MOUNTAIN-PLAINS CONSORTIUM

MPC 19-406A | D.R. Katti, K.S. Katti, K.B. Thapa, and H.M. Nasrullah Faisal

Development of Models for the Prediction of Shear Strength of Swelling Clays

INTERIM REPORT

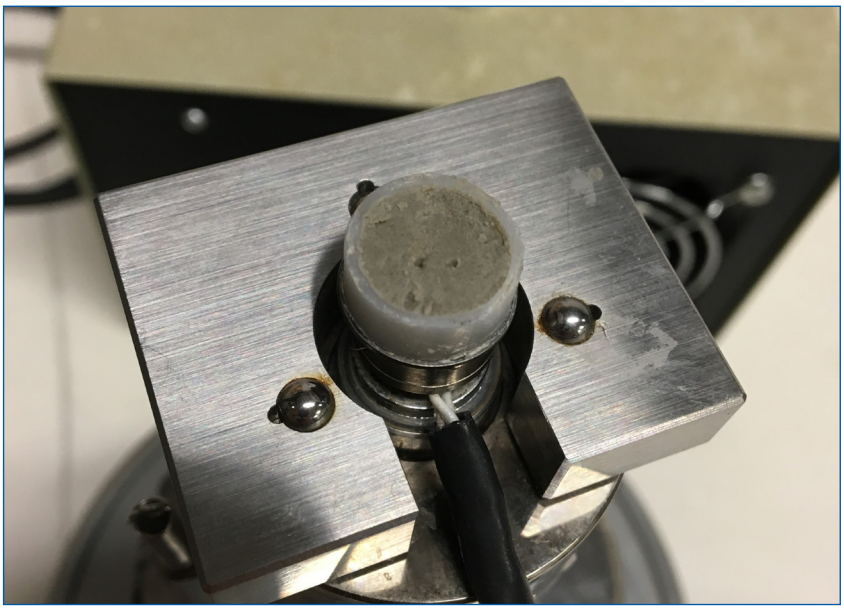

MOUNTAIN-PLAINS CONSORTIUM REGION 8

A University Transportation Center sponsored by the U.S. Department of Transportation serving the Mountain-Plains Region. Consortium members:

Colorado State University
North Dakota State University
South Dakota State University
University of Colorado Denver
University of Denver
University of Utah
Utah State University
University of Wyoming

Development of Models for the Prediction of Shear Strength of Swelling Clays

INTERIM REPORT

Dr. Dinesh R. Katti, P.E., F. EMI

Dr. Kalpana S. Katti, F.AIMBE

Keshab B. Thapa

H. M. Nasrullah Faisal

Department of Civil and Environmental Engineering
North Dakota State University, Fargo

December 2019

Acknowledgments

The authors acknowledge the support of USDoT Mountain-Plains Consortium (MPC) grants MPC-506 (agreement #DTRT13-G-UTC38) and MPC-548 (agreement #69A3551747108) for conducting the research presented in this report. The authors also thank the director of the Upper Great Plains Transportation Institute (UGPTI) Dr. Denver Tolliver and the staff at UGPTI for the opportunity and assistance. The computations for this research were conducted at the NDSU Center for Computationally Assisted Science and Technology (CCAST) (NSF #1229316). The experiments were conducted with instruments obtained from NSF grants (NSF #s 0923354, 0320657, and 0315513).

Disclaimer

ABSTRACT

Accurate prediction of the shear strength of swelling clays is critical for the design of infrastructure. Damage caused to U.S. infrastructure by swelling clays is estimated to be about $13 billion per year. Overestimation of strength can lead to failures, and underestimation can lead to an increase in project cost. Due to the small size of the clay particles and the nature of clay minerals, molecular interactions between the clay and fluids strongly influence engineering properties. In this research, we investigate the role of molecular interactions on the shear strength of swelling clay. This understanding can lead to the development of robust capabilities for accurate prediction of the shear strength of swelling clays. In this interim report, we present the results from our ongoing work that include the findings of the role of molecular interactions on the swelling, compressibility and shear response of montmorillonite clay interlayer using molecular dynamics. Results from unconfined compression tests and nanoindentation tests on saturated samples at 0% swelling are presented, and experiments with increasing swelling are ongoing. The development of molecular-scale clay tactoid, clay aggregate, and coarse-grained models to evaluate interparticle shear responses are in progress.

TABLE OF CONTENTS

LIST OF TABLES

LIST OF FIGURES

EXECUTIVE SUMMARY

Accurate prediction of the shear strength of swelling clays is critical for the design of roads, railway infrastructure, foundations, embankments, slopes, canals, erosion control, retaining walls, etc. Swelling clays are found in various parts of the United States and the world. Overestimation of strength parameters can lead to failures, and underestimation can lead to a significant increase in the cost of the project. Shear strength of soils with high swelling clay content can vary from high values when swelling is restrained due to significant degradation in strength or even complete loss of strength due to swelling. Due to the small size of the clay particles and the nature of clay minerals, molecular interactions between the clay and fluids strongly influence engineering properties. In this research, we are investigating the role of molecular interactions on the shear strength of swelling clay. This understanding would lead to the development of robust capabilities for accurate prediction of the shear strength of swelling clays. In this interim report, we present the results from our ongoing work.

We conducted molecular dynamics (MD) simulations to evaluate the role of fluid polarity on the swelling of Na-montmorillonite (MMT) clay, a swelling clay mineral. In this work, Fourier-transform infrared (FTIR) spectroscopy and MD simulations were carried out to investigate the swelling behavior of Na-MMT clay minerals with a wide range of organic fluids: formamide, water, methanol, and acetone. The shifts in the Si—O stretching band and Fe—OH deformation bands were observed in the FTIR spectra of Na-MMT clay, with higher polarity fluids showing larger band shifts than clay with low polarity fluids. This result indicates there are significant nonbonded interactions between clay and polar fluids. Our MD simulations indicate that the attractive nonbonded interactions between clay and polar fluids are significantly higher than those in clay and low polar fluids and consistent with the band shifts in FTIR studies, validating FTIR as a tool to evaluate clay-fluid molecular interactions. The larger the nonbonded interactions between the clay and fluids, the larger the clay swelling. Steered MD simulations (SMD) were conducted to evaluate the role of clay-fluid molecular interactions on the compressibility of clay interlayer. The results indicate that the clay interlayer is more compressible with low polar fluids than with high polar fluids, where nonbonded interactions are higher. Similar observations were noted in our experimental work at the macroscale. To scale the role of molecular interactions from the clay interlayer scale to clay aggregate (particle) scale, MD models of clay tactoids (stacked clay sheets) and clay aggregates (assembly of clay tactoids) are constructed, and SMD simulations are conducted to evaluate the mechanical behavior of the tactoids and aggregates to compressive and shear stresses. The simulations are in progress and results are forthcoming. Also, under development, is a coarse-grained model of clay for scaling up molecular modeling of interparticle interactions to support future discrete element modeling efforts Modeling details and results are provided in sections 1 through 5. Undrained shear strength experiments are conducted on Na-MMT clay samples swollen to various amounts of swelling from a specially fabricated device. Nanoindentation experiments are conducted on identically swollen samples. A new technique has been developed to conduct nanoindentation experiments on saturated clay samples. Details of the experimental work are presented in sections 6 and 7. Sections 1 through 7 in this report are presented verbatim from our published papers/manuscripts under review or manuscripts under preparation.

1. ROLE OF MOLECULAR INTERACTIONS ON SWELLING IN EXPANSIVE CLAYS

This section is presented verbatim from our publication (1).

1.1 Background

Swelling clays are found all over the world. The understanding of the expansive behavior of these clays is of significant importance in geotechnical and geoenvironmental applications, in petroleum and industrial engineering, and for the design of polymer-clay-nanocomposites. The volume of swelling clay increases when it interacts with water, resulting in a significant increase in swelling and swelling pressure. The infrastructure, such as buildings, roads, retaining walls, dams, and irrigation canals, are prone to damage from swelling pressure (2-4). However, this type of clay has also been used for landfill liners (5), borehole stabilization when drilling mud (6), enhancing the material properties in clay-nanocomposites (7), biomedical application (8), and modifying asphalt in pavement construction (9).

Sodium-montmorillonite (Na-MMT), in many cases, is the main component of swelling clay mineral found in these clays. The mineral consists of a tetrahedral-octahedral-tetrahedral (T-O-T) structure where octahedral clay sheet is sandwiched between two tetrahedral clay sheets (10). Na-MMT clay is used extensively as a barrier material in geotechnical and geoenvironmental engineering due to its high surface area and low hydraulic conductivity. Hence, understanding the swelling mechanisms and evaluating the interactions occurring on the molecular scale of Na-MMT clay with various organic fluids is crucial for predicting swelling clay response, designing landfill clay liners, and avoiding enormous damages caused by swelling clays. Landfill leachate includes a wide range of organic fluids. The United States Environmental Protection Agency (EPA) has labeled fluids such as toluene, trichloroethylene (TCE), acetone, methanol, and formamide among other fluids as toxic and dangerous to health. The interactions between Na-MMT clay and organic fluids are very important in determining the appropriate use of clays in the landfill liners. In swelling clays, swelling is categorized as inner crystalline swelling and osmotic swelling (11). The inner crystalline is due to initial hydration of exchangeable interlayer cations of dry clays when they come in contact with an aqueous phase such as water. The clay-water interactions have been studied using diffuse double layer theory (12). However, the interlayer hydration of swelling clay was not described accurately by these theories.

In our previous work, swelling pressure of saturated bentonite clay at a predetermined swelling level has been studied experimentally and showed that clay particles break down to a smaller size with increases in swelling level and reduction of swelling pressure (13). Fourier-transform infrared (FTIR) spectroscopic is a nondestructive technique (14) and used for the analysis of clay-fluid interactions. Extensive studies on Na-MMT clay with water have been carried out using FTIR (15), and the disorientation of clay sheets increase due to clay-water interactions with increasing swelling magnitude. In our prior work, the hydraulic conductivity of the Na-MMT clay interlayer region is studied using polarized FTIR spectroscopy. In addition, the change in Si—O stretching band in tetrahedron clay sheets, O—H stretching of a structural hydroxyl group, and H—O—H bending vibration band of bulk water at the molecular scale showed a significant interaction between clay and water. Extensive experimental studies have been carried out on Na-MMT clay with high polar fluids, formamide and water, medium polar fluids, methanol, and low polar fluids, acetone, chloroform, trichloroethylene, and toluene (16, 17). The interactions between Na-MMT and organic fluids are nonbonded in nature—the nonbonded interactions are very high for polar fluids and almost negligible for low polar fluids. Therefore, the clay-fluids molecular interactions control the evolution of the macroscopic structure of Na-MMT clay. The macro-scale mechanical properties, such as hydraulic conductivity, consolidation, and swelling pressure, of Na-MMT clay with these fluids, are studied. The hydraulic conductivity decreases dramatically with the

increase in polarity of fluids (17). Furthermore, the initial swelling of montmorillonite clay depends on the type of interlayer cations and hydration energy of interlayer cations (18), and the clay particles break down due to a significant cation-fluid hydration energy.

In addition to these experimental studies, the computational techniques have been used to investigate the behavior of swelling clays at the molecular level. Molecular dynamics (MD), Monte Carlo (MC), and discrete element method (DEM) have been carried out to study the interaction between clay and water (19-33). In our previous work, the mechanical behavior dry and hydrated Na-MMT clay interlayer and clay-water interactions are studied using steered molecular dynamics (SMD); and it has been observed that the solvation of interlayer cations and clay sheets play a significant role in the swelling properties of Na-MMT clay (28, 29, 34-36). DEM studies showed that particle subdivision of Na-MMT clay causes an increase in swelling pressure (30). The attractive interactions between sodium and clay hold the clay sheets together in dry clay; however, when water is introduced, the attractive interactions between sodium and water result in the formation of solvation shell around the cations, resulting in decreased attractive interactions between clay sheets and sodium ion, in turn increasing the crystalline swelling, and with increased interlayer hydration, causing exfoliation and particle breakdown of swelling clay (32, 37). The initiation of the crystalline swelling mechanism of Na-MMT clay has been carried out using MD simulations. Interlayer sodium cations attract the water molecules into the interlayer, and there is also a significant attractive nonbonded interaction between them, which initiates interlayer swelling (32). Furthermore, interactions of Na-MMT with formamide, water, methanol, acetone, and toluene have been quantitatively studied in a previous work. We have observed the significantly higher nonbonded interactions between clay and polar fluids than between clay and low polar fluids (38). Previous studies on clay-fluid interactions have been conducted either experimentally or computationally but not concurrently on the same system. In the current work, we attempt to link interaction energies from MD simulations to observed changes in the experimentally obtained FTIR spectroscopy spectra. The molecular models used in the study resemble the clay used in the experiments. Also, by conducting MD studies at the observed d-spacing values of samples used in FTIR studies, the fluid content in the interlayers in MD and FTIR experiments is similar, providing an insight into molecular mechanisms. This current study presents our FTIR and MD simulation results on Na-MMT clay with a wide range of organic fluids and provides insight into nonbonded interactions quantitatively at the molecular scale. In addition, the conformations of each organic fluids in close proximity to interlayer sodium cations are presented.

1.2 Materials

Na-MMT (SWy-2, Crook County, Wyoming, USA) clay was acquired from Clay Minerals Repository at the University of Missouri in Columbia, Missouri. The cationic exchange capacity of this clay is about 76.4 meq/100g. The fluids used were 90% to 100% purity formamide and 99.9% purity acetone obtained from Mallinckrodt Baker Inc., New Jersey, and 99.9% purity methanol obtained from Alfa Aesar in Massachusetts. The deionized water used was obtained from our laboratory at North Dakota State University. The fluids used in this study range from high dielectric constant to low dielectric constant, reflecting highly polar to low polar fluids. Formamide and water have a high dielectric constant of 110 and 80, respectively; methanol has a medium dielectric constant of 33, and acetone has a low dielectric constant of 20.

1.3 Experimental Method

A comprehensive infrared spectroscopic study on Na-MMT clay and organic solvents samples were described in our previous work (16). Briefly, Na-MMT was first ground and passed through a No. 325 sieve (45 μm mesh). The consistent moisture content was acquired by drying clay in an oven at 50°C for 24 hours prior to each sample preparation. The thin layer of Na-MMT was placed on the gold-coated

metal substrate with a glass slide, and fluid was added to the surface of the sample. For transmission FTIR spectroscopy study, the powder samples were gently compressed against a silicon window with a glass side, and then the fluids were added to the surface of the clay. Another silicon window was used to sandwich the sample by gently pressing them together to make a thin layer of sample between silicon windows. The homogeneous samples for formamide and water were prepared by mixing clay with fluids in a porcelain dish to obtain a thin layer of slurry. The sample was smeared on a silicon window, and gold coated a substrate for transmission and reflectance FTIR experiments, respectively. Data acquisition was accomplished immediately after the samples were wetted. The FTIR spectroscopy experiments were performed using a Nicolet 850 FTIR spectrometer with KBr beam splitter in the range of 4000-400 cm^{-1} at a spectral resolution of 4 cm^{-1}. A wire grid polarizer was used to yield a p-polarized IR beam, and angle of incidence was at 45° for the reflectance experiment, and the gold-coated metal substrate was used for obtaining background spectra. The clean silicon windows and gold coated metal substrate were used, respectively, for background spectra in transmission and reflectance experiments.

1.4 Model Construction

The chemical formula of the Na-MMT SWy-2 unit cell is $NaSi_{16}(Al_6FeMg)O_{20}(OH)_4$. The initial coordinates were obtained from the model proposed in the literature (39). Also, the atomic charges were obtained from the literature (21). The Na-MMT 4x2 model was initially constructed (28) in our previous studies—the dimensions of unit cell were 5.28Å x 9.14Å x 6.56Å. The structural charges in the molecular models of clay sheets are consistent with the experiments. The chemical formula for clay used in the experiments (40) is $(Ca_{0.12}Na_{0.32}K_{0.05})[Al_{3.01}Fe(III)_{0.41}Mn_{0.01}Mg_{0.54}Ti_{0.02}][Si_{7.98}Al_{0.02}]O_{20}(OH)_4$. Almost all of the unbalanced charge in the clay sheet comes from isomorphous substitution and is reported as 0.53e. In our models, the charge due to isomorphous substitution in the octahedral sheet is 0.5e per unit cell (29). This model has been extensively used for clay-fluid interactions (29, 32, 37, 41) using CHARMM force field parameters (27, 29). The sodium montmorillonite clay layers have a tetrahedral-octahedral-tetrahedral (T-O-T) structure, and each octahedral clay sheet is sandwiched between tetrahedral clay sheets. In our work, the clay model has 6x3 unit cells, and the dimensions of the unit cell are 31.68 Å x 27.44 Å x 24.16 Å. The molecular model consists of 6 unit cells in X-direction and 3 unit cells in Y-direction as shown in Fig. 1.1. A detailed explanation of the model construction is described in our previous work to study polymer clay nanocomposites [41].

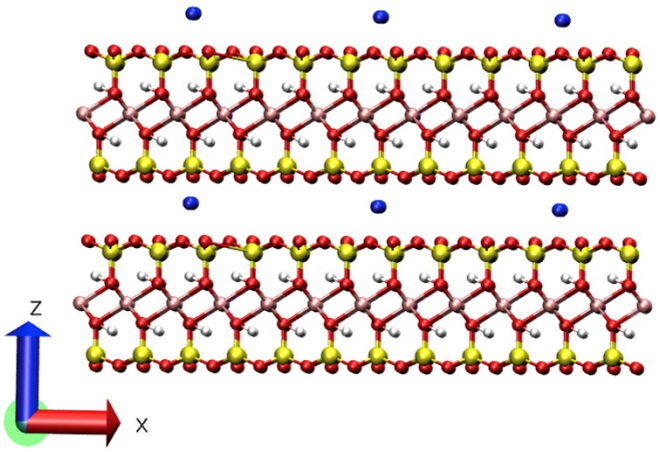

Figure 1.1 Molecular model of sodium (Na)-montmorillonite showing clay sheets and interlayer cations

The negative charge was developed on the individual clay sheets due to isomorphic substitution in the octahedral sheet. In the 6x3 model, nine aluminum (Al^{+3}) cations are substituted by nine iron (Fe^{+3}) cations, and nine aluminum (Al^{+3}) cations are substituted by nine magnesium (Mg^{+2}) cations. Thus, nine sodium (Na^{+}) cations were introduced in the interlayer to balance the negative charge (-0.5e per unit cell) of the clay sheets.

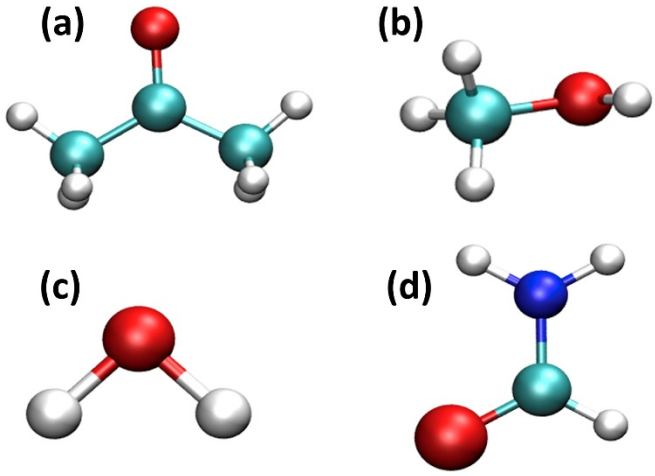

Figure. 1.2 The molecular structure of (a) acetone, (b) methanol, (c) water, and (d) formamide.

The Na-MMT and fluids models were developed using Material Studio™ and PSFGen plug-in of Visual Molecular Dynamics (VMD 1.9.2) software (42). The force field parameters for formamide, methanol, and acetone were obtained from CHARMM GUI Archive-CHARMM small molecule (43), and the water molecule was transferable intermolecular potential 3 point (TIP3P) (44). FTIR spectroscopy experiments were conducted on samples created by clay slurries of clay+acetone and clay+methanol. In addition, samples were prepared with clay mixed with a predetermined amount of water and clay mixed with a predetermined amount of formamide. Under the same condition, XRD experiments were conducted on the samples to evaluate d-spacing. Inverse calculations were conducted to evaluate the amount of fluid in the interlayer by comparing d-spacing obtained from MD simulations with d-spacing values found from XRD experiments. The molecular models with the computed amounts of fluid molecules in the interlayer were used to evaluate the interaction energies. The d-spacing values for the molecular models with 10% acetone, 20% methanol, 30% water, and 30% formamide matched with the d-spacing results from the XRD experiments. In order to compare FTIR spectroscopy results with the MD interaction energy results, the representative clay models consist of 10% acetone, 20% methanol, 30% water, and 30% formamide in the interlayer (16, 17, 45, 46). The detailed procedure of the model construction is described in our previous work (38). CHARMM force field parameters have been used for both organic fluids and Na montmorillonite clay (27-29). The CHARMM parameters have been found and validated by the authors. Based on the molecular weight of individual molecules, 10% fluid content is equivalent to 24 molecules of acetone, 40 molecules of methanol, 64 molecules of water, and 48 molecules of formamide. In addition, 20% methanol has 80 methanol molecules, 30% water has 216 water molecules, and 30% formamide has 90 formamide molecules in the clay interlayer.

1.5 Simulation Details

Molecular dynamics (MD) simulations and visual molecular dynamics (VMD 1.9.1) were used for the molecular modeling of Na-MMT clay with different organic fluids. In molecular dynamics, Nanoscale Molecular Dynamics (NAMD 2.9) software was used, which was developed by Theoretical and Computational Biophysics Group, Beckman Institute, the University of Illinois at Urbana-Champaign (47). All interaction energies were computed using VMD, which was compatible with the CHARMM

force field (48). The simulations were run using 2.66 GHz Intel Xenon X5550 processor and 127 nodes, each node consisting of 8 processor core, at the Center for Computationally Assisted Science and Technology (CCAST) at North Dakota State University.

The conjugate method was carried out for the minimization of all models. The temperature 0 K, and the pressure 0 atmospheres are used during minimization. All the simulations were run at room temperature and atmospheric pressure, resulting in the isothermal-isobaric ensemble. The temperature was raised in three steps, 0 K through 300 K, with an increment of 100 K. The pressure was raised in four steps, 0 kPa through 101 kPa (1 atmosphere), with increment of 25 kPa while keeping the temperature constant at 300 K. The pressure was controlled by the Langevin piston Nose-Hoover method (49) and temperature by Langevin dynamics.

All the simulations were run for 150,000 steps, which is equivalent to 75 ps (10^{-12} s), with the time step of 0.5 fs (10^{-15} s). The infinite number of clay sheets were mimicked by applying the period boundary conditions. Although the clay sheets were restrained in X and Y directions, they were allowed to move in the Z direction. All the organic fluids were free to move in all directions, mimicking experimental conditions. The d-spacing of each model was measured by the distance between the corresponding surface oxygen atoms of clay sheets in the Z-direction. The interaction energies were computed considering the last 20 ps of the trajectory of simulation. Nonbonded interaction, such as electrostatic energy, was computed using the Particle Mesh Ewald (PME) method. For all models, the van der Waals switch and cut off distances were 16 Å and 17 Å, respectively.

1.6 Results and Discussion

In our previous work, a detailed vibrational spectroscopic study on clay-fluid interactions was described using transmission and reflection FTIR experiments (16). The combined IR spectra for dry Na-MMT and Na-MMT with acetone, methanol, water, and formamide is shown in Figure 1.3 (a-d).

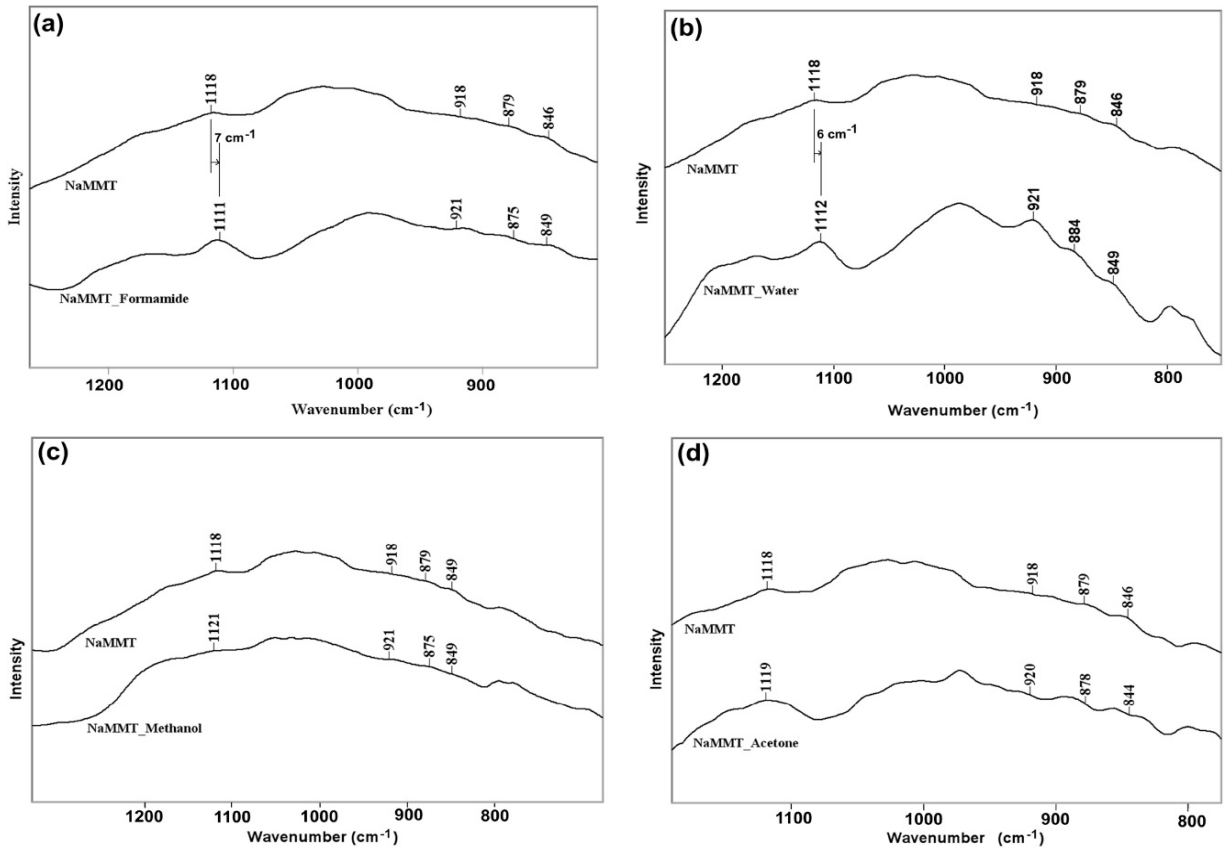

Figure 1.3 IR spectra for (a) mixture of Na-MMT and formamide in the energy range of 800-1275cm^{-1}, (b) mixture of Na-MMT and water in the energy range of 750-1250 cm^{-1}, (c) mixture of Na-MMT and methanol in the energy range of 675-1325 cm^{-1}, and (d) mixture of Na-MMT and acetone in the range of 775-1200 cm^{-1}

Table 1.1 shows the band assignments obtained from the literature (50-53). The band at 1118 cm^{-1} in the IR spectra of dry Na-MMT is attributed to the Si—O stretching. It is observed in Figure 3 (a-b) that the Si—O stretching band has a shift of 7 cm^{-1} and 6 cm^{-1} to lower energy for the clay-formamide complex and the clay-water complex, respectively.

Table 1.1 FTIR band assignment for dry Na-Montmorillonite clay

Band position (cm^{-1})	Band assignment
688	Si-O deformation (50)
788	Si-O stretch from quartz and silica (50, 51)
846	Mg-OH deformation (50, 51)
879	Fe-OH deformation (50, 51)
918	Al-OH deformation (50, 54)
1065	Si-O stretching (50, 52)
1118	Si-O stretching (50-52)

The band shift observed in the spectra suggests that the alteration in the orientation of silica tetrahedral region due to swelling characteristics, as the polar fluids enter into the clay interlayer galleries. The shift also signifies there is nonbonded interaction between surface oxygen of clay and interlayer solvents; this phenomenon has been observed in prior work in literature to study the polymer clay nanocomposites (55), evolution of clay microstructures (15-17), and interaction between clay and organic matter (52). The band

shifts are not significant in the Si—O region in the case of clay-methanol and clay-acetone complexes, which indicates that intermediate polar and low polar fluids have lower nonbonded interactions in Si—O region. Furthermore, Mg—OH deformation band at 846 cm^{-1} and Al—OH deformation band at 918 cm^{-1} of dry clay have no significant shifts in any clay-fluids complexes, indicating insignificant nonbonded interactions in the octahedral clay sheets. Fe—OH deformation band of dry Na-MMT at 879 cm^{-1} is shifted toward lower energy by 9 cm^{-1} and 5 cm^{-1} in the spectra of the clay-formamide complex and clay-water complex, respectively. These shifts are significant because of no overlapping bands in IR spectra. From the spectra of clay-methanol and clay-acetone complexes, no significant band shifts are observed in the tetrahedral or octahedral region of clay sheets. The shifts toward either lower or higher energy observed in the Si-O stretching band and the Al-OH, Fe-OH, and Mg-OH deformation bands suggest that the molecular interactions between clay and polar fluids are significantly higher than those in clay and medium and low polar fluids.

The experimental d-spacing of dry Na-MMT clay is 9.85 Å (16). The molecular dynamics simulation showed the average d-spacing of dry Na-MMT to be 10.70 Å, resulting in the representative clay model for this study. Similarly, the experimental d-spacing of Na-MMT with acetone, methanol, water, and formamide were found to be 13.07 Å, 17.14 Å, 18.32 Å, and 18.99 Å, respectively (16, 34, 38, 56). The d-spacing of the clay model with 10% acetone, 20% methanol, 30% water, and 40% formamide were approximately 13.38 Å, 17.60 Å, 17.89Å, and 18.46 Å, respectively, indicating that the interlayer fluid content increased with an increase in dielectric constant of fluids. These results are consistent with experimental results and can be related to the high swelling and swelling pressure, particle breakdown, low permeability, and low compression of the expansive clay in the presence of polar fluids (17). In this study, the swelling of the interlayer is associated with an increase in the distance between two clay sheets, however, the thickness of clay sheet remains constant. The clay-fluid molecular models consist of clay sheets, sodium ions, and interlayer fluids. The nonbonded interactions among these constituents provide insight into swelling behavior of the expansive clay.

Visual molecular dynamics was used to compute the interaction energies quantitatively. Energies were computed by considering the interlayer fluids in the clay interlayer after a simulation period of 75 ps. The snapshots of molecular models of Na-MMT with acetone, methanol, water, and formamide after simulation are shown in Figure 1.4 (a-d).

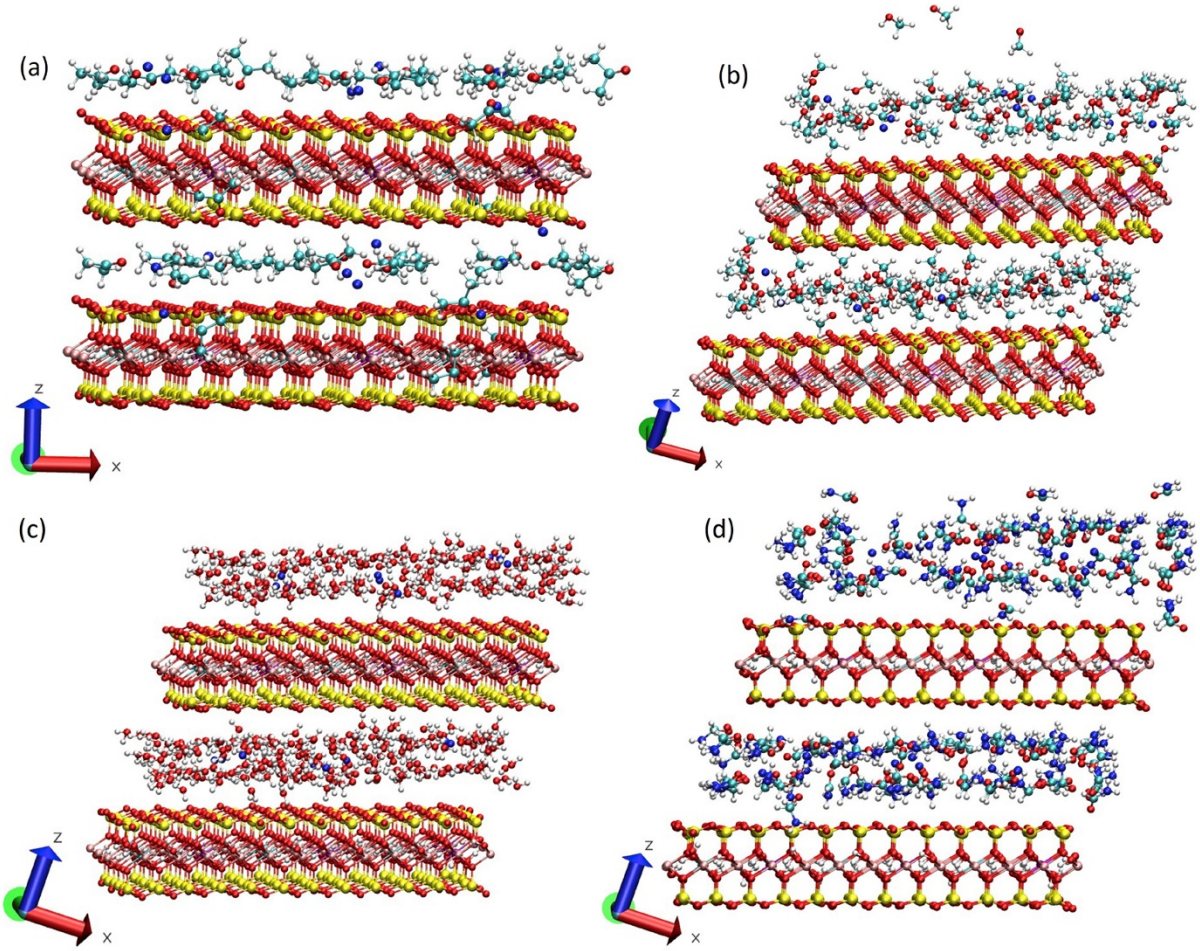

Figure 1.4 Na-MMT models with different interlayer fluids after simulation up to 75 ps (a) 10% acetone, (b) 20% methanol, (c) 30% water, and (d) 30% formamide

The sum of the electrostatic energy and Van der Waals energy is the total nonbonded energy. The electrostatic interaction energy is the function of the charge and distance between two sets of atoms; whereas, Van der Waals interaction energy depends only on the distance between two sets of atoms. The negative interaction energy represents the attractive interaction, and the positive interaction energy represents the repulsive interaction between two atoms.

Figure 1.5 shows the interactions energy between clay sheets in the dry state and various interlayer fluids (polar, medium polar, and low polar fluids). In the case of the dry interlayer, clay-clay interactions are the highest and predominated by Van der Waals energy. The repulsive electrostatic interaction was due to a negative charge in each clay sheet. When fluids are introduced in the interlayer, the attractive nonbonded interactions are decreased with the increasing amount of interlayer fluids and polarity of fluids, and interactions are rapidly diminished almost to zero at 30% of formamide. As shown in Figure 6, the attractive nonbonded interactions between sodium and clay layers are the highest in the dry condition, and these attractive interactions are primarily electrostatic and hold the clay sheets together.

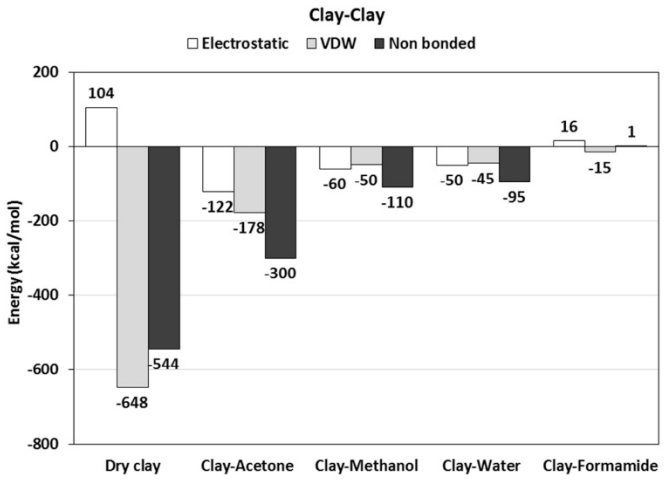

Figure 1.5 Interaction energies between clay sheets for fluids with a wide range of dielectric constants

This observation has also been studied on Na-MMT swelling clay with increasing water content using molecular dynamics (37). At equilibrium, sodium ions are found to be in close proximity to the clay sheets in the molecular model of Na-MMT with acetone and methanol, but sodium ions are located near the center of the interlayer in the molecular model of Na-MMT with water and formamide. The attractive interaction is also decreased with increasing polarity of fluids and fluid content. The electrostatic energy between sodium and clay sheets in dry Na-MMT clay is 1.5 times higher than Na-MMT with 10% acetone, and it is almost the same for Na-MMT with 20% methanol, 30% water, and 30% formamide, and the Van der Waals energy is negligible.

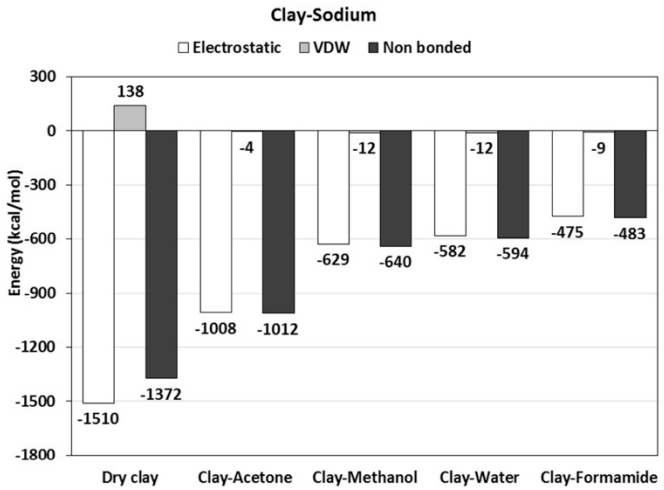

Figure 1.6 Interaction energies between clay sheets and sodium ions for fluids with a wide range of dielectric constants

Figure 1.7 shows the attractive interactions between sodium ions and interlayer fluid molecules are the highest, followed by clay-sodium interactions and clay-clay interactions. The electrostatic energy between sodium ions and 20% methanol was more than two times greater than sodium ions and 10% acetone. Similarly, the electrostatic energy between Na-MMT and 30% water was 1.5 times greater than Na-MMT and 20% methanol. The total nonbonded interaction energy between Na-MMT and 30% water is slightly greater than Na-MMT and 30% formamide. The nature of these interactions is predominantly (attractive)

electrostatic, whereas (repulsive) Van der Waals interactions are negligible. Thus, sodium ions have more significant interactions with polar fluids than those with low polarity fluids; the solvation of swelling clay was initiated by hydration of interlayer sodium ions, resulting in the initial interlayer swelling.

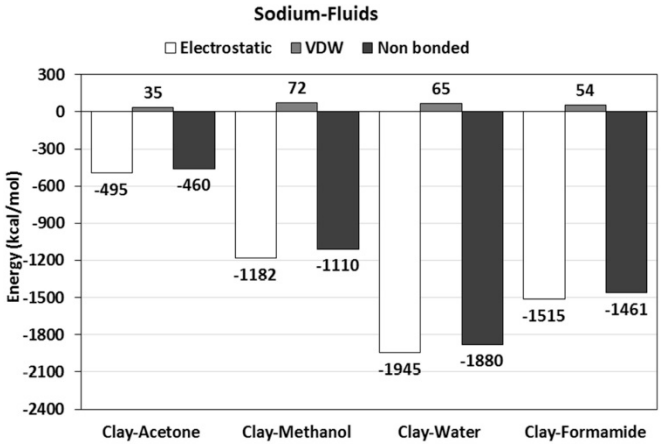

Figure 1.7 Interaction energies between fluids and sodium ions for fluids with a wide range of dielectric constants

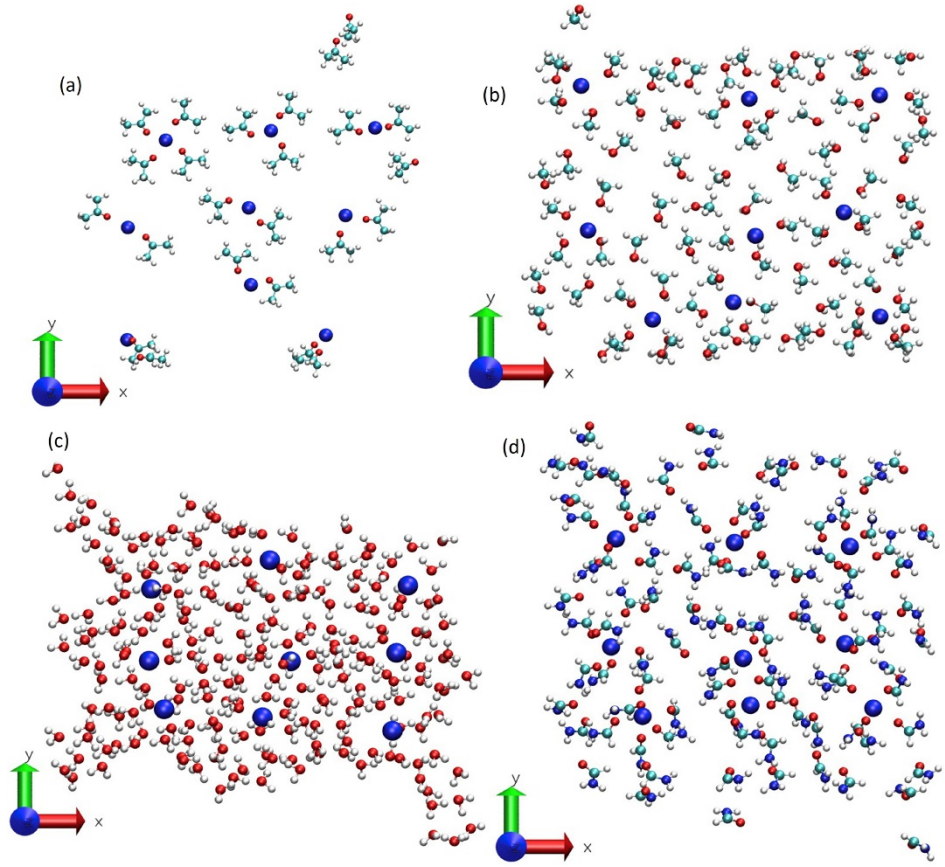

Figure 1.8 Snapshots displaying conformation of molecules of fluids in proximity to sodium ions (a) acetone (b) methanol (c) water, and (d) formamide

Figure 1.8 shows the snapshots of the representative models of Na-MMT with 10% acetone, 20% methanol, 30% water, and 30% formamide. This figure shows the planar view of conformation of the

interlayer fluids with sodium ions. It was found that the oxygen atoms were attracted and directed to the sodium ions, and hydrogen atoms were attracted to oxygen atoms, resulting in the formation of an organized pattern. It can be seen that two oxygen atoms and four oxygen atoms are in proximity of the sodium ions in the cases of Na-MMT with 10% acetone and Na-MMT with 20% methanol, respectively. In addition, the clustering and proximity of fluid molecules to the sodium ions increase dramatically as the fluid content, and the polarity of fluids increased; this formation resulted in the well-organized pattern for high polar fluids such as water and formamide. All these fluid molecules lay on the same plane as sodium ions.

The nonbonded interaction energy of Si—O of tetrahedral clay sheets with acetone, methanol, water, and formamide is shown in Figure 1.9. The interaction energy between Si—O, and fluids increased as the polarity of fluids increased. The repulsive electrostatic energy between Si—O, and water is more than 5.5 times greater than Si-O and acetone. Although the total nonbonded interaction energy between Si—O and formamide is slightly greater than Si—O and methanol, the corresponding electrostatic energy is similar and attractive in nature. These interaction energies agreed with shifts of Si—O band in our FTIR experimental analysis (Figure 1.3). These shifts suggest strong nonbonded interactions between the surface oxygen of clay sheets and fluid molecules, and strong interactions may change the orientations of silica tetrahedral sheets of clay.

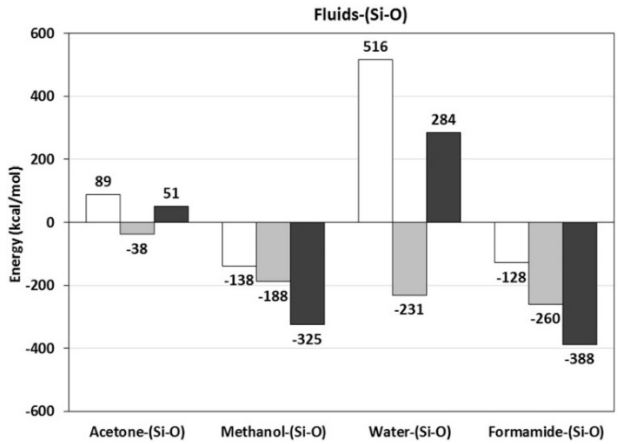

Figure 1.9 Interaction energy of Si-O with (a) acetone (b) methanol (c) water and (d) formamide

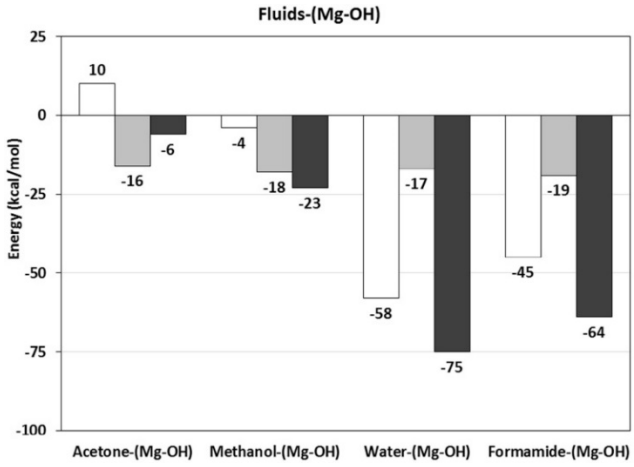

Figure 1.10 Interaction energy of Mg-OH with (a) acetone (b) methanol (c) water and (d) formamide

Figure 1.10 plots the variation of interaction energy between Mg—OH of octahedral clay sheet and fluids. The attractive nonbonded energy between Mg—OH and methanol is 3.5 times greater than acetone; however, Van der Waals energy is similar in both cases. The nonbonded interaction energy between Mg-OH and water is approximately same for Mg—OH and formamide, and these attractive interactions are predominantly electrostatic in origin. Nevertheless, Van der Waals energy is almost the same for both cases.

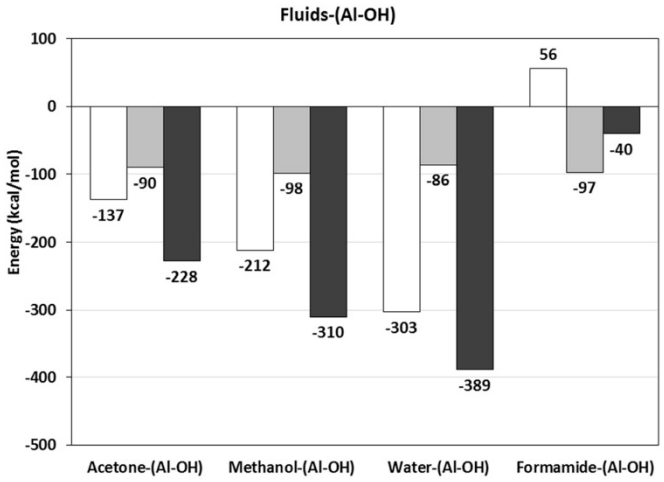

Figure 1.11 Interaction energy of Al-OH with (a) acetone (b) methanol (c) water and (d) formamide

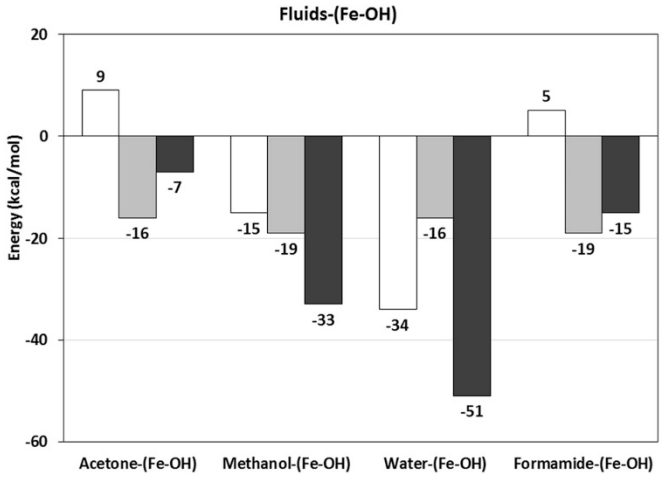

Figure 1.12 Interaction energy of Fe-OH with (a) acetone (b) methanol (c) water and (d) formamide

The nonbonded interaction energies of Al—OH and Fe—OH of octahedral clay sheet with fluids are shown in Figure 1.11 and Figure 1.12. Attractive electrostatic interaction energy between Al—OH and water is two times greater than acetone and almost 1.5 times greater than methanol. On the other hand, the electrostatic interaction between Al—OH and formamide is repulsive in nature. Van der Waals energy remains almost the same for all cases. Similarly, the total nonbonded energy between Fe—OH and water is more than three times greater than acetone and 1.5 times greater than methanol, but the (repulsive) electrostatic interaction between Fe—OH and formamide is not significant compared with other fluids. These results were consistent with the FTIR studies, which indicate that the interaction between polar fluids and clay increases with the increase in polarity of fluids. Thus, the FTIR and molecular dynamics simulation studies showed significantly higher nonbonded interactions between clay, formamide, and water than in clay, methanol, and acetone. In addition, simulation results indicated that clay and

formamide interactions were predominant. The results also show that the various entities of the clay sheet interact differently with the fluid molecules, even for fluid molecules with similar dielectric constants.

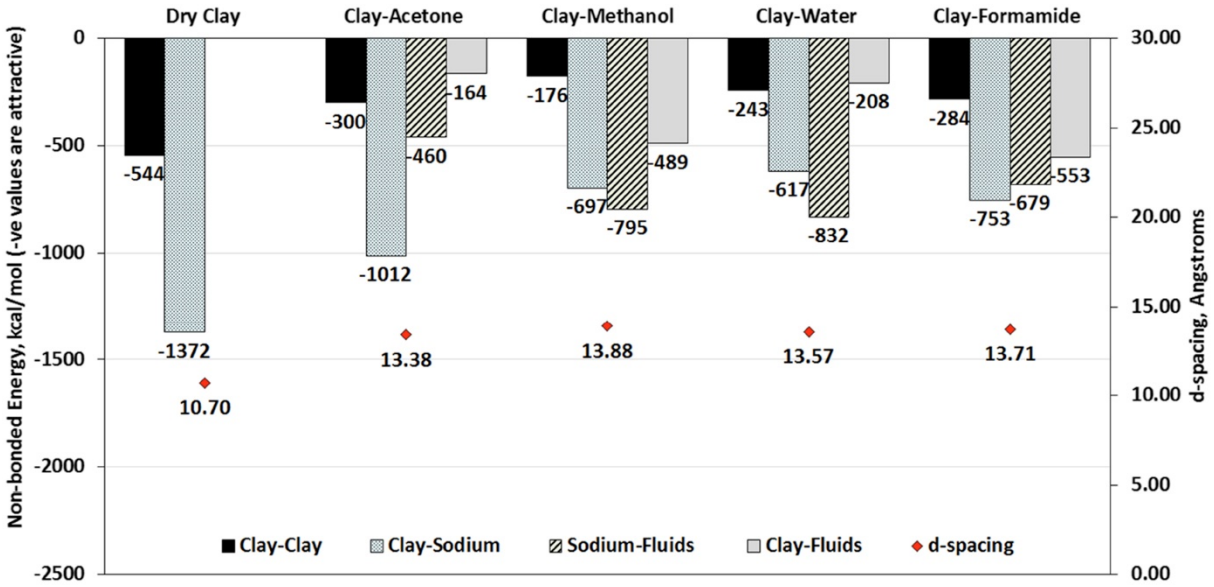

Figure 1.13 Nonbonded interaction energies between clay sheets for 10% acetone, methanol, water, and formamide and corresponding d-spacing. The interaction energies shown are clay-clay, clay-sodium, sodium-fluids, and clay-fluids.

Figure 1.13 shows the evolution of nonbonded interaction energies between the various components of the clay with 10% of fluid content in the interlayer with d-spacing. The d-spacing corresponding to 10% acetone, 10% methanol, 10% water, and 10% formamide were 13.38 Å, 13.88 Å, 13.57 Å, and 13.71 Å, respectively. The figure indicates that although the fluid content is the same, the molecular interactions in the interlayer are significantly different. Although the clay interlayer contained the same fluid content, each of the clay-fluid models had different d-spacing, and the clay-clay, clay-sodium, sodium-fluids, and clay-fluids interactions were also different. The nonbonded interactions between clay sheets decreased with an increase in d-spacing. The 10% of interlayer methanol had the highest d-spacing, resulting in the lowest nonbonded interactions between clay sheets. With the increase in d-spacing, the clay-sodium attractive nonbonded interactions decreased, but the interaction for formamide remained slightly higher than for water. The sodium-fluids attractive nonbonded interactions increased with an increase in d-spacing; the sodium-methanol interactions were more than 1.5 times greater than sodium-acetone; and the sodium-water interactions were slightly greater than sodium-methanol and sodium-formamide. The clay-fluids attractive nonbonded interactions increased with an increase in d-spacing, but the interactions of water with clay layers had the lowest energy. Also, the interactions of methanol with clay layers were three times greater than that of clay layers with acetone and slightly less than that of clay layers with formamide. The clay-clay attractive interactions were predominated by Van der Waals energy for dry clay as well as clay with 10% fluids content, but the attractive clay-sodium, sodium-fluids, and clay-fluids interactions were primarily electrostatic in nature.

Figure 1.14 shows the conformation for each of four interlayer fluids with sodium ions. The acetone, methanol, water, and formamide molecules formed a well-organized pattern in proximity to sodium ions, and the oxygen atoms were also attracted and directed to the sodium ions. Although, the fluid molecules tend to cluster around the sodium ions, the distribution of fluid molecules in the interlayer over the plane parallel to the clay surfaces show conformational differences. This is particularly apparent with methanol and water, where the distribution of the fluid molecules is not as uniform as acetone and formamide. The greatest difference is observed in the case of water where the water molecules are aligned along the y-axis

of the model. The size of the molecules, molecular charge distribution, and the number of molecules seem to affect the molecular distribution of fluid molecules in the interlayer. The water molecules are the smallest size fluid molecules among the fluids used and are most in number for the same 10 weight percent. As shown in Figure 1.13, the sodium-water attractive interactions are significantly larger than clay-formamide interactions, some of which may be attributed to more clustering of water molecules with sodium ions (Figure 1.14). The figure also shows larger clay-formamide interactions compared with clay-water interactions, which may be because the formamide molecules are more uniformly distributed over the entire plane parallel to the clay surface. The relationship between the fluid molecular conformations and effect on interaction energies is qualitative based on the snapshots, and more work will be needed to introduce the effect of size and conformations, in addition to fluid polarity on clay swelling.

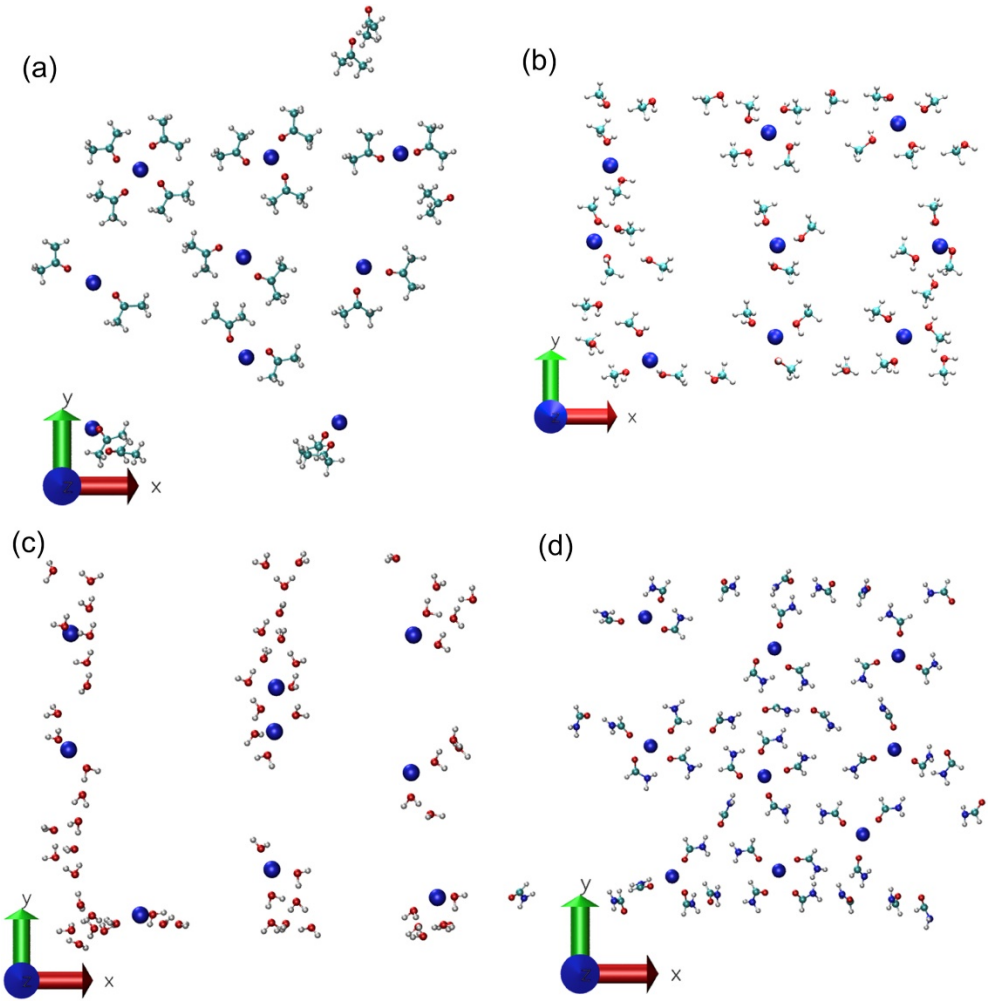

Figure 1.14 Planar view showing the conformation of molecules of fluids in proximity to sodium ions (a) 10% acetone, (b) 10% methanol, (c) 10% water, and (d) 10% formamide

1.7 Conclusions

In this work, FTIR and MD simulations were carried out to investigate the swelling behavior of Na-Montmorillonite (NA-MMT) clay mineral with a wide range of organic fluids: formamide, water, methanol, and acetone. The shifts in the Si—O stretching band and Fe—OH deformation bands were observed on the FTIR spectra of Na-MMT clay, with formamide and water showing larger band shifts than clay with methanol and acetone. This result indicates there are significant nonbonded interactions

between clay and polar fluids, resulting in the change in orientation of tetrahedral and octahedral clay sheets. The molecular models of Na-MMT clay with fluids were developed, and the representative clay-fluids models were validated by comparing MD simulation d-spacing with the experimental results. The MD simulations were used to provide insight into conformation and quantitative nonbonded interactions of clay with formamide, water, methanol, and acetone at the molecular level. The results of our simulations indicate that the attractive nonbonded interactions, which are primarily electrostatic in nature, between clay, formamide, and water are significantly higher than those in clay, methanol, and acetone. These results are consistent with the shifts of bands in FTIR studies. Furthermore, the nonbonded interactions play a significant role in the conformations of fluid molecules in proximity to sodium ions in the interlayer. A planar view of the conformations shows a well-organized pattern as the amount and polarity of interlayer fluids increase. The modeling study with 10 weight percent of the four fluids in the interlayer gallery showed that the molecular interactions between clay sheets, sodium ions, and fluid molecules are significantly different. The d-spacings in all four cases were different and ranged from 13.38Å to 13.88Å. The clay-clay interactions decreased with increasing d-spacing. The sodium-fluid and clay-fluid interactions appear to relate to the size, number of fluid molecules, and the physical distribution of the molecules in the interlayer. These studies provide an insight into the molecular mechanism and indicate that the polarity of fluids plays a significant role in the interlayer swelling, alternation in the orientations, and evolution of microstructure of swelling clays at the molecular scale.

2. COMPRESSION OF SWELLING CLAY WITH VARIOUS ORGANIC FLUIDS AT THE MOLECULAR SCALE

This section is presented verbatim from our publication under review.

2.1 Background

Swelling clays are found throughout the world and are of great importance in geotechnical engineering, geoenvironmental applications, and industrial processes due to high swelling capacity (57), high specific area (58), and low hydraulic conductivity (59). These clays have also been used as barrier liners in landfills (5) and for high-level radioactive waste disposal (60), drug delivery in biomedical applications (61), and modifiers in pavement construction (62). However, civil infrastructures are susceptible to damage due to clay swelling, resulting in enormous damage to the buildings, roads, bridges, and embankments (2, 63).

Sodium-montmorillonite (Na-MMT) clay is one of the major constituents of smectite clay minerals (64). This mineral consists of a tetrahedral-octahedral-tetrahedral (T-O-T) structure where an octahedral clay sheet is sandwiched between tetrahedral clay sheets (10). A negative charge on the individual clay sheets is developed due to isomer substitution by metal ions in the tetrahedral or octahedral clay sheets (65). These charges are balanced by adding sodium cations, which are naturally found inorganic species in clays, in the interlayer. In this study, a wide range of polar fluids—formamide (110), water (80), methanol (33), and acetone (20)—are chosen for the clay-fluid interactions. The values in parentheses are the dielectric constant (DEC) of the fluid. Some of these fluids are commonly found in landfill leachates and identified as toxic and hazardous to health by the United States Environmental Protection Agency (EPA).

Understanding the swelling nature and molecular mechanism of swelling clays by including clay-fluid interactions is essential to avoid their detrimental consequences and thus utilize their benefits. In swelling clays, the hydration of the interlayer cations triggers the interlayer crystalline swelling (11, 19). The earlier double-layer models (66-68) attempt to evaluate the clay-water interactions in the clay interlayer (12), but these theories were not able to predict the interlayer swelling at smaller layer spacing.

The previous experimental study has shown that the particles of the saturated swelling clays successively break down into a small size with increased swelling level and a reduction of swelling pressure (13). This phenomenon is further incorporated into the computational model to capture the role of the particle subdivision on swelling and swelling pressure (69). The evolution of microstructures, mechanical properties, and fluid flow behavior of Na-MMT clay with various organic fluids are experimentally studied. The interactions of Na-MMT clay with these fluids are primarily nonbonded in nature at the molecular level, and the nonbonded interactions for polar fluids are significantly higher than those of low and medium polar fluids (16). With an increase in the polarity of the fluids, the swelling pressure increases, but the hydraulic conductivity decreases dramatically (17). Thus, the clay-fluid interactions at the molecular level control the macroscopic properties of Na-MMT clay.

A number of computational studies—molecular dynamics (MD), Monte Carlo (MC) method, and discrete element method (DEM)—have been used to evaluate the nature of interactions of swelling clays with various interlayer cations (70-73) and water at a different levels of hydration (22, 74, 75) and organic matter (76, 77). The swelling mechanism and hysteresis loop of expansive clay have been studied at the molecular level (25). Steered molecular dynamics (SMD) simulation is a computational technique in which the external forces are applied to the molecules to guide a system from one state to another at an atomic scale. The evolution of the mechanical response of the dry state and hydrated Na-MMT clay with multiple layers of water is evaluated using SMD simulations. The stress-deformation response of the clay

interlayer is linear for dry clay and clay with one monolayer of water and nonlinear for clay with two and three monolayers of water in the interlayer (28). The level of hydration, solvation of interlayer cations, and clay-fluid interactions control the interlayer spacing and modulus of swelling of Na-MMT clay upon compression. The elastic properties of swelling clays have been studied using MD simulations, and it has been reported that the water content, nature of interlayer cation, and temperature influence the stiffness tensor of montmorillonite clays (78). The stiffness of the layer silicates in presence of the surface charges is calculated using density functional theory (DFT) and MD simulations (79). The elastic tensors of Na-MMT clays over a wide range of hydrations have been computed using MD simulations (80). The nanoscale hardness of tobermorite and montmorillonite clay has been computed using a local structure optimization (LSO) approach by applying biaxial deformation or stress (81).

For the dry case, the stability of the stacked structure is maintained by the nonbonded interactions between sodium ions and clay sheets (37, 82). However, these attractive interactions decrease as soon as the water molecules are introduced in the swelling clay interlayer. The sodium ions also attract the water molecules in the interlayer, and the sodium-water interactions are higher than clay-clay interactions, resulting in the initiation of interlayer swelling of Na-MMT clay (32). The nonbonded interactions of Na-MMT clay with toluene, acetone, methanol, water, and formamide have been studied experimentally and computationally on the same system, and it has been observed that the polar fluids have higher interactions with clay than those of low and medium polar fluids (38, 83). However, the nonbonded interactions and mechanical behavior of Na-MMT clay with these fluids have not been investigated at the molecular level. These clay-fluid interactions and the interlayer response of swelling clays upon compression are essential to predict the reliable shear failure mechanism that is crucial for the effective and economic design of infrastructures and for public safety. In this study, we present our results from SMD simulations on Na-MMT clay with a wide range of organic fluids. This work also provides an insight into the role of the fluid content and the polarity of the fluids on the interlayer spacing, volume, strain, modulus, and nonbonded interactions upon externally applied stresses at the molecular level. Furthermore, the conformation of all four fluid molecules in the interlayer in close proximity to the sodium ions before and after compression is captured.

2.2 Model Construction

The chemical formula for Na-MMT clay used in the experiments(84) is

$(Ca_{0.12}Na_{0.32}K_{0.05})[Al_{3.01}Fe(III)_{0.41}Mn_{0.01}Mg_{0.54}Ti_{0.02}][Si_{7.98}Al_{0.02}]O_{20}(OH)_4$,

which has both octahedral and tetrahedral isomer substitutions. The chemical formula of the clay model is simplified to $NaSi_{16}(Al_6FeMg)O_{20}(OH)_4$. The coordinates of the unit cell are obtained from Skipper et al. (24), and the atomic charges are obtained from Teppen et al. (21). The dimensions of the unit cell of this model are 5.28 Å x 9.14 Å x 6.56 Å. This work uses a large 6x3 Na-MMT model, which has six unit cells in X-direction and three unit cells in Y-direction, as shown in Figure 2.1.

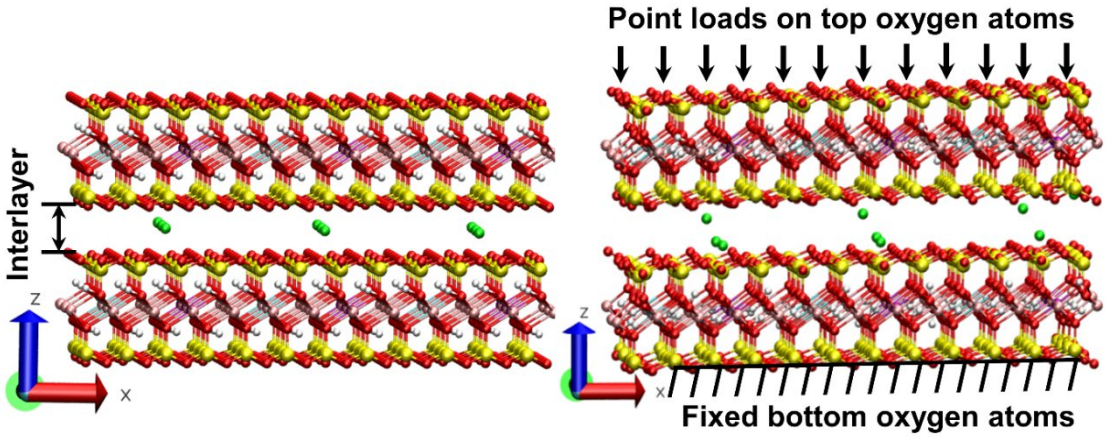

Figure 2.1 (a) Initial molecular model of dry Na-MMT and (b) equilibrium Na-MMT clay at 300 K temperature and 1 atmospheric pressure

The isomer substitution by metal atoms in the octahedral sheet takes place and results in a negative charge on the individual clay sheets. During isomer substitution, nine aluminum (Al^{3+}) cations were replaced by nine iron (Fe^{3+}) cations and another nine aluminum (Al^{3+}) cations by magnesium (Mg^{2+}) cations in the 6x3 Na-MMT model. These negative charges of the clay sheets were balanced by inserting nine sodium (Na^{+}) cations. The detailed construction of the 6x3 model is explained in our previous work. (85) The overall dimensions are 31.68 Å x 27.44 Å x 24.16 Å. The Na-MMT and fluids models are developed by using Material Studio and PSFGen plug-in of Visual Molecular Dynamics (VMD 1.9.3) software (47). The CHARMM force field parameters for formamide, methanol, and acetone are received from the Chemistry at Harvard Macromolecular Mechanics (CHARMM) force field parameters GUI Archive-CHARMM small molecule (43), and the water molecule was transferable intermolecular potential 3 point (TIP3P) (44). In this study, the representative clay models consist of 10% acetone, methanol, water, and formamide, as well as 30% methanol, water, and formamide in the interlayer. Depending upon the molecular weight of the individual atom, 10% fluid content has 24 acetone molecules, 40 methanol molecules, 64 water molecules, and 48 formamide molecules. Similarly, 30% fluid content is equivalent to 120 molecules of methanol, 216 molecules of water, and 120 molecules of formamide. The interlayer fluid molecules are initially placed in a single layer for 10% fluid and three layers for 30% fluid.

2.3 Simulation Details

In this study, MD and SMD simulations of dry and hydrated 6x3 unit Na-MMT clay models were carried out by using NAMD 2.12 that is developed by Theoretical and Computational Biophysics Group, Beckman Institute at the University of Illinois at Urbana-Champaign (86). The CHARMM force field parameters (48) were also used for the clay. Visual molecular dynamics (VMD 1.9.3) was used for visualization and interaction energy computation. An isothermal-isobaric (NPT) ensemble was used for running the MD simulations. The model was minimized by using a conjugate gradient method. After minimization, the temperature was increased from 0 K to 300 K in three steps with an increment of 100 K using the Langevin dynamics control method (49). The pressure was increased from 0 bar to 1.01 bar in four steps with 0.25 bar increments using the Nose-Hoover Langevin piston control method (87) while keeping the temperature constant at 300 K. The simulation was run for an additional 400 ps. The total simulation time up to this point was 1 ns.

The displacement of clay interlayer spacing responses of dry and hydrated 6x3 unit Na-MMT clay molecular models was carried out using constant-force SMD simulations. The interlayer spacing is the void space between adjacent clay layers, and the sum of the interlayer spacing and thickness of the clay

sheet is the d-spacing. The interlayer strain is similar to the strain in solids and measured by a change in interlayer spacing upon the application of a load relative to the original position. A uniform compressive point load was applied in the z-direction on each of the oxygen atoms lying on the top surface of the clay sheet. A total of 108 oxygen atoms on the top surface of the clay sheet were selected, and the average projected load-bearing area was 729.63 $Å^2$ in the x-y plane. Also, the 108 oxygen atoms of the bottom surface of the clay sheet were fixed in all x, y, and z directions, mimicking the unconfined compression experiment. The clay sheets are unrestrained in the z-direction but restrained in x and y directions. All the fluid molecules are allowed to move in all directions, simulating standard experimental conditions. A wide range of compressive loads on each atom of the top clay sheet were 0, 25, 50, 75, 100, 150, 200, 300, 400, and 600 pN (10^{-12} N) per atom for dry and hydrated Na-MMT clay models, and the equivalent stresses were 0, 0.37, 0.74, 1.11, 1.48, 2.22, 2.96, 4.44, 5.92, and 8.88 GPa. Furthermore, these normal stresses were divided into two groups, where the stresses varied from 0 to 1.48 GPa for region-I and from 2.22 to 8.88 GPa for region-II.

SMD simulations were run for 400,000 steps with a time step of 0.5 fs (10^{-15} s) for a total simulation time of 200 ps (10^{-12} s). Thus, the total simulation time up to this point was 1.2 ns. The last 20 ps of constant-force SMD simulation trajectory were averaged to compute the nonbonded interaction energy. The switch and cut-off distances for van der Walls and electrostatic were 16 Å and 17 Å, respectively. All simulations were run with 200 processors using a 2.66 GHz Intel Xenon X5550 processor at the Center for Computationally Assisted Science and Technology (CCAST) at North Dakota State University.

2.4 Results and Discussion

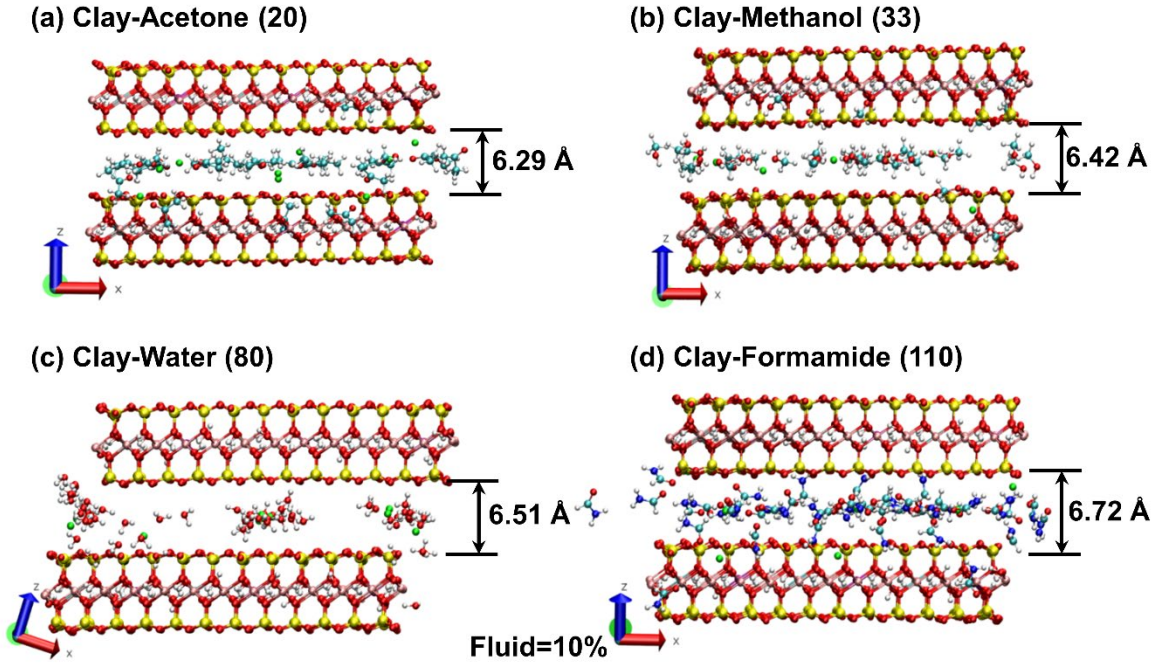

Figure 2.2 Na-MMT clay models with 10% interlayer fluids showing the interlayer spacing: (a) clay-acetone (20), (b) clay-methanol (33), (c) clay-water (80), and (d) clay-formamide (110). The values in the parentheses are the dielectric constant of the fluid.

For the representative dry clay and the hydrated clay acetone, methanol, water, and formamide, the interlayer spacing after MD simulation was measured by computing the vertical distance between the corresponding surface oxygen atoms of the top and bottom clay sheets. For the dry Na-MMT clay, the

average interlayer spacing and d-spacing are 3.96 Å and 10.52 Å, respectively. These values are obtained from equilibrated MD simulation and consistent with the experimentally obtained value from a previous study (16). The interlayer spacing for Na-MMT clay with 10% acetone, methanol, water, and formamide is 6.29 Å, 6.42 Å, 6.51 Å, and 6.72 Å, respectively, as shown in Figure 2.2. The interlayer spacing for Na-MMT clay with 30% methanol, water, and formamide is 9.94 Å, 10.85 Å, and 6.72 Å, respectively. These results are also consistent with our previous study (38). It is observed that the interlayer spacing is increased with an increase in the polarity of fluids and increased in the fluid content. Thus, the dry clay and hydrated clay-fluid molecular models are further used for the constant-force SMD simulations to study the mechanical response of the interlayer spacing.

For dry clay, a drop in the interlayer spacing is observed from 0 to 1.48 GPa stress, but the interlayer spacing is on the same order of magnitude from 2.22 to 8.88 GPa, as shown in Figure 2.3 (a). For 10% clay-fluid models, it is observed that the gradual and linear decrease in interlayer spacing from 0 to 1.48 GPa is followed by a nonlinear drop in the interlayer spacing from 2.22 to 8.88 GPa. Also observed is a significant reduction in the interlayer spacing upon compression from 0 to 1.48 GPa for Na-MMT with 30% clay-fluid models, as shown in Figure 2.3 (b), followed by an abrupt and nonlinear drop in the interlayer spacing from 2.22 to 8.88 GPa.

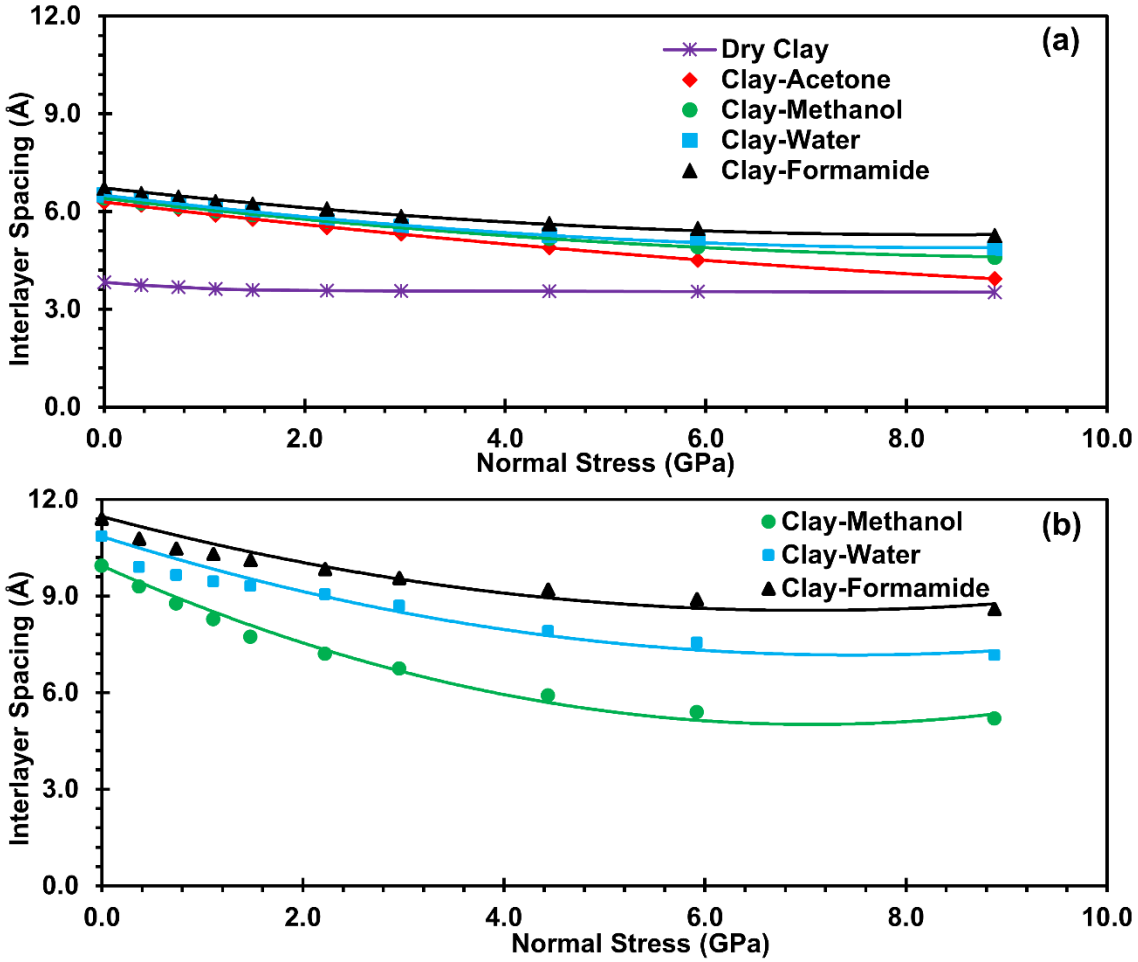

Figure 2.3 Decrease in fluid polarity for identically applied normal stress for (a) Na-MMT dry clay and clay with 10% fluid and (b) Na-MMT clay with 30% fluid.

For Na-MMT clay with 10% and 30% fluid, the compression of the interlayer volume at 8.88 GPa with respect to 0 GPa for polar fluids is significantly lower than that for medium and low polar fluids. Therefore, the interlayer strain for the polar fluids is lower than that of the medium and low polar fluids for given compressive stress at 8.88 GPa, indicating that the internal swelling pressure opposes the compression of the clay sheets. As the external stress is applied on the clay sheet, the interlayer spacing for dry clay is decreased, but the clay sheets remained the same. Interlayer spacing is dropped linearly from 3.83 Å to 3.59 Å for the stress of 0-1.48 GPa in region-I, resulting in a strain of 0.06. However, the interlayer spacing is decreased from 3.58 Å to 3.45 Å linearly and undergoes a maximum strain of 0.08 from 2.22 GPa to 8.88 GPa in region-II. Thus, two distinct stress-interlayer spacing responses are observed for regions I and II. An attempt is carried out to evaluate the interlayer modulus by using the least-squares method. The interlayer moduli for dry clay in region-I and region-II are found to be 21.39 GPa and 476.16 GPa, respectively. These values are in the same order of magnitude with our previous experimental and computational studies.(7, 29).

Figure 2.4 (a) shows the stress-strain characteristics along the swelling axis for clay with 10% fluid. For all models, the strain in region-I increases linearly to about 0.08, which is consistent with the previous SMD simulations of hydrated Na-MMT clay (28) and organically modified clay (88), where the interlayer deformation is very small in the level of stresses from 0-1.48 GPa. However, the strain in region-II is increased from 0.12 to 0.37 for clay-acetone, 0.11 to 0.28 for clay-methanol, 0.12 to 0.25 for clay-water, and 0.10 to 0.22 for clay-formamide. Figure 2.4 (b) shows the stress-strain behavior of clay with 30% fluid. In region-I from 0-1.48 GPa, the interlayer spacing yields a strain of to 0.22 for clay-methanol, 0.14 for clay-water, 0.11 for clay-formamide. From 2.22 to 8.88 GPa, the interlayer undergoes a maximum strain of 0.48 for clay-methanol, 0.34 for clay-water, and 0.25 for clay-formamide. The final interlayer strain increases with an increase in the amount of the fluid content, as well as with a decrease in the polarity of fluid. Another significant observation is that the shape of the stress-strain plots of clay with high polar fluids is considerably different from clay with medium and low polar fluids. The stress-strain plot of the medium polar fluid methanol falls between the low polar fluid acetone and high polar fluids formamide. Our previous consolidation experiments have also shown that a nonlinear response of void ratio versus effective stress for medium polar fluid lies between the low and high polar fluids, and the void ratio for Na-MMT clay with polar fluid is significantly higher than that for low polar fluid for given effective stress (17). Therefore, a profound effect of the polarity of fluid under compression of swelling clay is observed, not only at the micro-scale but also at the molecular level.

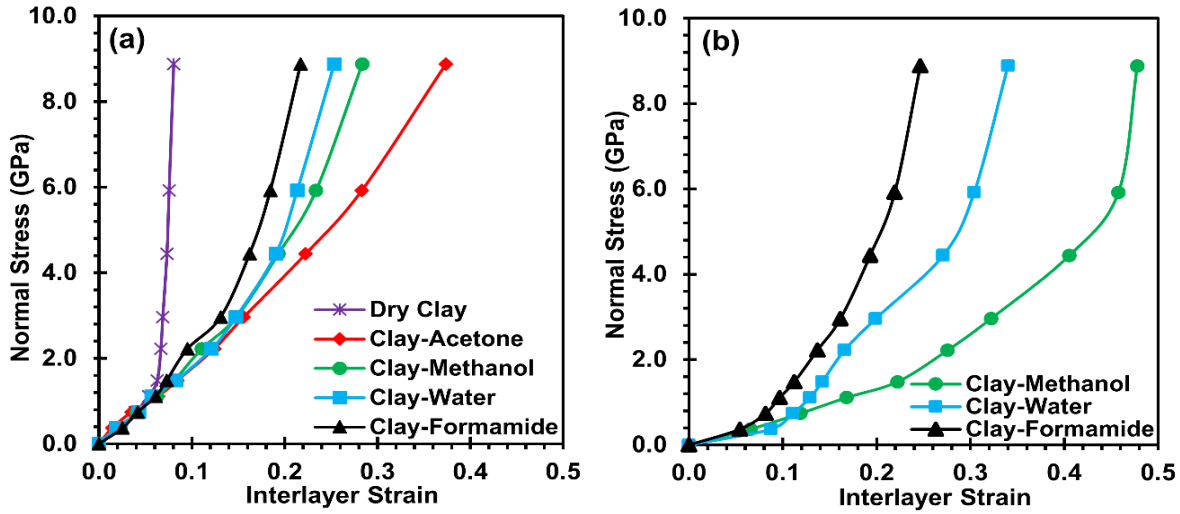

Figure 2.4 Stress versus interlayer strain for (a) dry clay and clay with 10%, (b) clay with 30% fluid

The interlayer modulus for all 10% clay-fluid models is calculated from the slope of the trend line of the stress-strain plot. The stress-strain plot for clay with all four fluids is linear with a shallow slope from 0-1.48 GPa in region-I. The interlayer moduli in this level of stress are found to be 21.39 GPa for dry clay, 18.46 GPa for clay-formamide, 18.25 GPa for clay-water, 18.03 GPa for clay-methanol, and 18.02 GPa for clay-acetone. The interlayer modulus in region-I is decreased relative to the interlayer modulus of dry clay, indicating that a soft and weak interlayer response is observed for clay-fluid models under compression as the clay layers are separated more by introducing the fluids in the clay interlayer. In region-II, the slope of the stress-strain plot is steeper for clay with polar fluid than that with low polar fluid. The interlayer moduli in region-II are 26.30 GPa, 38.05 GPa, 49.37 GPa, and 52.61 GPa for clay-acetone, clay-methanol, clay-water, and clay-formamide, respectively. Similarly, the interlayer moduli in region I and region II for Na-MMT with 30% methanol, water, and formamide are also computed. The interlayer modulus in region-I is 7.07 GPa for clay-methanol, 20.42 GPa for clay-water, and 19.18 GPa for clay-formamide. Although the magnitude of the interlayer modulus of dry clay and clay with 30% polar fluids is on the order of the same magnitude, a much softer interlayer response is observed for clay-methanol. Additionally, the interlayer moduli in region-II are 37.96 GPa for clay-methanol, 41.98 GPa for clay-water, and 69.57 GPa clay-formamide, resulting in an increase in the interlayer modulus with an increase in the fluid polarity. Similarly, the higher value of elastic modulus can be correlated with high internal swelling pressure developed within and between clay particles as high polar fluids interact with clay and offer a tremendous resistance to change in the interlayer spacing upon compression.

Figure 2.5 shows the planar view at the end of 8.88 GPa and exhibits the conformational difference of the fluid molecules in the vicinity of the sodium ions. Upon compression, the proximity of the fluid molecules around the sodium ions is increased with an increase in the polarity of the fluids, resulting in the formation of a well-organized pattern for high polar fluids. At 8.88 GPa, the oxygen atoms are attracted and oriented toward the sodium ions, suggesting a shell formation around the fluid molecules. At the end of 8.88 GPa, there are 11 of 24 acetone, 18 of 40 methanol, 31 of 64 water, and 21 of 48 formamide molecules out of the clay interlayer.

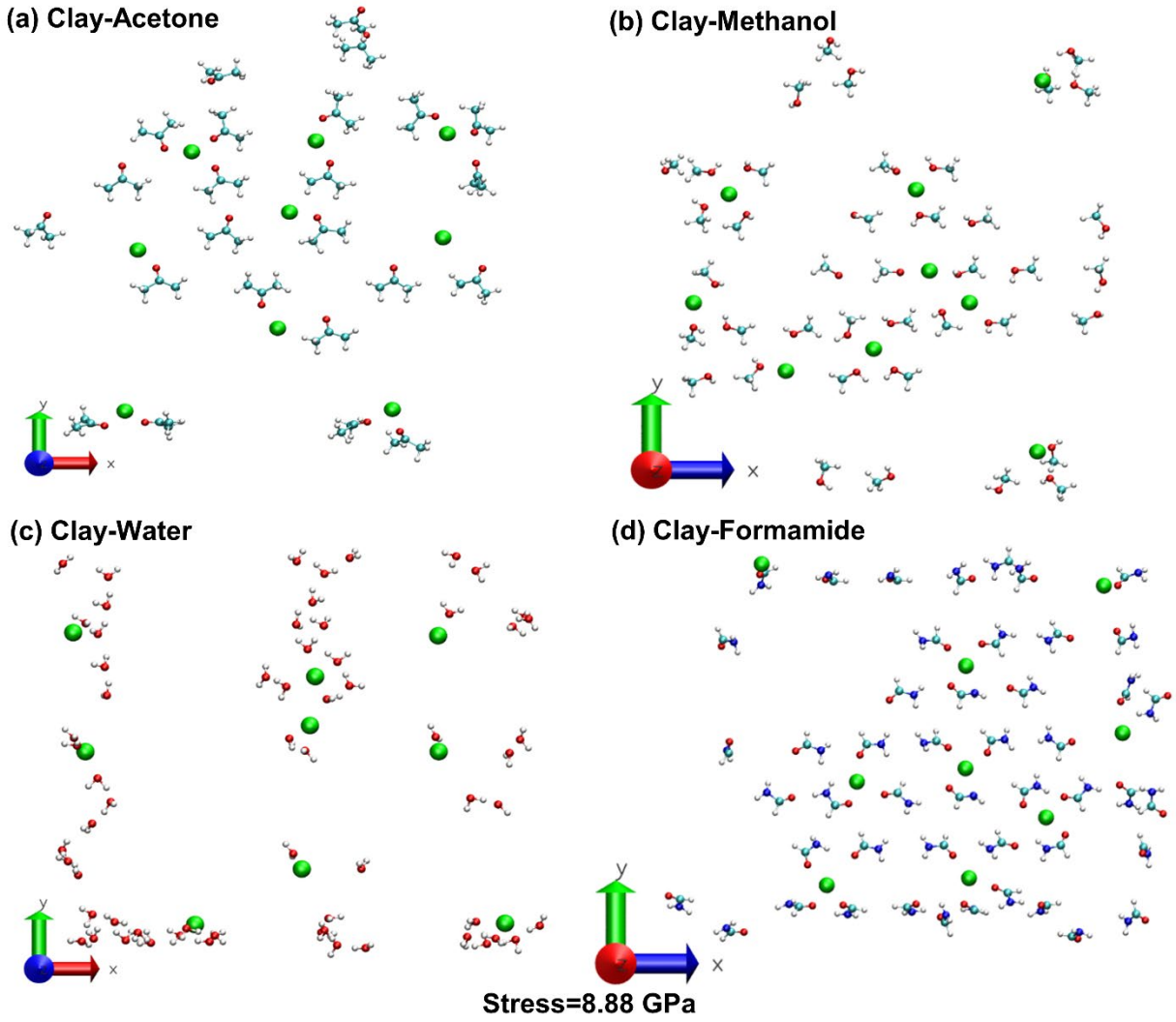

Figure 2.5 Planar view displaying the conformation of 10% fluid in proximity to sodium cations at 8.88 GPa: (a) clay-acetone, (b) clay-methanol, (c) clay-water, and (d) clay-formamide

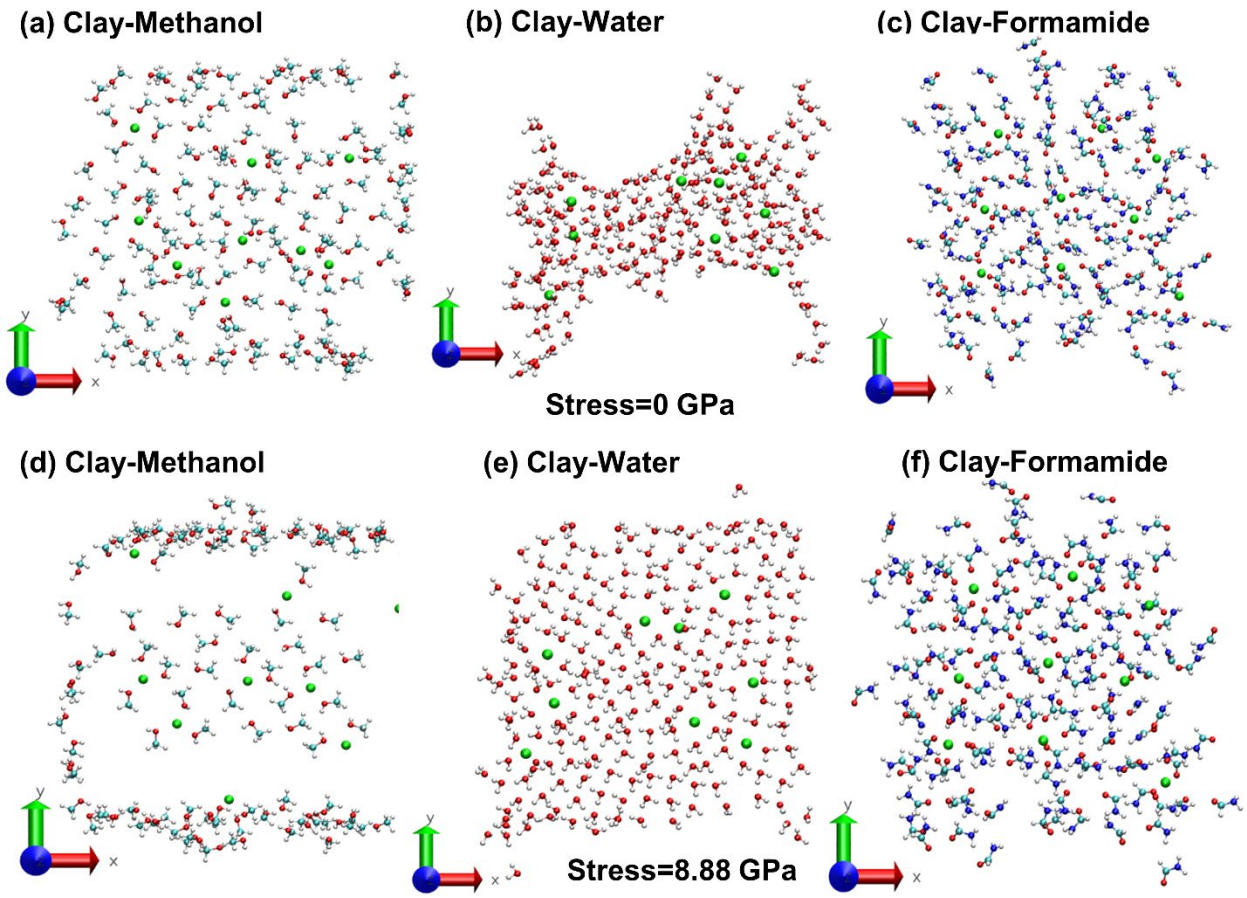

Figure 2.6 Planar view of 30% fluid around sodium cations for Na-MMT with methanol, water, and formamide at 0 GPa (a-c) and at 8.88 GPa (d-f).

Figure 2.6 (a-c) shows the hydration of the sodium ions for Na-MMT with 30% fluid at 0 GPa in XY-plane. Similarly, Figure 6 (d-f) shows the change in conformation of the fluid molecules around sodium ions at 8.88 GPa. There are 48 of 120 formamide molecules, 64 of 216 water, and 94 of 120 methanol out of the clay interlayer at 8.88 GPa. It is seen that three oxygen atoms of interlayer methanol and five oxygen atoms of water and formamide molecules are attracted and oriented to the sodium ions, resulting in the well-organized formation.

For 10% fluid content, although the fluid molecules in the interlayer remained in the single-layer before and after compression, the polar fluids formamide and water behave more like a relatively rigid layer of constant thickness relative to the low medium polar fluids. Figure 2.7 shows the conformation of 30% fluid in XZ-plane at 0 GPA and 8.88 GPa. It is observed that the two monolayers of the methanol and water at 0 GPa have been noticeably compressed to one distinct monolayer at 8.88 GPa, resulting in a sudden decrease in the thickness of the fluid molecules from 3.67 Å to 1.43 Å for methanol and from 5.25 Å to 2.74 Å for water, as shown in Figure 2.7. However, the two monolayers of the interlayer formamide molecules are compressed from 5.83 Å to 4.76 Å, which indicates that the two formamide layers have remained comparatively rigid as compared with methanol and water**.** Therefore, the total interlayer deformation upon compression is not only due to the compression of the void space between the clay sheets and fluids, but also the compression of the fluid molecules in the interlayer for clay with 30% fluid. The role of fluid polarity and the nature of the total nonbonded interactions—whether electrostatic or van der Waals—provides an insight into the molecular mechanism of the clay interlayer. The nonbonded interaction energies between clay-clay, clay-sodium, sodium-fluid, and clay-fluid for dry Na-MMT clay

and clay with 10% and 30% fluids before and after compression are presented in Table 2.1. The magnitude of the nonbonded interactions between clay sheets are approximately the same for Na-MMT clay with 10% acetone, methanol, water, and formamide at 8.88 GPa, but these interactions as compared with 0 GPa are increased by 46%, 89%, 112%, and 85% for clay-acetone, clay-methanol, clay-water, and clay-formamide, respectively. The repulsive electrostatic energy for dry clay is due to negatively charged clay sheets, and the total clay-clay interactions at 8.88 GPa is 16% less than clay-clay interactions at 0 GPa. The nature of clay-clay interactions before and after compression is predominantly attractive van der Waals energy, which maintains the structural stability of stacking of dry clay sheets, but the attractive electrostatic interactions are negligible.

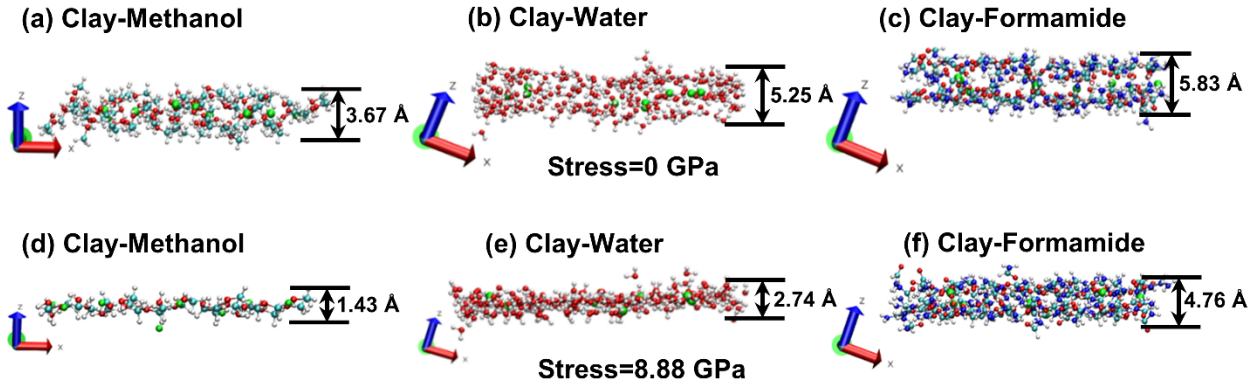

Figure 2.7 The conformation showing the thickness of 30% fluid in proximity to sodium cations for Na-MMT with methanol, water, and formamide at 0 GPa (a-c) and at 8.88 GPa (d-f)

The total attractive clay-sodium interactions at 8.88 GPa are the highest and decrease with an increase in the fluid polarity, as shown in Figure 8 (a). These interactions at 0 GP and 8.88 GPa are on the order of the same magnitude. The predominant attractive electrostatic interactions are due to negatively charged clay sheets and positively charged sodium ions. However, the nature of attractive van der Walls energy at 0 GPa results in repulsive energy at 8.88 GPa. This is due to the decrease in the distance between clay sheets and sodium ions at high stresses, and the repulsive nature of short-range van der Waals energy predominates. Although the total sodium-fluid interactions at 8.88 GPa are lower than those at 0 GPa, as shown in Table 2, the attractive interactions of the sodium ions with the fluid molecules indicate these fluid molecules are hydrated and strongly bound at 8.88 GPa. These attractive interactions are predominantly electrostatic in nature, hold the fluid molecules in proximity to the sodium ions. However, the repulsive van der Waals interactions in both cases are negligible. The total sodium-fluid interactions increased with an increase in the polarity of the fluids.

The repulsive clay-clay electrostatic interaction for clay with 10% acetone at 0 GPa is diminished almost to zero at 8.88 GPa, as shown in Table 2**.** However, the attractive electrostatic interactions of clay sheets with 10% methanol, water, and formamide at 0 GPa are decreased rapidly at 8.88 GPa, as also presented in Table 2. Another significant observation is that the attractive van der Waals interactions of clay sheets with these four fluids at 0 GPa changed dramatically to repulsive interactions at 8.88 GPa. The short-range repulsive van der Waals interactions become extremely strong because of the higher-order distance dependence. The applied external stresses push the top clay sheet in close proximity to the fluid

molecules by reducing the interlayer spacing, thus the clay sheets and fluid molecules repel each other strongly.

Table 2.1 Nonbonded interaction energies of clay-clay, clay-sodium, sodium-fluid, and clay-fluid for dry clay and clay with 10% and 30% fluid content upon compression at 0 GPa and 8.88 GPa

Fluid	Interactions	Molecular Models	Energy (kJ/mol)					
			At 0 GPa			At 8.88 GPa		
			ELE	VDW	Total	ELE	VDW	Total
10%	Clay-Clay	Dry Clay	+372	-2766	-2389	+259	-2268	-2013
		Clay-Acetone	-510	-761	-1272	-393	-1469	-1862
		Clay-Methanol	-280	-644	-925	-88	-1657	-1745
		Clay-Water	-397	-686	-1088	-8	-2301	-2310
		Clay-Formamide	-347	-707	-1050	-238	-1703	-1941
	Clay-Sodium	Dry Clay	-6456	+644	-5816	-6385	+879	-5506
		Clay-Acetone	-4188	-17	-4205	-4531	+92	-4439
		Clay-Methanol	-3305	-46	-3351	-3623	+243	-3381
		Clay-Water	-2548	-50	-2598	-3640	+343	-3293
		Clay-Formamide	-3937	-21	-3958	-4113	+310	-3803
	Sodium-Fluid	Clay-Acetone	-2084	+151	-1933	-887	+54	-833
		Clay-Methanol	-3582	+264	-3322	-2598	+184	-2414
		Clay-Water	-3724	+238	-3485	-1724	+230	-1498
		Clay-Formamide	-2519	+176	-2343	-1820	+159	-1665
	Clay-Fluid	Clay-Acetone	+54	-678	-628	+4	+1322	+1326
		Clay-Methanol	-1008	-870	-1879	-222	+1234	+1013
		Clay-Water	-431	-423	-854	-163	+920	+761
		Clay-Formamide	-736	-1251	-1992	-372	+736	+377
30%	Clay-Clay	Clay-Methanol	+29	-146	-117	-25	-1435	-1460
		Clay-Water	-222	-38	-259	-247	-745	-992
		Clay-Formamide	-155	-29	-184	-439	-209	-649
	Clay-Sodium	Clay-Methanol	-3180	-50	-3230	-4540	+197	-4343
		Clay-Water	-2297	-33	-2330	-3151	-59	-3209
		Clay-Formamide	-1761	-25	-1787	-2464	-50	-2515
	Sodium-Fluid	Clay-Methanol	-6895	+318	-6577	-2243	+255	-1987
		Clay-Water	-9586	+259	-9330	-6757	+402	-6355
		Clay-Formamide	-5983	+218	-5766	-3795	+297	-3498
	Clay-Fluids	Clay-Methanol	-4289	-2067	-6351	-113	+1100	+987
		Clay-Water	-1042	-1084	-2125	-63	-1029	-1092
		Clay-Formamide	-1234	-1849	-3084	-301	-808	-1109

ELE=Electrostatic; VDW=van der Waals; and Total=ELE+VDW=Nonbonded

The nonbonded interaction energies at 0 GPa and 8.88 GPa for Na-MMT with 30% methanol, water, and formamide are also presented in Table 2.1. The attractive clay-clay interactions, which are predominated by van der Waals energy, at 8.88 GPa, are decreased with an increase in the polarity of fluids, as shown in Figure 2.8(b). Moreover, these interactions, as compared with 0 GPa, are significantly increased by 1146%, 282%, and 252% for clay-methanol, clay-water, and clay-formamide, respectively. Similarly, the nonbonded clay-sodium interactions at 8.88 GPa are increased with an increase in the fluid polarity, and the nature of the interactions is electrostatic energy. These interactions, relative to 0 GPa, are increased by 34%, 38%, and 41% for clay-methanol, clay-water, and clay-formamide, respectively. The sodium-fluid interactions upon compression at 8.88 GPa for clay-formamide and clay-water are higher than clay-methanol. These interactions, with respect to 0 GPa, are decreased by 70%, 32%, and 39% for clay-methanol, clay-water, and clay-formamide, respectively. The attractive nonbonded clay-fluid interaction for clay with 30% methanol at 0 GPa is dramatically changed to the repulsive energy. The interaction is predominated by repulsive van der Waals energy**.** However, these attractive nonbonded clay-fluid interactions at 8.88 GPa, as compared with 0 GPa, are decreased 49% for clay-water and 64% for clay-formamide.

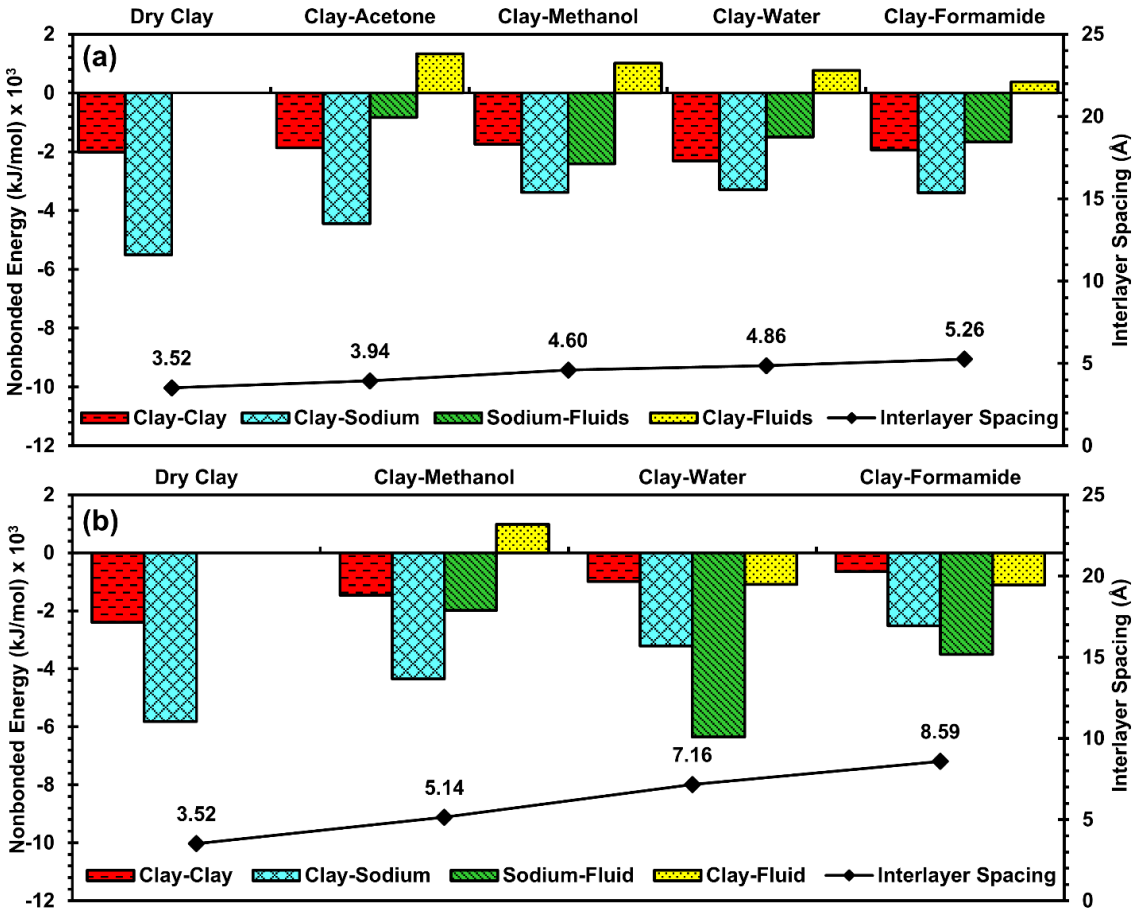

Figure 2.8 Interlayer spacing increased with the increase in the fluid polarity and the corresponding nonbonded interaction energies at 8.88 GPa of clay with (a) 10% and (b) 30% fluid

Although the clay interlayer has the same fluid content for all fluids, the interlayer spacing values have been significantly varied before and after the application of normal stress on the top of the clay sheet. When the clay interlayer spacing of dry clay is compared with that of the clay with four fluids, the interlayer spacing is increased with an increase in the fluid polarity as well as with the increase in the fluid content in the interlayer. It is also observed that the presence of the fluids in the interlayer caused the

interlayer to behave weaker in compression than dry clay. The clay-formamide model has the highest interlayer spacing because of the larger separation between clay sheets. For given normal stress, interlayer strain is significantly lower for clay with polar fluids than that of low polar fluid both for 10% and 30% fluid content, which indicates that the externally applied normal stress is more resisted by the internal swelling pressure in the interlayer for clay with polar fluids. The interlayer spacing of Na-MMT clay with 10% and 30% formamide is compressed about the same value; however, the compression of the interlayer spacing is increased when the fluid content is increased from 10% to 30% for methanol and water. Although the fluid molecules have maintained the well-organized pattern around the sodium ions, the tendency of the fluid molecules to come out of the interlayer for 30% fluid is higher than 10% fluid, and these fluid molecules are much more randomly oriented upon compression. For Na-MMT with 10% fluid, the compression of the fluid molecules with increasing stress is very small, whereas the abrupt compression of the fluid layers has occurred for 30% fluid. It can be concluded that the compression of the space between the clay sheets and fluid molecules contributes to the overall interlayer strain for Na-MMT with 10% fluid in the interlayer. However, it appears that the overall strain upon compression for Na-MMT with 30% fluid is not only due to the compression of the void space between the clay sheets but also the compression of the fluid molecules in the interlayer.

When the fluid molecules are introduced into the clay interlayer, the clay-clay and clay-sodium interactions are decreased, but the sodium-fluid and clay-fluid interactions are increased both for 10% and 30% fluid content. Thus, the fluid molecules that enter into the interlayer are the dominating factor to clay swelling. Relative to dry clay, the clay-clay interactions at 0 GPa for 10% fluid are slightly decreased, but these interactions are negligible for 30% fluid. The clay-clay interactions upon compression at 8.88 GPa are slightly decreased for dry clay, but significantly increased in the presence of the greater amount of fluids in the interlayer. As the amount of fluid molecules in the interlayer increases, the clay-sodium interactions are reduced, and these interactions have been increased upon compression. The nature of the clay-sodium interactions before and after compression is primarily attractive electrostatic energy. The clay-sodium and clay-clay interactions are reduced more with the increase in the fluid polarity. However, the sodium-fluid interactions are increased with an increase in the fluid content. This indicates that the hydration level of the sodium ions is continually augmented upon compression as well. These interactions, however, are significantly decreased upon compression.

The attractive clay-fluid interactions are further increased with an increase in fluid content. Therefore, increasing the amount of the fluid molecules not only initiates the clay swelling but maintains the intercalated clay structure as well. Under stress of 8.88 GPa, the clay-fluid interactions are rapidly changed from attractive to repulsive energy for Na-MMT with 10% acetone, methanol, water, and formamide. The attractive clay-fluid interaction before compression is dramatically changed to repulsive energy upon compression only for clay with 30% methanol, but significantly decreased for clay with 30% water and formamide. This suggests the hydration of the clay sheets also persists in the presence of the greater amount of polar fluids even upon compression.

2.5 Conclusions

In this study, steered molecular dynamics (SMD) simulation is used to quantitatively evaluate the mechanical response of the interlayer of dry Na-MMT clay and clay with 10% and 30% fluid content with a wide range of organic fluids: acetone, methanol, water, and formamide. Upon the application of normal stress ranging from 0 to 8.88 GPa to the top of the clay sheet, the interlayer spacing decreased, whereas the clay sheets remain rigid. For dry Na-MMT clay, the interlayer spacing is decreased abruptly and linearly from 0-1.48 GPa in region-I but remained approximately constant from 2.22 to 8.88 GPa in region-II. While the stress-deformation response of the clay interlayer is linear from 0-1.48 GPa, it is nonlinear from 2.22 to 8.88 GPa for clay with the increase in the fluid content in the interlayer of 10% and 30% fluids. The compression of the interlayer spacing is not only increased with an increase in the

amount of the fluid content but also with a decrease in the polarity of fluids. Furthermore, the reduction of the interlayer volume of Na-MMT clay decreases with increases in the polarity of the fluids. Although the interlayer moduli of the clay-fluid models are on the order of the same magnitude in low normal stress of region-I, a softer interlayer response, as compared with that of dry clay interlayer, is observed when the more fluid molecules are introduced in the clay interlayer. Thus, the clay with polar fluid is much stiffer than clay with low and medium polar fluids. Although a well-organized pattern of the fluid molecules around the sodium ions is observed, the number and volume of the fluid molecules coming out of the interlayer upon compression for clay with 30% fluid are greater than clay with 10% fluid. An abrupt compression of the thickness of the fluid layers is only observed for clay with 30% fluid, and the compression of the layers is increased with a decrease in the fluid polarity.

Upon compression, the clay-clay interactions are increased for dry clay as well as with an increase in the fluid content in the interlayer, and these interactions are mostly dominated by van der Waals energy. The attractive clay-sodium interactions upon compression are increased relative to that of interactions before applying stresses. These interactions are predominated by electrostatic energy before and after compression. The attractive clay-fluid interactions are increased when increasing the number of fluid molecules in the interlayer. Conversely, these interactions are decreased upon compression, and the nature of the interactions are also electrostatic in nature before and after compression. Furthermore, the attractive clay-fluid interactions are increased when the fluid content is increased, which indicates that the presence of more fluids in the interlayer initiates the clay swelling and retains the structures of the clays sheets. For Na-MMT clay with 10% acetone, methanol, water, and formamide, the nature of attractive clay-fluid interactions are changed to the repulsive interactions upon compression. The attractive nature of clay-fluid interaction for Na-MMT with 30% methanol is changed to repulsive upon compression; whereas, the clay-fluid interactions for Na-MMT clay with 30% water and formamide have remained attractive. This indicates that the hydration of the clay sheets upon compression continues when the more polar fluid molecules are present in the interlayer.

Therefore, the major components that influence the overall compressibility of the interlayer of swelling clays are the compression of the distance between the clay sheets and fluid molecules, the number and volume of fluid molecules coming out of the interlayer, the polarity of the fluids, and nonbonded interactions among clay sheets, sodium ions, and fluid molecules. The results from this study provide a framework for the development of multiscale modeling for swelling clays and reliable prediction of the shear failure mechanism by taking into account the clay-fluid interactions, which are not only essential for effective analysis and design of civil infrastructures but also for enhancing the public safety in areas with swelling clay.

3. MOLECULAR DYNAMICS SIMULATIONS OF CLAY TACTOID

This section is presented verbatim from our publication under preparation.

3.1 Background

Reactive soil has always been a great topic of interest among researchers. It undergoes significant change in shape and structure due to its exposure to specific physical or geological conditions. Among the available three types of reactive soils (expansive, collapsible, and chemically reactive), expansive soil is the most predominant in the United States and Canada. Structural changes of expansive soil following the variation in moisture content affects the infrastructural economy by causing damage to buildings, foundations, highways, dams, etc. Highly active montmorillonite (MMT) clay minerals constitute a large portion of expansive soil. MMT swells significantly upon reaction with water. If the swelling is allowed to occur, then MMT can expand up to 15 times its original volume. However, if the swelling is constrained, it exerts a large amount of swelling pressure (89, 90). MMT, as a swelling clay mineral, also finds its beneficial application in geotechnical and geoenvironmental engineering, polymer clay nanocomposites, and in the pharmaceutical, cosmetics, and petroleum industries.

MMT clay mineral is a member of the smectite group. Clay mineral can be defined as a fine-grained, earthy, natural material that exhibits plasticity when water is added to it (91). Smectite belongs to the aluminum phyllosilicate group, a varying combination of tetrahedral silica sheet (t) and octahedral alumina sheet (o). Sodium Montmorillonite (Na-MMT) is a 2:1 (T-O-T) phyllosilicate with an alumina octahedral sheet sandwiched between two silica tetrahedral sheets (92, 93). Isomorphous substitution of aluminum ions from the octahedral sheet causes the development of negative charge generally balanced by interlayer cations (Na, K, Ca, and Cs).

The swelling of Na-MMT clay minerals is characterized by structural changes both in nanoscale and microscale. Clay interlayer space increases with an increasing amount of hydration in the nanometer dimension (31). Breakdown of Na-MMT particle occurs during swelling in the micrometer level (13). Discrete element modeling (DEM) studies on swelling clays provided the evidence of particle breakdown (69). In order to bridge the gap of swelling behavior in nanoscale and microscale, it is primarily essential to model the MMT structure in both levels. According to a handful of earlier studies, Na-MMT clay is considered to possess a hierarchical structure from different viewpoints. Investigation of clay porosities through SEM, SAXS, XRD, and MIP referred to three sizes of porosity, i.e., interlayer porosity, inter-particle porosity, and inter-aggregate porosity (57, 94-97). Analysis of the difference between hydration of clay-rich material and hydration of porous granular material led to the exploration of the multiscale structure of clays (98-102). This multiscale structure consists of the microscopic scale (T-O-T layer), mesoscopic scale (stacks of T-O-T layers) and macroscopic scale (random combination of stacks). The hierarchical structure of smectite (layer, particle, single aggregate, multiple aggregates) was also described to define its different hydration sites as a function of scale (103). Thermoporometric study of mesoscopic swelling of Na-MMT clay mineral also referred to its stratified architecture (104, 105). Unit clay layer (T-O-T) of Na-MMT clay mineral does not exist separately at standard condition. Several unit clay layers stay together by forming a stack along Z direction. This stack is termed as clay tactoid. Previous X-ray diffraction studies showed the formation of Na-Mt clay tactoids containing ten clay layers stacked to each other in Z axis (106). Clay tactoid also behaves as the primary clay particle which forms aggregates upon different gathering orientation.

Molecular dynamics (MD) simulation has long been utilized by the researchers to investigate different properties (molecular interactions, hydration) of clay minerals as it forecasts the behavior of molecular systems (20-22, 39, 107, 108). Steered molecular dynamics (SMD), a special plugin of MD package, was utilized to explore the mechanical properties of Na-MMT clay mineral (28, 29, 41, 109). Interactions of

different fluid molecules with clay layer were also studied using MD to observe the effect of different fluid polarity (1, 110). Swelling of Na-MMT clay mineral is governed by the swelling of interlayer space inside Na-MMT clay tactoids (103). Therefore modeling the properties of Na-MMT clay tactoid will provide an insight into different behaviors of the clay mineral, including the swelling mechanism. The present study seeks to investigate the molecular interactions and mechanical properties of Na- MMT clay tactoid by using both MD and SMD.

3.2 Construction of the Tactoid Molecular Model

The Katti research group performed various experimental and modeling studies on Na-MMT clay minerals (SWy-2) collected from the clay mineral repository at the University of Missouri, Columbia [7, 31, 32]. Though the actual chemical formula of this Na-MMT is $(Ca_{0.12}Na_{0.32}K_{0.05})[Al_{3.01}(III)_{0.41}Mn_{0.01}Mg_{0.54}Ti_{0.02}][Si_{7.98}Al_{0.02}]O_{20}(OH)_4$ (111), the simplified version of the formula, $NaSi_{16}(Al_6FeMg)O_{20}(OH)_4$, has been utilized for model construction. Previously proposed coordinates (112) and partial charges (21) have also been employed. Isomorphous substitution takes place in the octahedral sheet (o) as one of every four Al^{3+} ions is replaced by Mg^{2+} and Fe^{3+} ions. Development of negative charge in the clay layer due to isomorphic substitution is balanced by introducing interlayer Na cation.

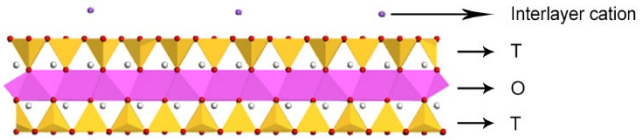

Figure 3.1 Molecular model of a single Na-MMT clay layer

The present study will to utilize an Na-MMT 6×3 clay model as used by previous studies (1, 77, 110). The clay layer unit cell dimensions are 5.28 Å×9.14 Å×6.56 Å. Therefore, the initial overall dimensions of a single 6×3 Na-MMT clay layer (T-O-T) are 31.68 Å×27.44 Å×6.56 Å. The initial interlayer space is considered to be 3.44 Å, which gives the initial d-value as 10 Å. Each 6×3 clay layer contains 720 atoms. As isomorphic substitution generates a charge of -0.5e in each unit cell, nine interlayer Na cations are introduced in the interlayer space to balance the charge of the 6×3 clay model. For building the Na-MMT clay tactoid model, 10 6×3 clay layers are stacked on top of each other in the Z direction. These 10 layers will be termed as B, C, D, E, F, G, H, I, J, and K layer, respectively, from bottom to top along the Z-axis. Therefore, the Na-MMT clay tactoid model can also be described as a 6×3×10 clay model. This orientation consists of nine interlayer spaces. Hence, the final vertical (Z) dimension of the Na-MMT clay tactoid will be 96.56 Å, the summation of the thickness of 10 clay layers (10×6.56 Å) and nine interlayer spaces (9×3.44 Å). The overall dimensions of the Na-MMT clay tactoid (6×3×10- model) are 31.68 Å×27.44 Å × 96.56 Å. Each interlayer space contains nine Na cations. Thus, the whole Na-MMT clay tactoid system consists of 7,281 atoms (7,200 clay atoms and 81 interlayer Na cations). Materials Studio 7.0 was used to build the Na-MMT clay tactoid model.

The Na-MMT clay tactoid has been parameterized using a CHARMm (Chemistry at HARvard Macromolecular Mechanics) force field (113). It contains a set of functions and associated constants to describe the energy expression of a molecular system. Consistent force field (CFF) parameters of Na-MMT clay developed in an earlier study (21) were converted to the CHARMm force field (28, 29, 109).

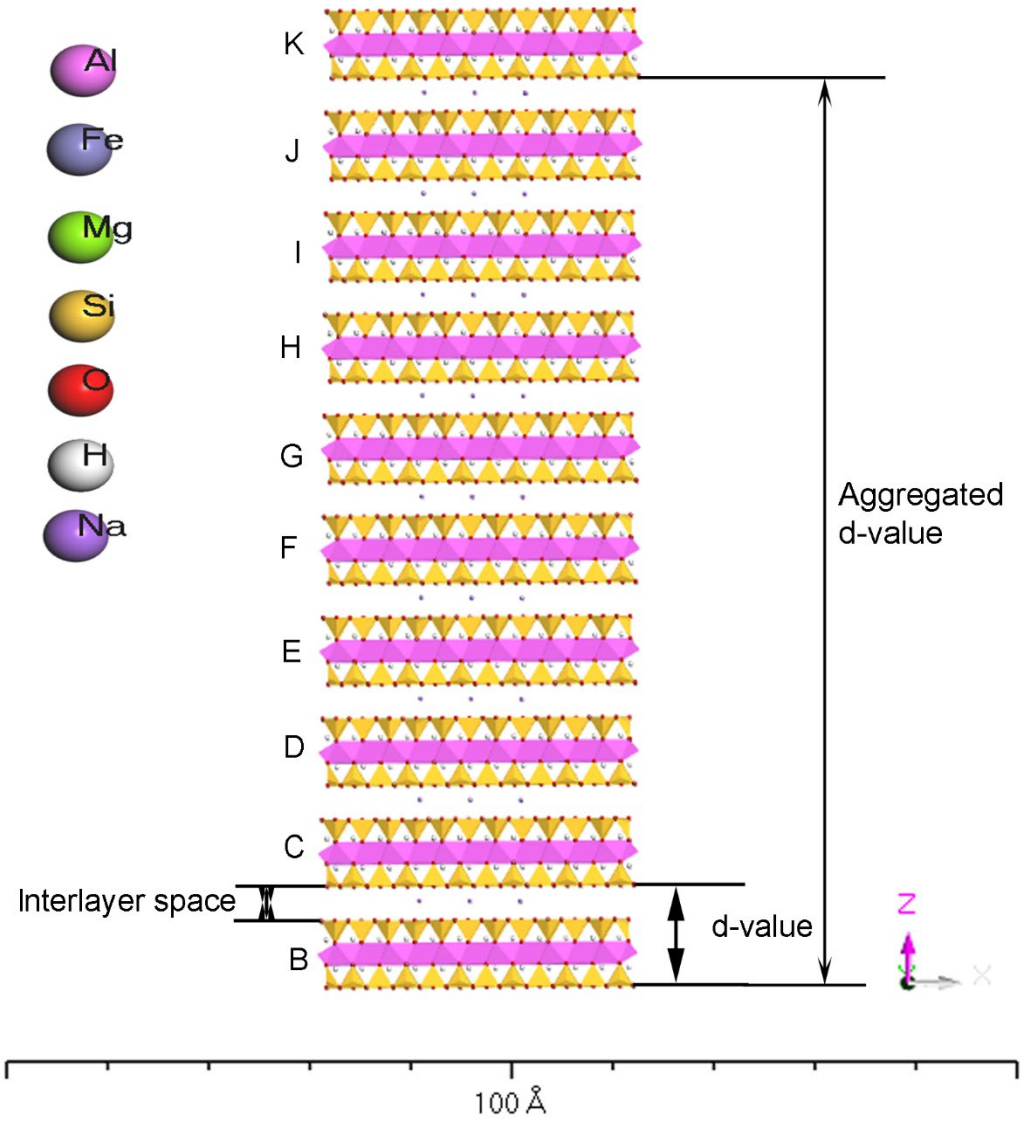

Figure 3.2 Molecular model of Na-MMT tactoid

3.3 Simulations Description

Both molecular dynamics (MD) and steered molecular dynamics (SMD) simulations of Na-MMT clay tactoid have been performed using NAMD 2.12 (47). NAMD was developed by the Theoretical and Computational Biophysics Group in the Beckman Institute for Advanced Science and Technology at the University of Illinois at Urbana-Champaign. All the simulations have been run on the Center for Computationally Assisted Science and Technology (CCAST), a parallel computing facility at North Dakota State University. All the simulations were executed using 1 node and 20 Intel Xeon 2.5GHz processors with 15GB DDR3 RAM at 1866 MHz.

The Na-MMT tactoid model was minimized at the beginning at vacuum condition (0 K temperature and 0 bar pressure) using a conjugate gradient method (114). Then the model was brought into normal temperature (300 K) and pressure (1.01325 bar) condition in a stepwise approach. The equilibrated Na-

MMT tactoid model was utilized to explore its mechanical properties. The compression behavior of tactoid was investigated by applying different magnitudes of opposing forces on the top clay layer (layer K) by keeping the bottom clay layer (layer B) fixed. The forces applied were 0, 25, 50, 75, 100, 150, 200, 250, 300, 400, 500, 600, 700, 800, 900, 1000, 1100, 1200, 1300, 1400, 1500, 1600, 1700, 1800, 1900, 2000, 2100, 2200, 2300, 2400, and 2500 pN, respectively (equivalent to stresses of 0, 0.37, 0.74, 1.11, 1.48, 2.22, 2.96, 3.70, 4.44, 5.92, 7.40, 8.88, 10.36, 11.84, 13.32, 14.80, 16.28, 17.76, 19.24, 20.72, 22.2, 23.68, 25.16, 26.64, 28.12, 29.60, 31.08, 32.56, 34.04, 35.52, and 37 GPa, respectively). Constant force SMD was used to apply these forces on the Na-MMT clay tactoid. The d-values of tactoid were measured after these constant-force SMD simulations reached equilibrium. The shearing behavior of the Na-MMT tactoid was also studied using constant-velocity SMD (k=9, v=0.0002 Å/time-step). We applied force on the surface of the top clay layer (K) along the X-direction. We measured the required force to completely deform the tactoid along the X-axis.

3.4 Results and Discussion

The equilibrated Na-Mt tactoid model after 2 ns of simulation at NTP condition (300K and 1.01325 bar) was seen to tilt along the horizontal axis (X-axis). However, this incident did not impact the parallelism of clay layers inside the tactoid. The initial and final distance between the bottom (B) and top (K) clay layers (aggregated d-value) was measured as 90 Å and 97.2 Å, respectively.

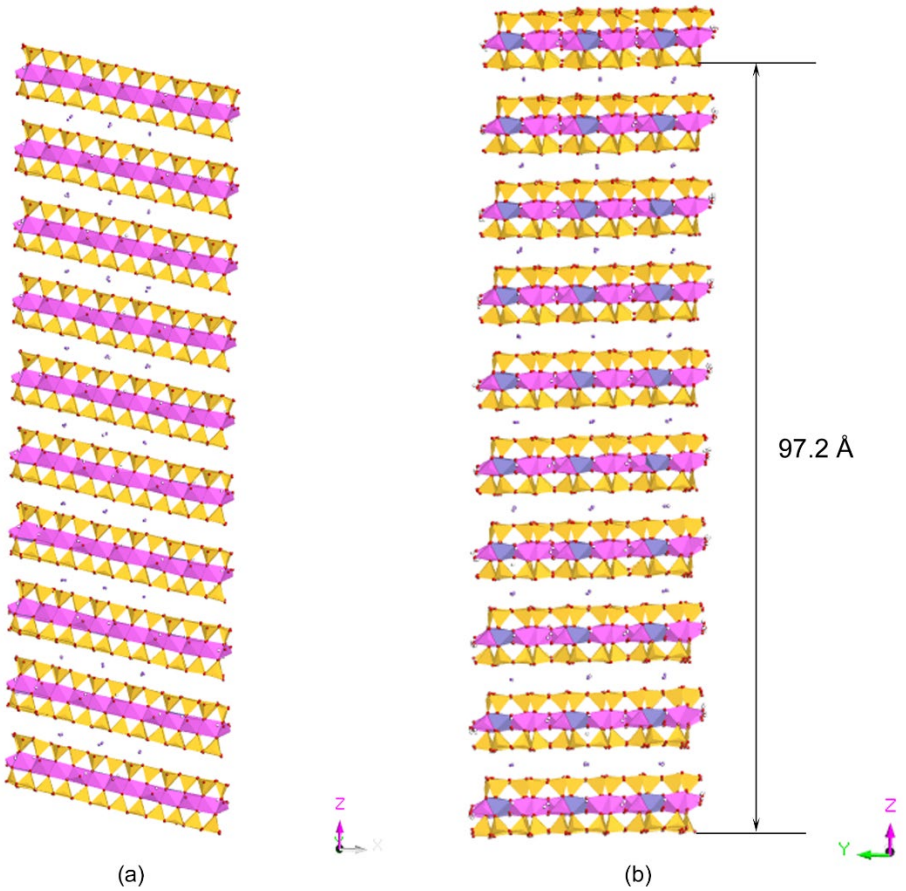

Figure 3.3 Equilibrated model of Na-MMT tactoid from two different directions

Table 3.1 Computed d-values between clay layers inside Na-MMT tactoid

Clay-layer pair	Equilibrated d-value (Å)
B-C	10.79
C-D	10.79
D-E	10.80
E-F	10.80
F-G	10.80
G-H	10.79
H-I	10.80
I-J	10.80
J-K	10.79

Table 3.1 exhibits the d-values between each pair of clay layers at an equilibrium condition. The average of these d-values is 10.795 Å (≈10.80 Å). Previous experimental and modeling studies validated these calculated d-values (31, 41, 50). The similarity in d-values proved the parallelism of clay layers inside the tactoid. Nonbonded interaction energies were calculated for clay layers inside the Na-MMT tactoid. Nonbonded interaction consists of electrostatic and Van der Waals interactions. Positive and negative values of interaction refer to repulsive and attractive interactions accordingly. Nonbonded energies between each pair of clay layers are represented in Table 3.2.

Table 3.2 Nonbonded energies (kJ/mol) acting between clay layers in Na-MMT tactoid

Clay-layer pair	Electrostatic (kJ/mol)	VDW (kJ/mol)	Nonbonded (kJ/mol)
B-C	751	-2597	-1846
C-D	750	-2596	-1846
D-E	752	-2597	-1845
E-F	746	-2599	-1853
F-G	745	-2599	-1854
G-H	745	-2600	-1855
H-I	744	-2601	-1857
I-J	743	-2602	-1859
J-K	761	-2603	-1842

The clay layers in the tactoid attracted each other with an equal amount of energies. The average value of Van der Waals energy (-2599 kJ/mol) was found to be 247% greater than average electrostatic energy (749 kJ/mol).

Nonbonded energy was also computed for each clay layer to identify its interactions with interlayer Na cations in the Na-MMT tactoid. We found that all the clay layers except the top (K) and bottom (B) layer interacted with interlayer cations with a similar order of magnitude. The interaction energies of interlayer Na cations with top and bottom clay layers were almost one-half of the interactions with the remaining clay layers. This energy discrepancy occurred because the top and bottom clay layers contained Na cations just on one side while the other clay layers contained cations on both sides. The attractive electrostatic energy was much higher than the repulsive Van der Waals energy in these Na-clay layer interactions. The Na-clay layer interaction energies are given in Table 3.3.

Table 3.3 Na-clay layer interaction energy in Na-MMT tactoid

Clay-layer	Electrostatic (kJ/mol)	VDW (kJ/mol)	Nonbonded (kJ/mol)
B	-3881	89	-3792
C	-6397	43	-6354
D	-6679	55	-6624
E	-6694	56	-6638
F	-6693	55	-6638
G	-6694	54	-6640
H	-6689	54	-6635
I	-6665	50	-6615
J	-6341	34	-6307
K	-3585	92	-3493

The binding energy of a single clay layer to its tactoid can be described as the total nonbonded attractive energy acting between the clay layer and rest of the tactoid (other clay layers and interlayer cations). Binding energy reflects how strongly a clay layer is bonded to the tactoid.

Table 3.4 Binding energy of each clay layer to tactoid

Clay-layer	Electrostatic (kJ/mol)	VDW (kJ/mol)	Nonbonded (kJ/mol)
B	-3140	-2511	- 5651
C	-5200	-5145	-10345
D	-5200	-5145	-10345
E	-5219	-5147	-10366
F	-5227	-5150	-10377
G	-5230	-5152	-10382
H	-5227	-5154	-10381
I	-5208	-5159	-10367
J	-4851	-5174	-10025
K	-2842	-2515	-5357

The calculated binding energies of the top (K) and bottom (B) clay layers were almost 53% of the binding energies of remaining clay layers (Table 3.4). This behavior can be attributed to the nature of interlayer cation and clay layer interactions. Electrostatic and Van der Waals energies contributed on the same order of magnitude to the binding energies of clay layers. Both of them imparted attractive interactions. The total attractive interaction between interlayer cations and all the clay layers was -59738 kJ/mol.
The response of the Na-MMT tactoid under an increasing amount of compression has been observed in the present study. Significant changes occurred in interlayer spaces of tactoid due to application of compressive stresses. Changes in clay layer thickness were considered minimal. The relationship between compressive stress and equilibrated distance between the top and bottom layer of tactoid is shown in Figure 3.4. The distance between the top and bottom layers of tactoid was measured by tracking the bottom oxygen atoms of the layers. This distance is also termed as “aggregated d-value” of tactoid, as it is the aggregate of all d-values inside the tactoid.

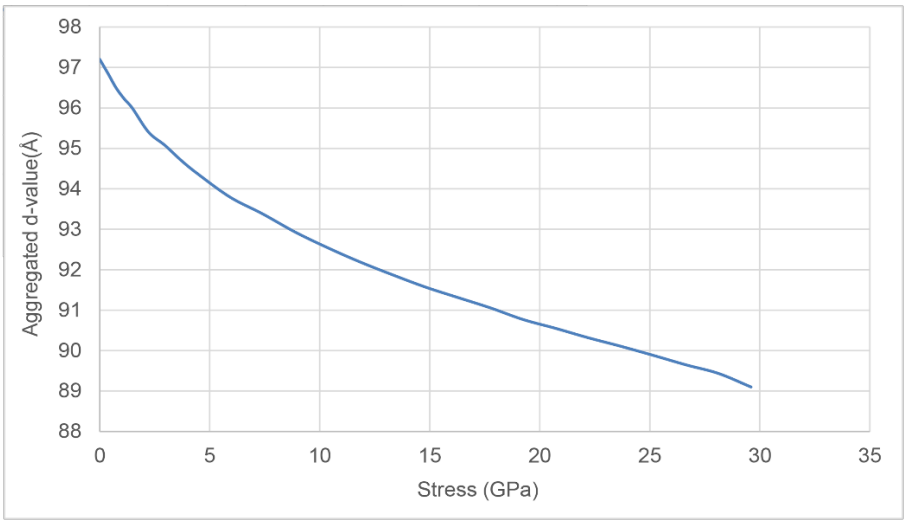

Figure 3.4 Applied stress vs. aggregated d-value of equilibrated Na-MMT tactoid

With the increasing amount of stress, the aggregated d-value of Na-MMT tactoid decreased. This occurrence was caused by the decrement of d-values between each pair of clay layers inside the tactoid. The apparent non-linear relationship between stress and aggregated d-value of the tactoid was a combination of two different linear relationships. The equilibrated aggregated d-value of Na-MMT tactoid under the compression of 0 GPa was 97.2 Å. As the applied stress was increased from 0 GPa to 2.96 GPa, the aggregated d-value decreased from 97.2 Å to 95.08 Å. As the compression was increased from 2.96 GPa to 3.70 GPa and so on, the earlier linear relationship between stress and aggregated d-value started changing and eventually transformed into a new one. Following the new relationship, the Na-MMT tactoid was able to withstand up to 29.6 GPa of stress with an aggregated d-value of 89.10 Å.

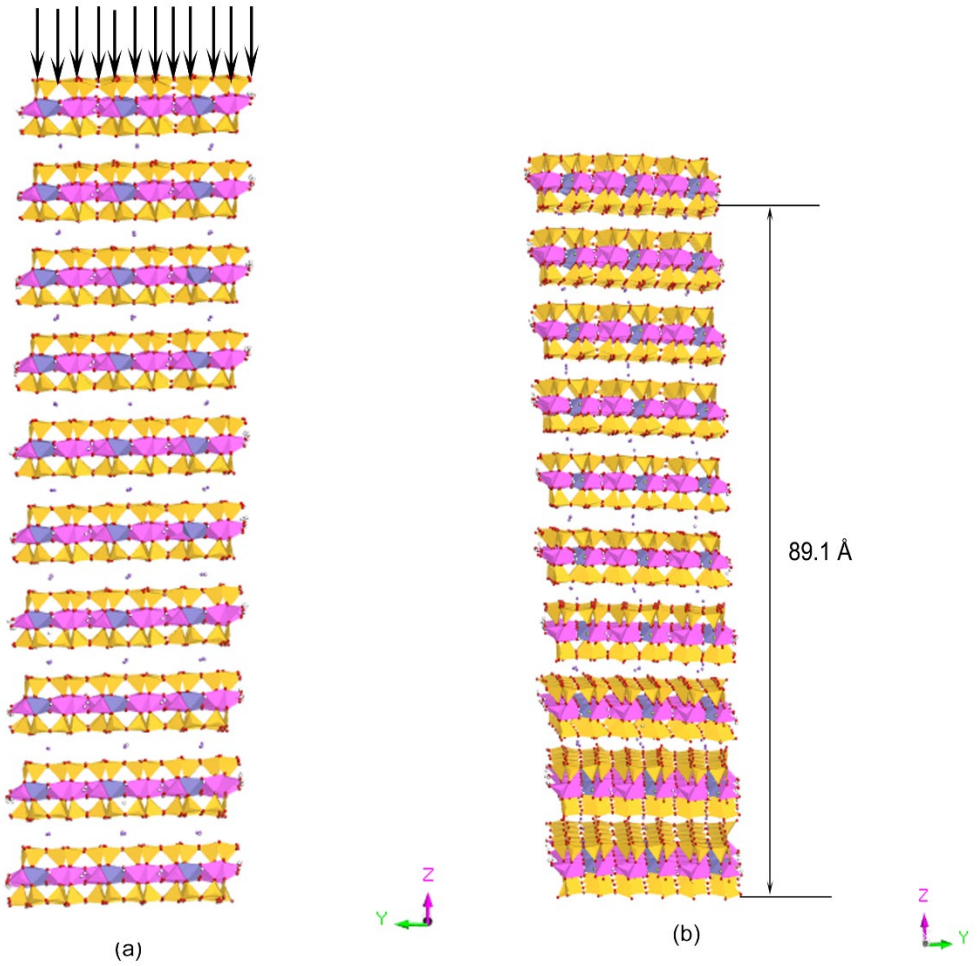

Figure 3.5 Compression of equilibrated Na-Mt tactoid at 29.6 GPa (a) initial and (b) final condition.

The Na-MMT tactoid became unstable beyond this stress as the interlayer space collapsed. The Na-MMT tactoid can be deformed, at most, about 8.1 Å under compression without collapsing the interlayer space. Table 3.5 represents the d-values between each pair of clay layers inside the Na-MMT tactoid under 29.6 GPa of compression.

Table 3.5 Calculated d-values between clay layers inside Na-Mt tactoid under 29.6 GPa stress

Clay-layer pair	Equilibrated d-value (Å) under 29.6 GPa
B-C	10.02
C-D	9.95
D-E	9.94
E-F	9.91
F-G	9.89
G-H	9.87
H-I	9.87
I-J	9.86
J-K	9.84

We can get a clear understanding of how the d-values inside the Na-MMT tactoid changed under compressive stress from the above-stated table. The top clay layers (H, I, J, and K) contained lower d-values while the bottom clay layers (B, C, D, and E) contained higher d-values. Hence the top portion of the tactoid became deformed more than the bottom portion of the tactoid due to compression. The maximum compression behavior of the Na-MMT tactoid was observed to be dependent upon the Van der Waals radii of tetrahedral oxygen atoms of clay layers. During compression of the tactoid, interlayer Na cations occupied the ditrigonal cavities of clay layers. The Van der Waals radii of tetrahedral oxygen atoms on both sides of the interlayer spaces were found to be 1.6 Å. The effective interlayer space subtracting the VDW radii of tetrahedral oxygen atoms was computed as 0.95 Å between the clay layers.

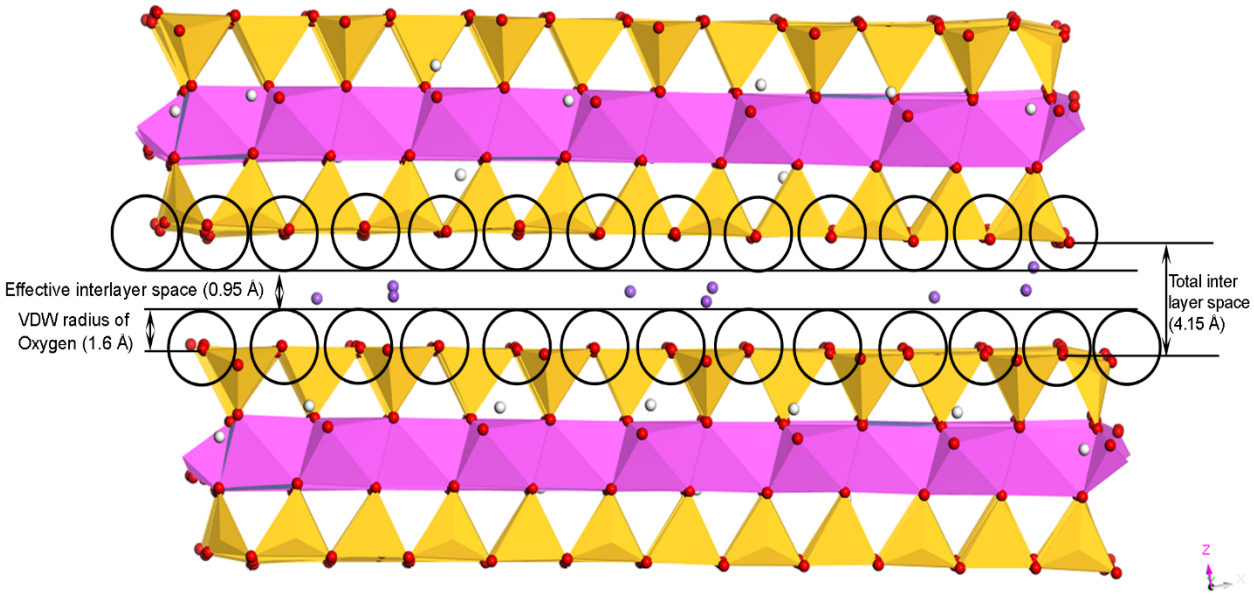

Figure 3.6 Effective interlayer space of Na- MMT clay model

The compression of the Na-MMT tactoid squeezed the interlayer spaces rather than shrinking the clay layers. The maximum possible reduction in interlayer space due to compression is equal to the magnitude of effective interlayer space (0.95 Å). Any significant reduction beyond this effective interlayer space (almost 8.1 Å reduction in aggregated d-value as there are nine interlayer spaces in the tactoid) caused the structural collapse of the tactoid.

The shearing of the Na-MMT tactoid was performed by pushing the topmost clay layer (K) along the horizontal direction to investigate its shear strength behavior. The top clay layer (K) started to move in the horizontal direction as soon as it was pushed. During the displacement of the top clay layer (K), other clay layers, along with the interlayer cations (from top to bottom), were gradually shifted toward the horizontal direction. The bottom-most layer (B) did not move as it was kept stationary. The migration of the clay layers and interlayer cations had continued until the Na-MMT tactoid was fully sheared (deformed). Further pushing beyond this stage caused the separation of the topmost clay layer (K) from the rest of the sheared tactoid.

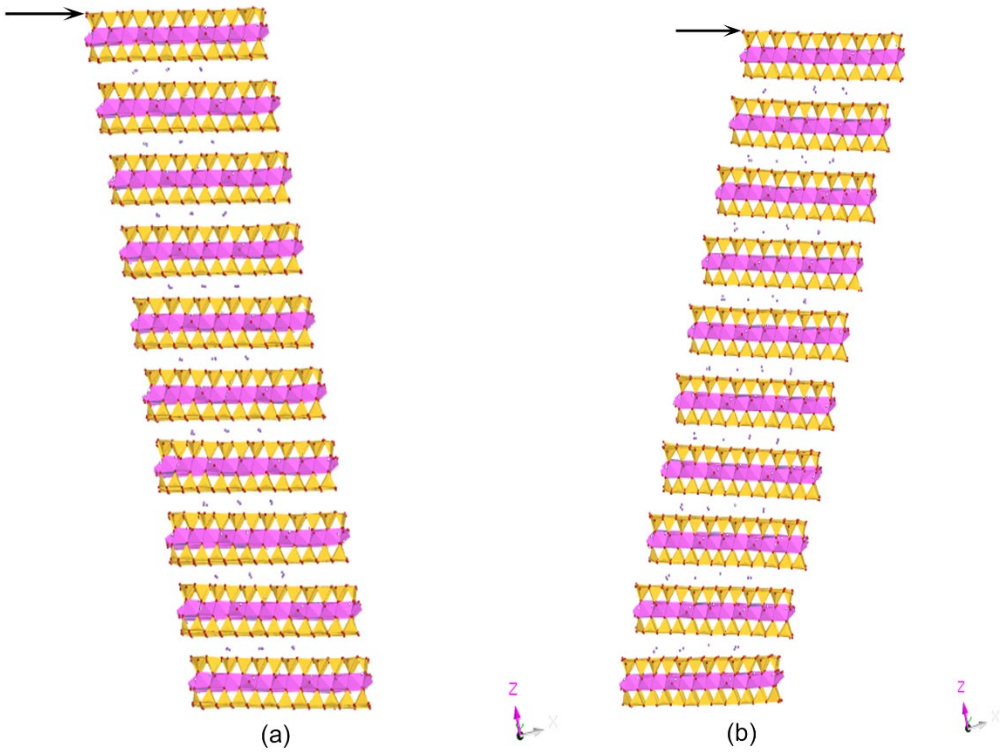

Figure 3.7 Shearing of individual Na-Mt tactoid (a) initial and (b) final condition (fully sheared)

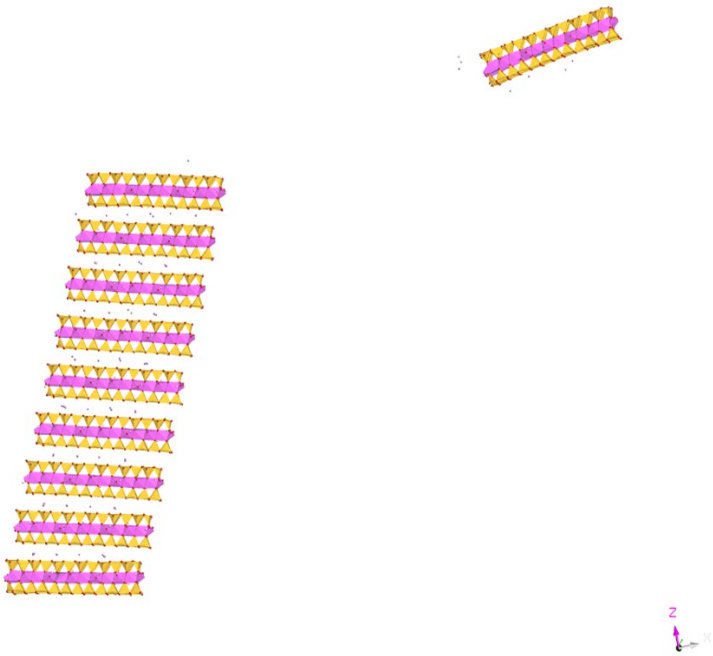

Figure 3.8 Separation of top clay layer from fully sheared tactoid due to further shearing

The shear stress-displacement curve of the Na-MMT tactoid also indicated this incident. The topmost clay layer, along with the other clay layers, were displaced linearly until the total shearing of the tactoid. Then the sudden steep increase of shear stress (maximum 6.87 GPa) referred to the further pushing of the top layer of the fully sheared tactoid. Finally, the reduction in stress was specified by the separation of the

top (K) layer from the remaining tactoid. A linear displacement profile for clay layers has been observed as the displacement of clay layers successively increased from bottom to top along the tactoid. The second most bottom layer (C) moved by 5.26 Å in the horizontal direction while the topmost layer (K) moved by 47.95 Å upon the total shearing of the tactoid. The Na-MMT tactoid was deformed by 28.34° in the horizontal direction due to the application of shear stress.

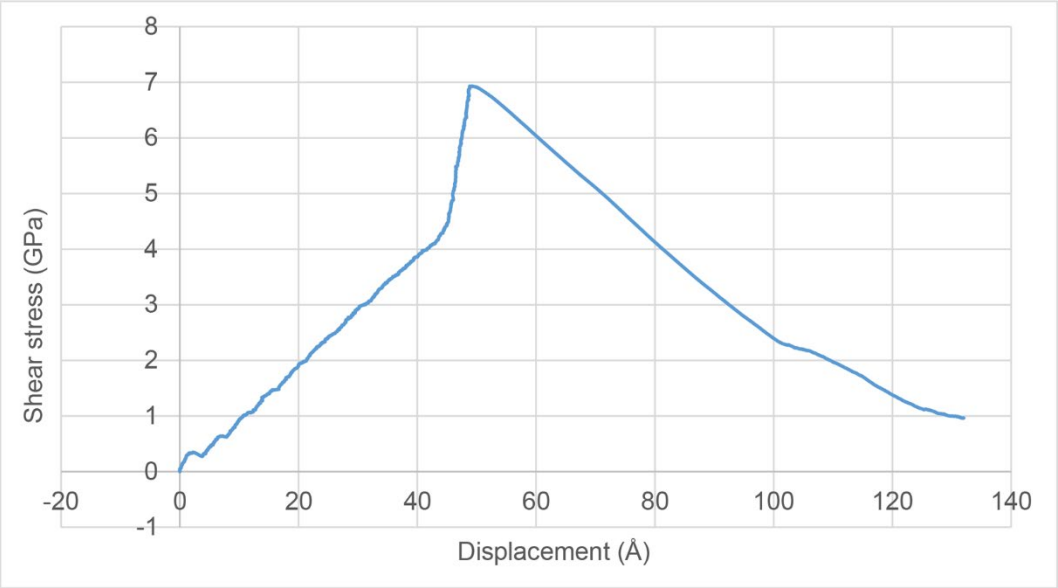

Figure 3.9 Shear stress vs. displacement of top clay layer due to shear stress application on tactoid

3.5 Conclusions

In the present study, a molecular model of the Na-MMT tactoid has been developed based on the hierarchical structure of clays. Molecular dynamics (MD) simulations have been performed to study the different features of an equilibrated tactoid in terms of energy. Steered molecular dynamics (SMD), a plugin of NAMD, was utilized to investigate the mechanical response of the Na-MMT tactoid under external loading conditions. The key findings of the current study are summarized below:

1) The mean d-value of equilibrated Na-MMT tactoid is 10.80 Å with an aggregated d-value of 97.20 Å.
2) In equilibrated Na-MMT tactoid at NTP condition, pairwise nonbonded interactions between the clay layers are attractive in nature having an average of -1850 kJ/mol. Attractive Van der Waals interactions dominate over the repulsive electrostatic interactions between the clay layers.
3) Clay layers of tactoid interact attractively with interlayer sodium cations. The nonbonded interactions between the interlayer cations and boundary clay layers (B and K) are almost one-half the interactions between cations and other clay layers.
4) The attractive nonbonded interaction between a clay layer and the rest of the tactoid is the binding energy of that clay layer. The binding energies of boundary (top and bottom) clay layers are almost 50% compared with the other clay layers. Electrostatic and Van der Waals interactions equally contribute to the binding energy of clay layers.
5) The maximum compressive stress that the Na-MMT tactoid model can withstand is 29.6 GPa. The aggregated d-value decreased from 97.20 Å to 89.10 Å under this compressive stress.
6) The compressive stresses deform the interlayer spaces rather than the clay layers. No interlayer space can be compressed by more 0.95 Å as it is the effective interlayer space excluding the Van der Waals radius of tetrahedral oxygen atoms.
7) The maximum applicable shear stress before detaching the top clay layer from the tactoid is 6.87 GPa. Upon the application of this stress, the Na-MMT tactoid is deformed by 28.34° in the horizontal direction.

4. MOLECULAR DYNAMICS SIMULATIONS OF CLAY AGGREGATE

This section is presented verbatim from our publication under preparation.

4.1 Background

Montmorillonite clay mineral swells upon the adsorption of water. It falls within the smectite group, which is a 2:1 aluminum phyllosilicate. Isomorphous substitution is attributed to the negatively charged montmorillonite clay sheets. Different alkaline cations minimize the negative charge of the clay sheets by occupying the interlayer space between them. Sodium-montmorillonite is a significant constituent of reactive soils found in different parts of the world (89, 90). Due to its swelling behavior, it is extensively used as barrier materials in landfill liners and in the petroleum industry. Pharmaceutical, cosmetics and geotechnical applications of clay minerals are also of significant importance. It is essential to have a clear idea about the clay particle structure to unravel its different properties.

Different researchers have reported various aspects of clay structure by observing its swelling mechanism. Clay layer is the primary building block of montmorillonite clay minerals in which one octahedral alumina sheet is sandwiched between two tetrahedral silica sheets (92, 93). Clay tactoid is considered the basic clay particle as the individual clay layer does not occur in normal condition. Clay tactoid consists of several clay layers stacked in Z-direction. The X-ray diffraction pattern showed the formation of clay tactoids composed of 10 clay layers stacked to each other in Z-direction (106). The water uptake during clay hydration was found to fall into two distinct classes. The interlayer water was contained by tactoid interlayer spaces, while the non-interlayer water was deposited on the tactoid external surfaces and inter-tactoid spaces (103). The inter-tactoid spaces are considered the inter-particular mesopores of clay minerals. These spaces possess strong orientational correlation (98). The inter-tactoid mesopores are located inside a clay aggregate. The electron diffraction pattern showed that the clay tactoids are rolled or crumpled to form clay aggregates (106). Part of the non-interlayer water was found to be stored in the inter-aggregate spaces, which are usually termed as clay macropores. Clay multiple-aggregates contain these macropores. The hydration of different clay water storage sites was observed to take place in a stepwise manner (104, 105). Based upon these observations, we can assume that Na-MMT clay consists of a hierarchical structure and it is composed of these four stages:

- Unit clay sheet/layer: T-O-T structure with interlayer Na ions.
- Tactoid: A number of clay sheets (about 10) stacked to each other to form a clay tactoid.
- Aggregate: A number of clay tactoids are gathered in different orientations to build a clay aggregate.
- Multiple aggregate/assembly of aggregates: Some clay aggregates are combined into a multiple-aggregate.

The behavior of molecular structures can be effectively predicted by MD simulations. It utilizes molecular mechanics calculations by employing a force field (115). MD simulations have proven to be successful in predicting the properties of clay minerals (20-22, 39, 107, 108). As we already built and determined different features of a clay tactoid model in our previous study, in the current report we develop the model of Na-MMT clay aggregate and analyze its different properties through MD simulations.

4.2 Construction of a Clay Aggregate Model

The Na-MMT clay aggregate is modeled based upon the Swy-2 montmorillonite acquired from the clay mineral repository at the University of Missouri, Columbia (13, 28, 29). Na-MMT 6×3 clay layer has been taken as the primary unit of aggregate. Ten 6×3 clay layers have been stacked in the Z-direction to

form a clay tactoid model. The dimensions of each 6×3 clay layer are 31.68 Å×27.44 Å×6.56 Å. By considering the initial d-value as 10 Å, the final dimensions of each tactoid become 31.68 Å×27.44 Å × 96.56 Å. An aggregate is a collection of several clay tactoids. As there is no fixed information regarding the number of tactoids in aggregate, we are assuming each aggregate is made up of three randomly oriented tactoids. In order to represent the orientation variability, we are building four different models of aggregate while each contains a distinct orientation of tactoids. These orientations are chosen randomly. The thickness of the aggregates is kept constant in the Y dimension. The three tactoids inside an aggregate are termed as T1, T2, and T3. Each tactoid consists of 7,281 atoms, of which 7,200 belong to 10 clay layers. The other 81 atoms are categorized as interlayer sodium ions. Therefore, each aggregate contains 21,843 atoms in total, where every 7,281 atoms represent a single tactoid.

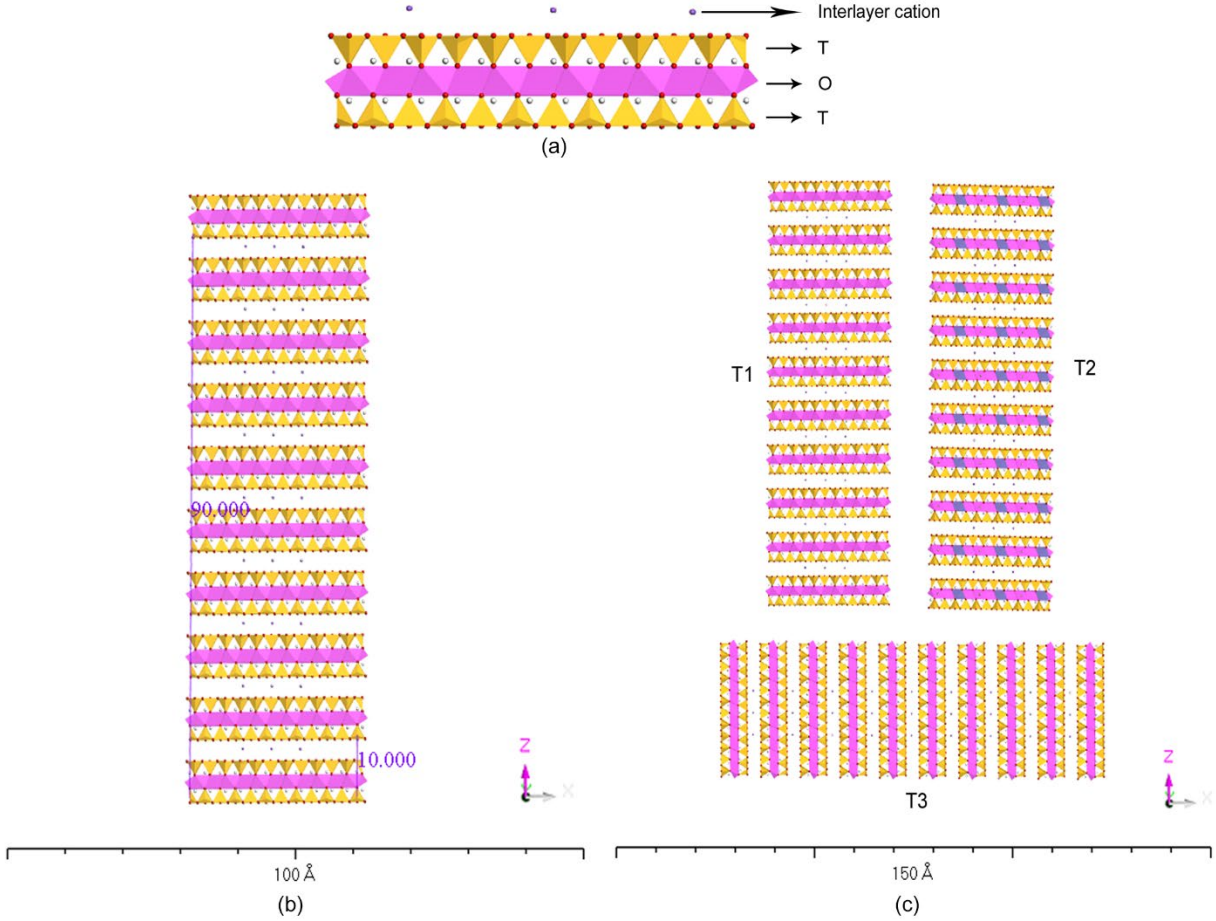

Figure 4.1 Hierarchical structure of Na-MMT clay mineral (a) single 6×3 clay layer (tetrahedral-octahedral-tetrahedral) with interlayer cations (b) tactoid of 10 stacked clay layers and (c) aggregate of three (T1, T2, T3) tactoids

The four different aggregate models are termed A1, A2, A3, and A4, respectively. The overall dimensions of aggregate A1 are 146.81 Å×27.44 Å×169.78 Å. The total dimensions of aggregate A2 are 96.98 Å×27.44 Å×136.51 Å. The model of aggregate A3 surpasses a volume of 157.51 Å×27.44 Å×132.11 Å in 3D space. The size of aggregate A4 is 218.10 Å×27.44 Å× 177.65 Å. Each model of aggregate has a thickness of 27.44 Å normal to XZ plane.

CHARMm (Chemistry at HARvard Macromolecular Mechanics) force field has been used to parameterize Na-MMT clay aggregate (113). The CHARMm force field parameters have been derived from consistent force field parameters (21) by a previous study from our group (109).

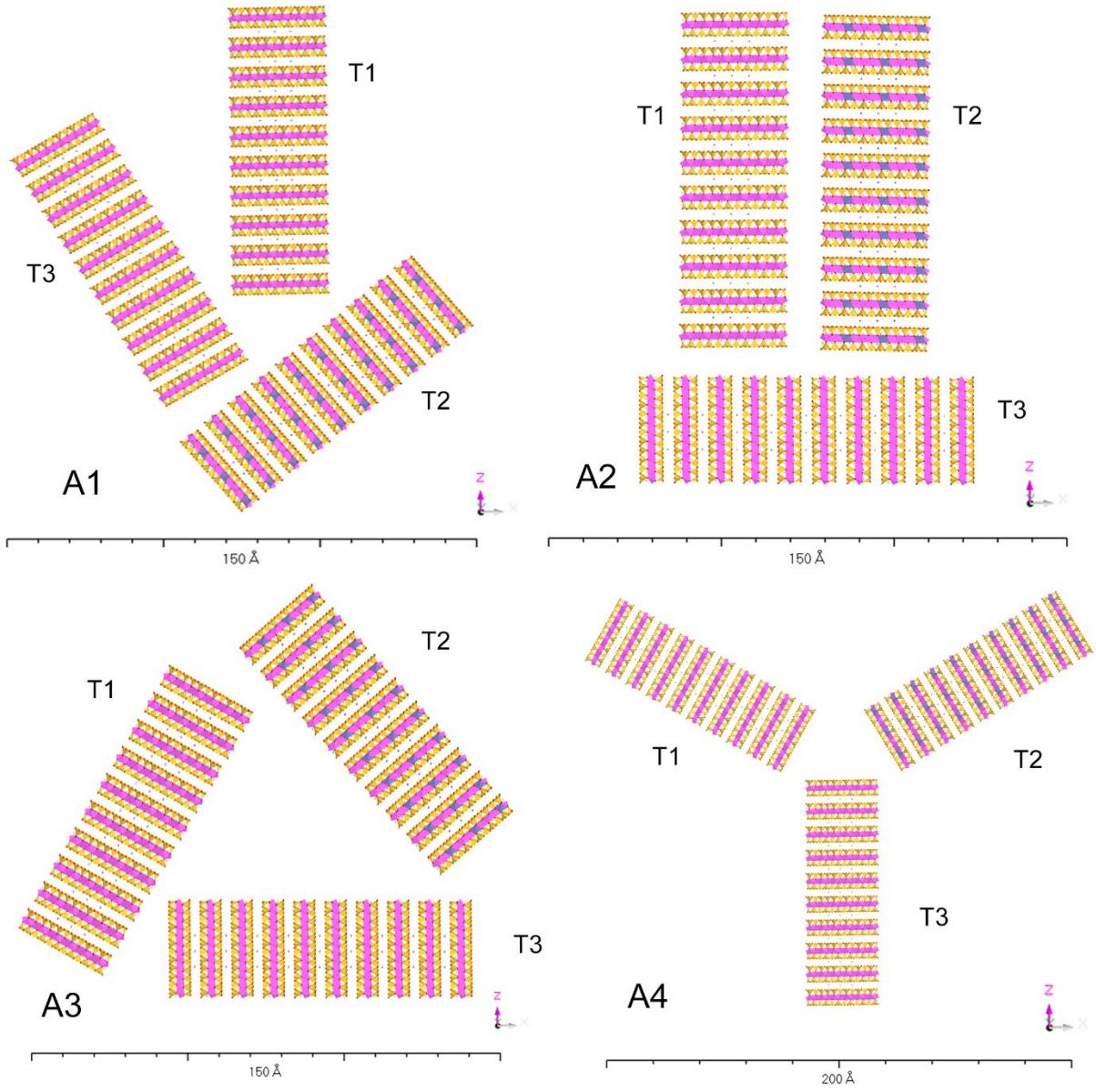

Figure 4.2 Molecular models of four different Na-MMT clay aggregates A1, A2, A3, and A4. Each of them contains a distinct orientation of tactoids T1, T2, and T3

4.3 Simulation Details

The MD simulations of each of the Na-MMT clay aggregates were performed using NAMD 2.12 (47). NAMD was developed by the Theoretical and Computational Biophysics Group in the Beckman Institute for Advanced Science and Technology at the University of Illinois at Urbana-Champaign. To start, all the aggregate models were minimized, utilizing a conjugate gradient method (114). Minimization was

performed at 0 K and 0 bar condition to attain minimum energy landscape by removing bad Van der Waals interactions. After minimization, the normal temperature (300K) and pressure (1.01325 bar) (NTP) were acquired for all Na-MMT clay aggregate models. The normal temperature was achieved in three steps (100K/step), while the normal pressure condition was obtained in four steps (0.25 bar/step). Finally, all the aggregate models were equilibrated at NTP condition by running the simulations for 3ns in an isobaric-isothermal environment. All the minimization and equilibration simulations utilized a time step of 0.5 fs. The CCAST, a parallel computing hub facilitated by NDSU, was used to run all the clay aggregate simulations. Each of the simulations utilized 1 node and 20 Intel Xeon 2.5GHz processors.

4.4 Results and Discussion

4.4.1 Aggregate A1

The three tactoids have been reoriented inside NTP equilibrated aggregate A1. All the tactoids were seen to be bent, while the clay layers of tactoid T2 moved significantly with respect to each other. However, all the clay layers maintained their parallelism inside tactoids (Figure 4.1). The overall dimensions of equilibrated aggregate A1 are 119.13 Å× 96.45 Å× 174.37 Å. The significant change in Y dimension occurred as the tactoids primarily bent towards the Y-axis. The d-spacing has been calculated for each pair of clay layers inside the component tactoids of aggregate A1. The average d-spacing for tactoid T1 was found to be 11.16 Å. The same value was computed as 10.96 Å and 11.06 Å for tactoids T2 and T3, respectively. The average d-spacing for the whole aggregate A1 was 11.06 Å.

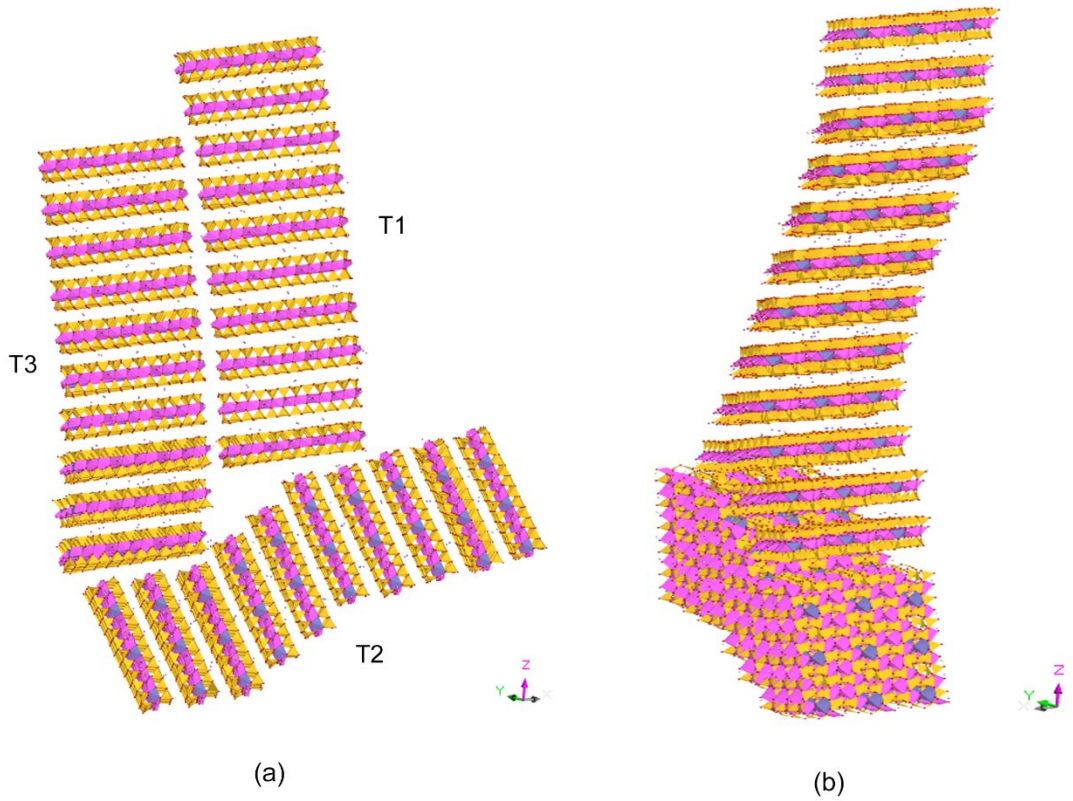

Figure 4.3 Equilibrated structure of aggregate A1 (a, b) from two different angles

The nonbonded interaction energies were calculated between each pair of tactoids. Nonbonded energy is the accumulation of electrostatic and Van der Waals energy. The nonbonded interactions acting inside T1-T2 pair, T2-T3 pair, and T1-T3 pair were -2891.76 kJ/mol, -3871.92 kJ/mol, and -10318.83 kJ/mol, respectively. The higher interactions between T1 and T3 may be attributed to their side-by-side occurrence for a longer region in three-dimensional space. These attractive nonbonded interactions are primarily governed by Van der Waals interactions.

4.4.2 Aggregate A2

The component tactoids of equilibrated aggregate A2 maintain their relative positions compared with the initial model. The bottom tactoid T3 is seen to be partially shifted along its mid-plane due to the pressing of T1 tactoid. The final dimensions of aggregate A2 were 109.03 Å× 46.85 Å× 158.56 Å. Tactoid T1 has an average d-spacing of 10.74 Å, which is analogous to the mean d-spacing of T2 (10.71 Å). Tactoid T3, which is placed at the bottom of T1 and T2, has a slightly higher d-value of 11.34 Å. The average d-spacing of all three tactoids is 10.93 Å.

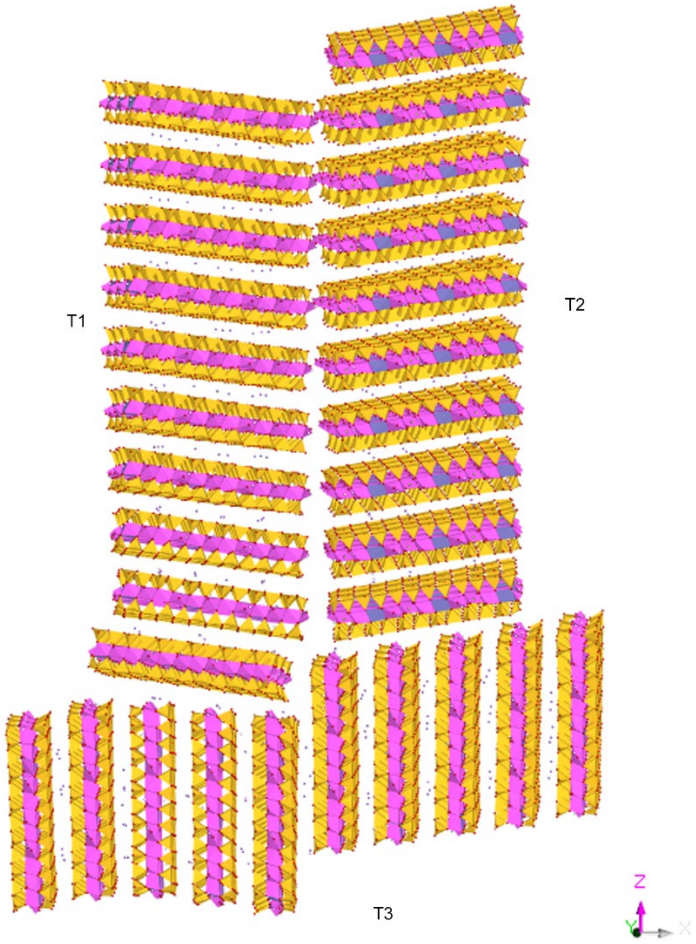

Figure 4.4 Equilibrated molecular model of aggregate A2

The nonbonded energy acting between T1 and T2 was -8910.71 kJ/mol. This value is significantly larger than the interactions in T1-T3 pair (-3947.89 kJ/mol) and T2-T3 pair (-2712.76 kJ/mol). The higher attractive interactions take place between T1 and T2 as they are equilibrated next to each other.

4.4.3 Aggregate A3

A compelling change of equilibrated aggregate A3 compared with its initial model has been caused by the structural and positional changes of tactoids. The top four clay layers of T2 were aligned in a different manner corresponding to the rest of the tactoid. It also migrated along the Y-axis to some extent. The bottom tactoid T3 partly lost its integrity along its middle section as half of the clay layers were rearranged. The d-spacing of tactoids T1 (11.35 Å), T2 (11.33 Å) and T3 (11.69 Å) resulted in an average value of 11.46 Å. This equilibrated A3 model was measured 195.44 Å in the x-direction, 70.54 Å in the y-direction, and 115.94 Å in the z-direction.

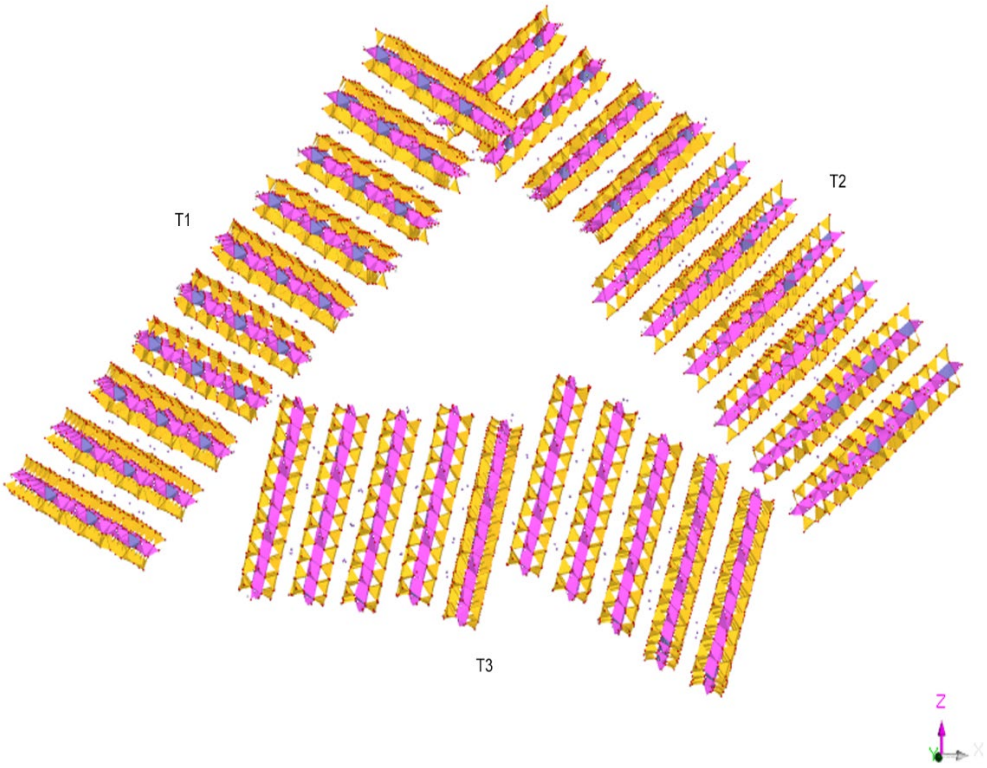

Figure 4.5 Equilibrated model of aggregate A3

4.4.4 Aggregate A4

In the equilibrated aggregate A4, tactoids T1 and T3 remained close while T2 moved away from the rest. Though the tactoids themselves changed their initial orientations, the parallel trend of clay layers inside them was not disrupted. Tactoid T1, T2, and T3 consist of an average d-spacing of 11.01 Å, 11.04 Å, and 10.79 Å, respectively. The mean of these d-values was determined to be 10.95 Å. The length of the final aggregate structure was 240.55 Å along X-axis, 46.85 Å along Y-axis, and 179.05 Å along Z-axis.

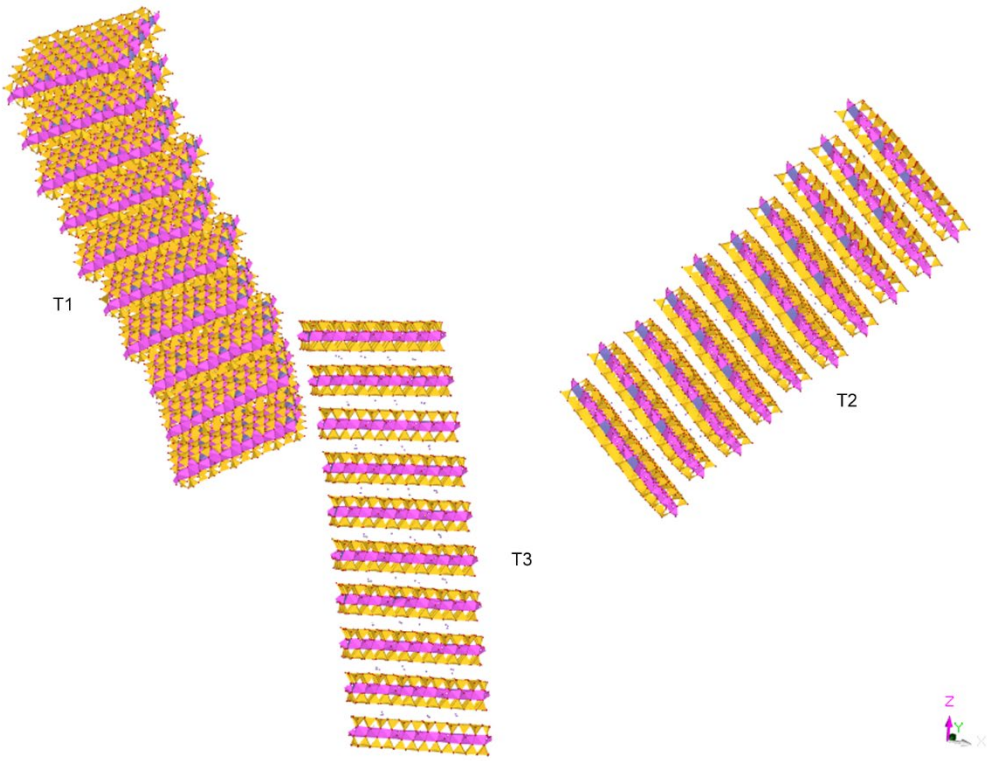

Figure 4.6 Equilibrated model of aggregate A4

5. COARSE-GRAINED MODELING OF SODIUM MONTMORILLONITE CLAYS

This section is presented verbatim from our publication under preparation.

5.1 Background

Sodium montmorillonite clay, a 2:1 aluminum phyllosilicate has long been attracting researchers due to its unique swelling behavior in the presence of water. This montmorillonite can expand up to 15 times its original volume when the swelling is allowed. However, it exerts a large amount of pressure when the swelling is constrained. High swelling pressure causes damage to buildings, foundations, highways, dams, etc. (89, 90). The swelling behavior of Na-montmorillonite (Na-MMT) has been utilized in geoenvironmental engineering, polymer clay nanocomposites, and the mining industry. Therefore, modeling the swelling phenomena of montmorillonite clays is of significant importance.

Na-MMT clay is composed of a hierarchical structure. Different experimental measures inspecting the clay porosities referred to the multiscale structure of clays (57, 94-97). A T-O-T clay layer is the fundamental building unit of Na-MMT clay. Isomorphous substitution of aluminum (Al^{3+}) ions from the octahedral sheet by iron (Fe^{2+}) or magnesium (Mg^{2+}) ions develops the charge deficiency in the clay layer. This phenomenon is neutralized by interlayer Na cations (92, 93). The d-spacing of Na-MMT clay is considered 10 Å. Tactoid is a clay particle built up of 10 clay layers stacked in Z direction (106). It behaves as the basic clay particle, as independent existence of a single clay layer in nature is rare. Several clay tactoids are rolled or crumpled to form a clay aggregate of 0.1 microns. At the uppermost stage of a clay hierarchical structure, a number of clay aggregates are combined in different directions to form multiple aggregates (>10 microns) (94). An investigation of clay hydration sites also exhibited the various stages of clay structure (103). In addition to the multi-scale structural features of clays, different numbers have also been reported to specify the clay particle size. A TEM micrograph of a Na-MMT clay particle showed the particle size ranged between 5nm and 750nm. This size range has a mean of 250 nm and a standard deviation of 180 nm (116). AFM imaging of Na-MMT clay particles reported the existence of two distinct sized populations of Na-MMT clay particles. The average length and width of larger-sized particles is 340 nm and 200 nm, respectively. Another group of clay particles is almost six times smaller than the larger particles i.e., mean length is 54 nm and mean width is 35 nm (117). Another study found the size of Na-MMT particle is 350~400 nm (118). These above-specified numbers represent the XY dimensions of clay layers.

Besides the utilization of different experimental techniques, we have been extensively performing molecular dynamics (MD) simulations to explore different properties of Na-MMT clay minerals at the molecular level. Molecular interactions with various fluids, hydration behavior, and nanomechanical properties of montmorillonite clays have been investigated through MD simulations (1, 28, 29, 41, 109, 110). These properties were successfully determined for 4×2 and 6×3 unit clay layer models where clay unit cell dimensions were 5.28 Å×9.14 Å×6.56 Å. However, the clay layer models should be larger enough (tens of nm) to mimic the behavior of real size clay particles. Moreover, the clay particle needs to be represented by a clay tactoid in which 10 clay layers will be stacked in the vertical direction. The atomistic model of a 50nm×50nm single Na-MMT clay layer contains 205,200 atoms. Therefore, a stack of 10 clay layers will result in an atomistic model of 205,2000 atoms. MD simulations of such massive atomistic models would require higher computing resources and large amount of time. This particular scale-related issue can potentially be addressed by using coarse-grained (CG) molecular dynamics.

CG modeling is a simplified version of atomistic modeling due to the lower degrees of freedom and removal of fine interaction details. This simplification is acquired by clustering a number of atoms into a bead (heavy pseudo atom) and then determining the interactions among the beads. The atom to bead conversion is constrained by the fact that the physical properties of the atomistic model should be reproduced in the CG model. This simplified bead-based CG model allows the simulation of large-scale (mesoscale) physical systems for an extended period of time.

6. EXPERIMENTAL EVALUATION OF SHEAR STRENGTH OF SWELLING CLAYS FOR VARIOUS MAGNITUDE OF SWELLING

This section is presented verbatim from our publication under preparation.

6.1 Background

The volume of swelling clay increases when it comes in contact with water, causing an increase in swelling, swelling pressure, and loss of strength. Some U.S. midwest regions have the most abundant clay, which has high swelling potential (119). Average annual damage caused by swelling clays to the U.S. infrastructure is over $13 billion. However, these clays are used as barrier material in landfills, polymer-clay-nanocomposites to enhance mechanical properties, and modifying in pavement construction.

Shear strength is a critical engineering property that controls the bearing capacity of clays. The shear failure occurs by the relative movements of the clay particles when the applied compressive stresses exceed the internal shear strength of the clays. Most of the civil engineering problems are related to the shear strength in one or another. Failure of building foundations and landslides are some examples of failures associated with clay's shear strength properties. Our previous experimental and modeling studies have shown that clay-fluid interaction at the molecular level has a tremendous impact on the evolution of important engineering properties, such as microstructure, swelling pressure, permeability, and consolidation of swelling clay (1, 17).

As the classical theory of bearing capacity does not account for clay-fluid interactions, a better understanding of shear failure mechanism accounting for clay-fluid molecular interactions is crucial, not only for economic project execution but also for public safety. Hence, the reliable prediction of shear strength of swelling clays would certainly improve design capabilities, prevent the failure of civil infrastructures, and reduce the cost of projects in swelling clay regions. Civil construction industry expenditures are about $10 trillion per year, and improving the fundamental theory used in the design and construction of the infrastructures will be an important contribution to the field and society. In this study, swelling pressure, undrained shear strength, and evolution of the microstructure of swelling clay at various level of swelling have been presented.

6.2 Materials and Equipment

Sodium (Na)-montmorillonite (MMT) clay in powder form is obtained from the Clay Minerals Society at Purdue University, West Lafayette, Indiana. The chemical formula of the Na-MMT clay mineral is $NaSi_{16}(Al_6FeMg)O_{20}(OH)_4$, which has a specific gravity of 2.67, an initial void ratio of 2.14, a density of 850 kg/m^3, and a cationic exchange capacity of about 76.4 mequiv/100 g. The deionized water was prepared in our laboratory in the Civil and Environmental Engineering Department, North Dakota State University.

6.3 Experimental Methods

Prior to each sample preparation, the Na-MMT clay mineral was ground finely and passed through a 76 μm mesh (No. 200 sieve). In order to have a consistent moisture content, the powder specimen was then placed in a drying oven at 105ºC for 24 hours.The controlled uniaxial swelling (CUS) device was used for saturating the samples. The CUS device allows the samples to saturate, and swelling in the uniaxial

direction and can be split vertically to remove the sample with minimum disturbance. The detailed design of the CUS device is explained in our previous work (13).

In this study, 233 grams of clay are placed in the controlled uniaxial (CUS) device of 70 mm internal diameter. To be consistent with our previous experiments, the clay sample is loosely compacted in four layers by gently tapping the CUS device to the height of 72 mm to maintain the void ratio of 2.14, as shown in Figure 6.1. Samples were kept in between porous stones and No. 40 Whatman filter paper. To maintain the zero volume change as well as prevent swelling of the sample in the vertical direction, the CUS device's piston was locked using a rectangular aluminum plate and hexagonal nuts, as shown in Figure 6.1.

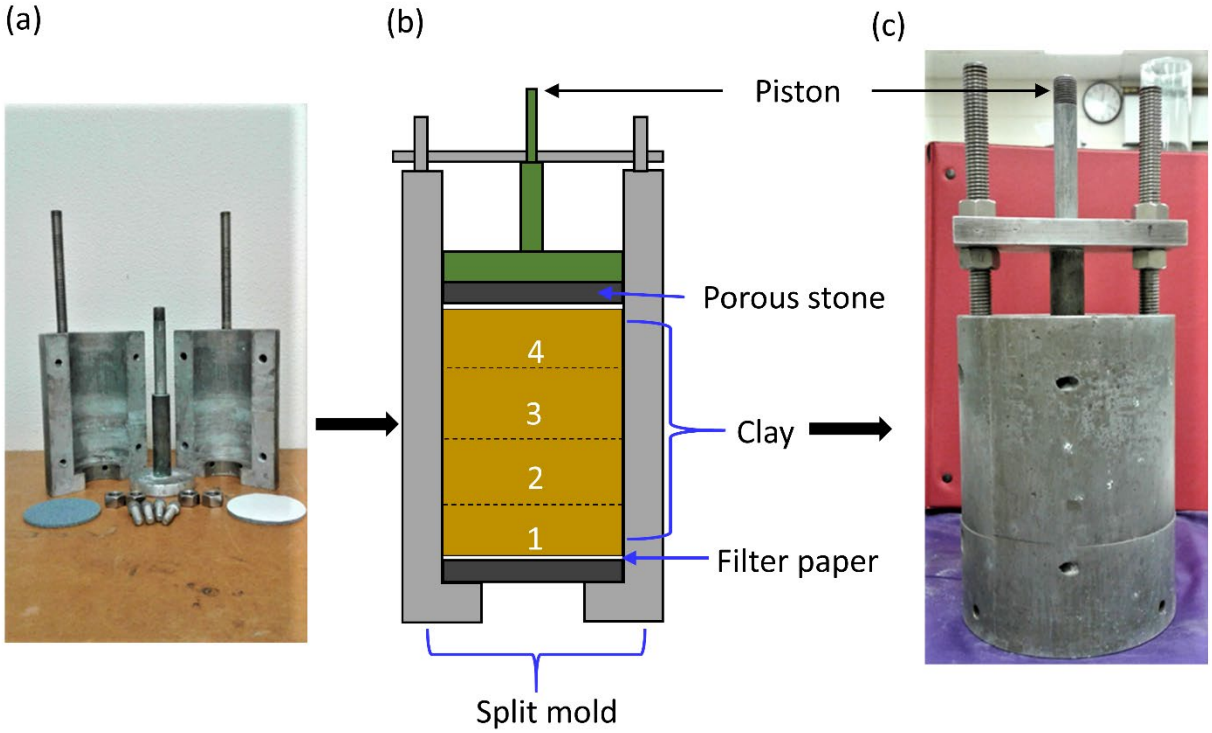

Figure 6.1 Assembly of clay sample (a) controlled uniaxial swelling (CUS) device, (b) schematic diagram showing the sample placed in four layers, and (c) CUS device with clay at zero swelling

The samples were then placed in the water-filled plexiglass tank for the saturation. All the samples are allowed to saturate in the plexiglass at least for 30 days, as shown in Figure 6.2. For the swelling pressure measurement, the CUS device and plexiglass were placed in SATEC 22 EMF universal testing equipment. The CUS device's piston was centered with the loading ram of the universal testing equipment, and the load-cell was brought in contact with the piston. The locking of the piston was released by unscrewing the hexagonal nuts. At this condition, the piston was maintained at zero swelling. The loading ram was moved up to remove the CUS device, and the sample was furthermore used to evaluate the microstructure, undrained shear strength, and nanomechanical properties.

Additionally, the loading ram can be moved up to the predetermined level of 3.6 mm for 5% swelling, 7.2 mm for 10% swelling, 10.8 mm for 15% swelling, and 18 mm for 25% swelling, and the swelling pressure at various swelling levels can be measured. To do this, the piston locking system is again released. The piston moves vertically up and touches the loading arm, and the corresponding swelling

pressure is measured similarly to how the swelling pressure is measured at zero volume change. Additionally, the swelling pressure measured samples are used to measure the microstructure, undrained shear strength, and nanomechanical properties at various levels of swelling.

Figure 6.2 The saturation of Na-MMT clay samples using four controlled uniaxial swelling (CUS) devices

In order to evaluate the undrained compressive strength of saturated swelling clays at various levels of swelling, a series of unconfined compression tests of swelling measured samples were accomplished. First, the zero percent swelled sample was removed from the CUD device. Figure 6.3 shows a cylindrical split mold of internal diameter of 35 mm, height of 70 mm, and thickness of 3 mm, which was used to take the sample from the CUS device. This cylinder was made up of polymethyl methacrylate (PMMA) white, which can be vertically split to two pieces. They were connected using 160-mm-long stainless steel cable tie. Before taking the sample for the compression test, the cylinder was lubricated with silicone high vacuum grease (Dow Corning Corporation, USA) to reduce the adhesion between sample and cylinder. The cylinder was then gently pressed on the swelling measured sample and removed upward gently. A sample with a diameter of 35 mm and height of 70 mm was then removed from the cylinder for the compression test. The strain rate of 1%/min was used for the unconfined compression test according to the ASTM D 2166-16. A Shimadzu loading frame (Shimadzu Scientific Instruments, USA) was used for the compression test. The degree of saturation of each sample after the test was also measured.

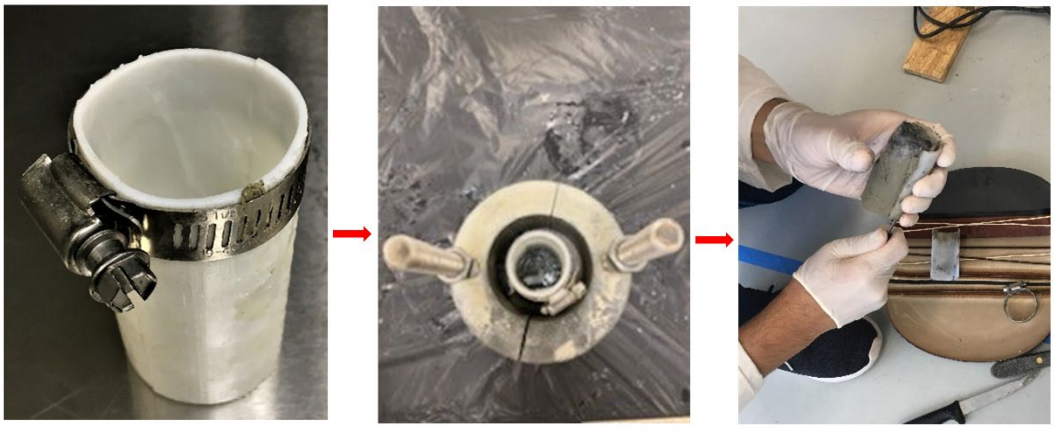

Figure 6.3 Taking sample for the compression test using a cylindrical split mold from the CUS device

6.4 Results

Figure 6.4 shows the unconfined compressive stress versus axial strain from the compression test for clay sample at no volume change condition. The plot shows that the continuous deformation and the pronounced stress-strain peak is observed at 8.35% strain. The maximum unconfined compressive stress is found to be 29.62 kPa, which is within the range for Na-MMT clay (120). The undrained shear strength, which is half of the unconfined compressive stress, is found to be 14.81 kPa. Figure 4.4 also shows that the compressive stress is gradually decreased, and the maximum strain axial is about 13%.

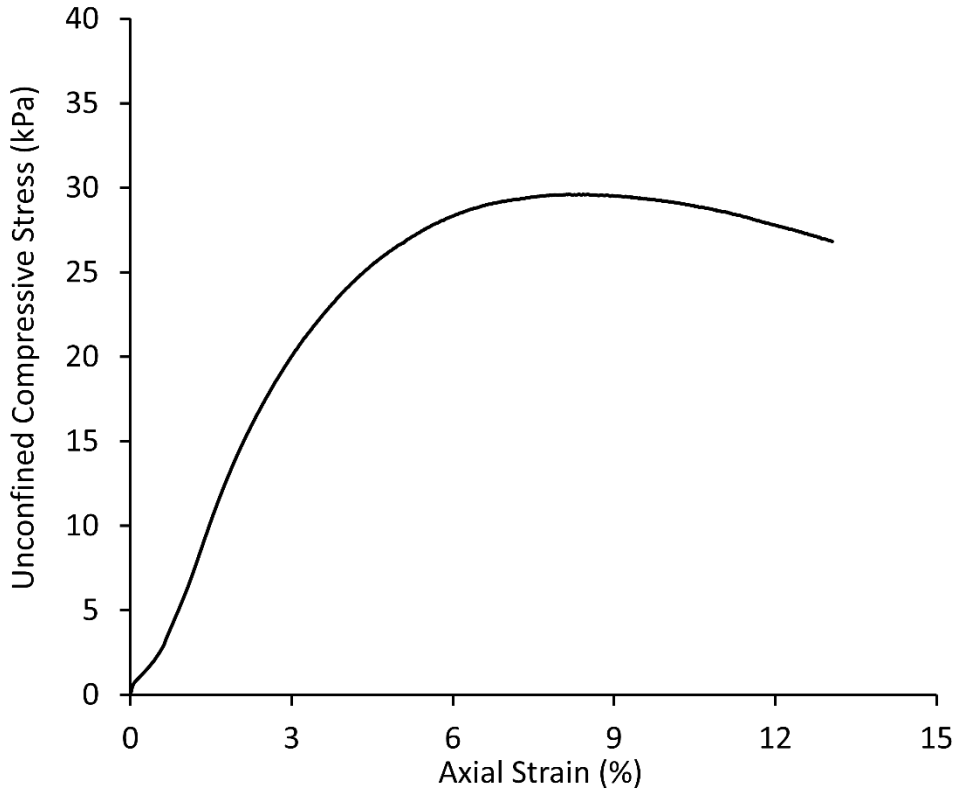

Figure 6.4 Stress-strain curve of saturated Na-MMT clay at no volume change condition

6.5 Discussion

The undrained shear strength of saturated Na-MMT clay at zero volume change is measured using the unconfined compressive strength test.

7. NANOMECHANICAL PROPERTIES OF SWELLING CLAYS

This section is presented verbatim from our publication under preparation.

7.1 Background

Swelling clays are found all over the world. These clays have been used as the barrier liners and to enhance the mechanical properties of clay-polymer-nanocomposities. Sodium-montmorillonite (Na-MMT) clay is the main component of the smectite clay mineral. The structure of Na-MMT clay consists of a tetrahedral-octahedral-tetrahedral (T-O-T) arrangement where an octahedral clay sheet is sandwiched between tetrahedral clay sheets. Knowing the fundamental mechanical properties of clay is essential for the design properties of the composite materials (7, 121). The mechanical behavior of the swelling clays is also necessary to the barrier liners in landfills as well as to store high-level radioactive waste (122). Understanding the fundamental mechanical properties of swelling clays is also essential for the efficient and economical extraction of oil and gas from oil shale—sedimentary rock (77, 123). The knowledge of elastic properties is used for analyzing the geophysical subsurface exploration and reservoir characterization using seismic waves (124). The mechanical properties of clays are furthermore required to evaluate the settlement of the laterally loaded foundations (125).

The elastic properties of clay minerals have great importance for the characterization and exploration of the shale formations, as clay minerals are common in the sedimentary formation and environments. The elastic modulus and hardness of air-dried layered aluminosilicates—muscovite and rectorite clay minerals—have been studied using load-controlled nanoindentation at various loading rates (126). The variation of the nanomechanical properties of bentonite and kaolinite clays subjected to an elevated temperature from 25^{o}C to 200^{o}C has been studied using nanoindentation. It has been observed that the resistance to penetration and elastic modulus increased with an increase in temperature, and bentonite clay has higher elastic modulus than kaolinite clay (127). The load-controlled nanoindentation of kaolinite clay mineral stabilized with oil-in-water emulsions and dried at room temperature is carried out, and the elastic modulus and hardness are found to be 0.5-3 GPa and hardness of 15-40 MPa, respectively (128).

The elastic properties at the macro-scale can be easily evaluated using uniaxial compression or tensile testing method. However, the elastic properties at the nano-scale, whether thin films on substrate or free-standing samples, require a sophisticated method. Nanoindentaion is an experimental technique to measure the mechanical properties of the materials at the nanoscale based on the theory of elastic contact. The frequently measured two mechanical properties are the elastic modulus (E) and the hardness (H). The indenter is allowed to press the sample at a specific load and then withdrawn. The load-displacement data are recorded from one complete loading and unloading cycle. The withdrawal of the indenter results in recovering the elastic deformation, and certain displacement remains as the plastic deformation, which is also known as residual indentation depth. The displacement during unloading is typically elastic in nature, and the initial portion of the unloading curve is used for the analysis. The indenter tip is made up of diamond that has high resistance to deformations.

Our previous studies have shown that the clay-fluid interactions for saturated swelling clays at the nano-scale control the macroscopic properties of swelling clays, such as microstructure, permeability, and consolidation (1, 17). The measurement of mechanical properties of swelling clays is challenging because of their affinity to water, being expansive in nature, and plate-like structures (129). Thus, in most of the reported literature, the elastic modulus and hardness of clay minerals are measured either in dry or very small water content conditions. In this work, we present our results from displacement-controlled nanoindentation on undisturbed dry and saturated Na-MMT clay samples. Furthermore, this study

captures insight into the role of water on the elastic modulus and hardness of the undisturbed clay samples at various levels of swelling.

7.2 Materials and Equipment

Na-MMT clay is obtained from the Clay Minerals Society at the Purdue University, West Lafayette, Indiana. The chemical formula of the Na-MMT clay is $NaSi_{16}(Al_6FeMg)O_{20}(OH)_4$. The clay has a specific gravity of 2.67, an initial void ratio of 2.14, a density of 850 kg/m^3, and a cationic exchange capacity of about 76.4 mequiv/100 g. We used deionized water from our laboratory in the Civil and Environmental Engineering Department, North Dakota State University, Fargo, ND.

7.3 Experimental Methods

Dry Na-MMT clay was ground and passed through 76 μm mesh (No. 200 sieve). The powder specimen was then placed in a drying oven at 105°C for 24 hours to have a consistent moisture content for all samples. For nanoindentation experiment for dry clay, 0.575 grams of clay was placed in the cylinder at a height of 6 mm, a diameter of 12 mm, and thickness of 1 mm by gently tapping the cylinder. This cylinder was made up of polymethyl methacrylate (PMMA) white, and the base of the cylinder was glued with a 15-mm diameter stainless steel disc to support the sample, as shown in Fig. 7.1. The undisturbed saturated sample was taken by gently pressing the same cylinder, which is used for dry indentation, from the controlled uniaxial swelling (CUS) device. The detailed design of the CUS device is explained in our previous work (13).

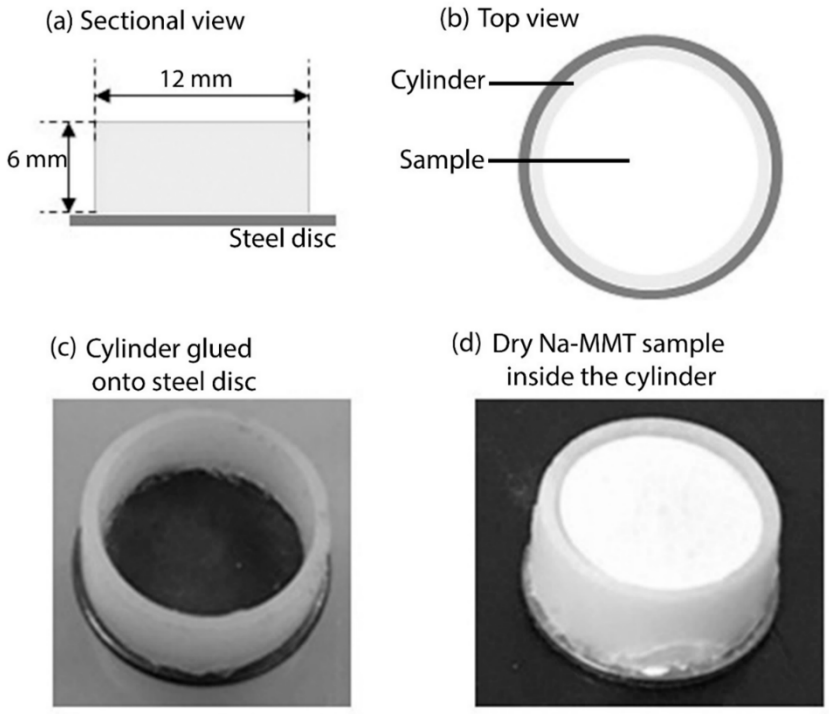

Figure 7.1 Schematic showing the specimen assembly for nanoindentation experiment

Nanoindentation tests were accomplished using contact mode with a Hysitron Triboscope nanomechanical testing instrument (Minneapolis, MN). The load resolution and displacement resolution of this instrument were 1 nN and 1 nm, respectively. A trigonal pyramid Berkovich diamond tip (100-200 nm tip radius) was used to perform the test. To evaluate how the nanomechanical properties of swelling clay change during saturation at different levels of swelling, the displacement-controlled indentation tests were carried to determine the elastic modulus and hardness of dry and saturated Na-MMT clay. In this work, the depth 500 nm was applied to the sample. Also, a triangular loading function was selected at a loading and unloading rate of 100 nm/s. An average of 10 indents were made on each sample, and the distance between the neighboring test locations is kept at least 5 µm. Furthermore, the indenter tip is cleaned after each indentation using acetone to reduce the interaction between the tip and clay sample.

The elastic modulus of the specimen is determined by calculating the stiffness and contact area from the load-displacement curve. The unloading curve for the measurement of stiffness is non-linear, and described by power-law relation:

$$P = B(h - h_f)^m$$

Where the constants B and m are determined by empirically using fitting parameters. The slope of the initial unloading curve, which is stiffness, is obtained by differentiating the above equation:

$$S = \left(\frac{dP}{dh}\right)_{h=h_{max}}$$

$$S = Bm(h_{max} - h_f)^{m-1}$$

The reduced modulus and the stiffness are related by

$$\mathrm{S} = \frac{2}{\sqrt{\pi}}\sqrt{A}\,\mathrm{E_r}$$

In addition, the tip area function depends on the geometry of the indenter. Indirect measurement of contact area between the tip and the sample is carried out by measuring the penetration depth and the known geometry of the indenter. Prior to each indentation test, area function is calculated by indenting on standard sample such as fused quartz. For a Berkovich indenter, the projected area of the tip (A) at the contact depth (hc) is described by polynomial equation:

$$A(h_c) = C_0 {h_c}^2 + C_1 h_c + C_2 {h_c}^{1/2} + C_3 {h_c}^{1/4} + \cdots + C_8 {h_c}^{1/128}$$

Where C_1 through C_8 are constants and C0=24.5. The first term, C_0, represents the ideal Berkovich indenter, and the other terms define the deviations from the Berkovich geometry because of tip blunting.

Hardness (H) is defined as the resistance of the material to plastic deformation. It is also known as the mean pressure that the material supports when a load is applied. It is calculated by dividing the peak load (P_{max}) by the projected contact area (A). The hardness and the reduced modulus were determined by using Oliver and Pharr method (130). In this method, unloading segment of the curve was described by a power-law function, and the contact area was obtained. The initial displacement segment of unloading curve was typically elastic, and the contact stiffness was calculated by differentiating the power-law relation. For each unloading segment, the hardness and the reduced modulus were computed using HYSITRON analysis software with the help of the peak-load, contact depth at peak-load, and contact stiffness. The indenter tip and the sample experienced elastic deformation—the elastic modulus of each

specimen was further calculated considering deformation of both of them. The relationship between the reduced modulus and the elastic modulus is as follows:

$$\frac{1}{E_r} = \frac{1-\nu^2}{E} + \frac{1-\nu_i^2}{E_i}$$

Where E_r= reduced elastic modulus, E=elastic modulus of the sample, E_i=elastic modulus of the indenter, ν=Poisson's ratio of the sample, and νi=Poisson's ratio of the indenter. For the diamond indenter tip, the elastic modulus of 1141 GPa and Poisson's ratio of 0.07 was used. An estimated Poisson's ratio of 0.255 was used for clay samples (131).

7.4 Results

Figure 7.2 shows the load-displacement curves on dry clay and saturated samples at indents of 500 nm. It has been observed that saturated clay exhibits a much stiffer response than that of dry clay. The values of an average peak load for dry and saturated clay are 32.16 µN and 90.40 µN, respectively. Our previous studies have shown that a significant amount of swelling pressure is exerted by clay during swelling (13, 17). To oppose this internal swelling pressure, it can be correlated that the force required to indent the saturated sample is significantly higher than that of dry clay.

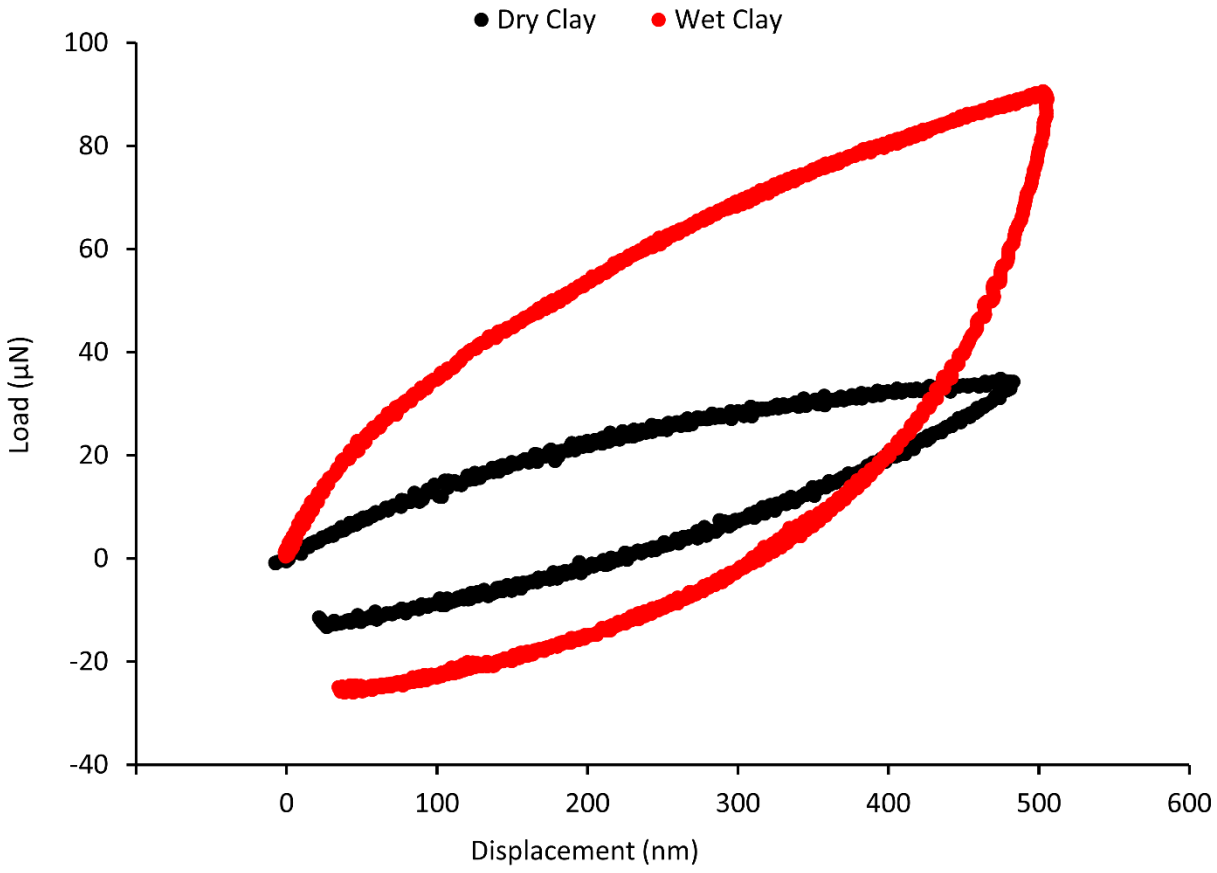

Figure 7.2 Typical load-displacement curve of dry clay and saturated clay sample by displacement-controlled test at 500 nm displacement

An average modulus of elasticity of dry clay is found to be 78.17 MPa, and the hardness is about 8.10 MPa. Similarly, for saturated clay, the modulus of elasticity is found to be 326.77 MPa, and the hardness is 17.61 MPa. Upon saturation, a significant increase in the nanomechanical properties of swelling clay is observed. The elastic modulus of saturated clay is more than four times greater than dry clay, and the hardness of saturated clay is twice the hardness of dry clay. Furthermore, the resistance to penetration of the indenter increases when the clay sample is saturated. This is due to clay particles breakdown upon adding water, and the void spaces between the clay particles are filled, and swelling pressure, which allows increasing the resistance to penetration upon indentation.

It has been observed there is an incomplete shape recovery of unloading curves for both dry and saturated clay, as shown in the load-displacement curves. The incomplete shape can be due to plastic deformation of clays upon indentation. The investigation of the plastic deformation can be explained by the residual indentation depth (h_f), which is also known as unrecovered displacement from the load-displacement plots. As seen in Figure 7.3, the residual indentation depths for dry and saturated clay are found to be 163.06 nm and 216.07 nm, respectively. It is observed that the residual depth increases when water is added to dry clay at zero swelling, which indicates that the mechanical plasticity increases with adding water with clay.

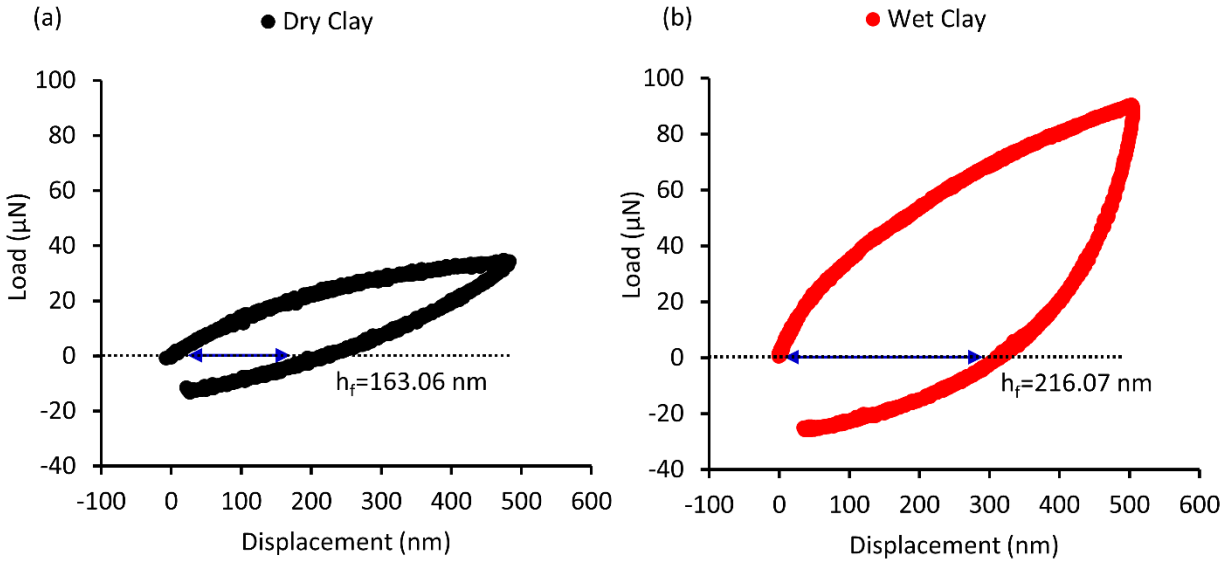

Figure 7.3 Typical load-displacement curve showing the residual depth (h_f) of dry clay and saturated clay sample by displacement-controlled test at 500 nm displacement

7.5 Discussion

The results from this study clearly show that the presence of water has a significant effect on the nanomechanical properties—elastic modulus and hardness—of swelling clays. The nature of nonbonded molecular interactions among clay sheets, interlayer cation, and water molecules appears to be the influencing factor for the difference in the modulus of elasticity and hardness of clay upon saturation. Dry clay sample response is softer than the wet clay response.Thus, the maximum force required to indent saturated clay is significantly greater than that required for dry clay. The mechanical plasticity increases with adding water on dry clay.

REFERENCES

1. Katti, DR, Thapa, KB, and Katti, KS. "The role of fluid polarity in the swelling of sodium-montmorillonite clay: A molecular dynamics and Fourier transform infrared spectroscopy study." *Journal of Rock Mechanics and Geotechnical Engineering*. 2018;10(6):1133-44. doi: 10.1016/j.jrmge.2018.07.001. PubMed PMID: WOS:000451767300011.
2. Chen, FH. *Foundations on expansive soils.* New York: Elsevier; 1988.
3. Rao, RR, Rahardjo, H, and Fredlund, DG. "Closed-Form Heave Solutions for Expansive Soils." *Journal of Geotechnical Engineering-Asce*. 1988;114(5):573-88. PubMed PMID: WOS:A1988N248000004.
4. Katti, RK, Katti, DR, and Katti, AR. *Behaviour of saturated expansive soil and control methods.* Lisse [Netherlands]; Exton, PA: Balkema; 2002.
5. Kayabali, K. "Engineering aspects of a novel landfill liner material: Bentonite-amended natural zeolite." *Engineering Geology*. 1997;46(2):105-14. doi: 10.1016/s0013-7952(96)00102-0. PubMed PMID: WOS:A1997XD83400004.
6. Murray, HH. *Applied clay mineralogy today and tomorrow.* Clay Minerals. 1999;34(1):39-49. doi: 10.1180/000985599546055. PubMed PMID: WOS:000079520300005.
7. Sikdar, D, Pradhan, SM, Katti, DR, Katti, KS, and Mohanty B. Altered phase model for polymer clay nanocomposites. Langmuir. 2008;24(10):5599-607. doi: 10.1021/la800583h. PubMed PMID: WOS:000255856100059.
8. Ambre, AH, Katti, DR, and Katti, KS. "Nanoclays mediate stem cell differentiation and mineralized ECM formation on biopolymer scaffolds." *Journal of Biomedical Materials Research Part A*. 2013;101(9):2644-60. doi: 10.1002/jbm.a.34561. PubMed PMID: WOS:000322061900019.
9. Abdelrahman, M, Katti, DR, Ghavibazoo, A, Upadhyay, HB, and Katti, KS. "Engineering Physical Properties of Asphalt Binders through Nanoclay-Asphalt Interactions." J*ournal of Materials in Civil Engineering*. 2014;26(12). doi: 10.1061/(asce)mt.1943-5533.0001017. PubMed PMID: WOS:000345330300008.
10. Mitchell, JK, and Soga K. *Fundamentals of soil behavior*, 2005.
11. Madsen, FT, and Muller-Vonmoos, M. "The swelling behaviour of clays." *Applied clay science*. 1989;4(2):143-56.
12. Jo, HY, Katsumi, T, Benson, CH, and Edil, TB. "Hydraulic conductivity and swelling of nonprehydrated GCLs permeated with single-species salt solutions." *Journal of Geotechnical and Geoenvironmental Engineering*. 2001;127(7):557-67. doi: 10.1061/(asce)1090-0241(2001)127:7(557). PubMed PMID: WOS:000169322500001.
13. Katti, D, and Shanmugasundaram, V. "Influence of swelling on the microstructure of expansive clays." *Canadian Geotechnical Journal*. 2001;38(1):175-82. doi: 10.1139/cgj-38-1-175. PubMed PMID: WOS:000167370700015.
14. Maria Gomez-Caravaca, A, Maggio, RM, Verardo, V, Cichelli, A, and Cerretani, L. "Fourier transform infrared spectroscopy-Partial Least Squares (FTIR-PLS) coupled procedure application for the evaluation of fly attack on olive oil quality." *Lwt-Food Science and Technology*. 2013;50(1):153-9. doi: 10.1016/j.lwt.2012.06.007. PubMed PMID: WOS:000309896600020.

15. Katti, KS, and Katti, DR. *Relationship of swelling and swelling pressure on silica-water interactions in montmorillonite.* Langmuir. 2006;22(2):532-7. doi: 10.1021/la051533u. PubMed PMID: WOS:000234647200006.

16. Amarasinghe, PM, Katti, KS, and Katti, DR. "Nature of organic fluid-montmorillonite interactions: An FTIR spectroscopic study." *Journal of Colloid and Interface Science.* 2009;337(1):97-105. doi: 10.1016/j.jcis.2009.05.011. PubMed PMID: WOS:000268111800014.

17. Amarasinghe, PM, Katti, KS, and Katti, DR. "Insight into Role of Clay-Fluid Molecular Interactions on Permeability and Consolidation Behavior of Na-Montmorillonite Swelling Clay." *Journal of Geotechnical and Geoenvironmental Engineering.* 2012;138(2):138-46. doi: 10.1061/(asce)gt.1943-5606.0000567. PubMed PMID: WOS:000301506000003.

18. Norrish, K. *The Swelling of Montmorillonite*. Discussions of the Faraday Society. 1954(18):120-34. PubMed PMID: WOS:A1954UL20500012.

19. Delville, A. *Modeling the Clay Water Interface.* Langmuir. 1991;7(3):547-55. doi: 10.1021/la00051a022. PubMed PMID: WOS:A1991FC98800022.

20. Chang, FRC, Skipper, NT, and Sposito, G. *Computer-Simulation of Interlayer Molecular-Structure in Sodium Montmorillonite Hydrates*. Langmuir. 1995;11(7):2734-41. doi: 10.1021/la00007a064. PubMed PMID: WOS:A1995RL57200065.

21. Teppen, BJ, Rasmussen, K, Bertsch, PM, Miller, DM, and Schafer, L. "Molecular dynamics modeling of clay minerals .1. Gibbsite, kaolinite, pyrophyllite, and beidellite." *Journal of Physical Chemistry B*. 1997;101(9):1579-87. doi: 10.1021/jp961577z. PubMed PMID: WOS:A1997WL35700015.

22. Shroll, RM, and Smith, DE. "Molecular dynamics simulations in the grand canonical ensemble: Application to clay mineral swelling." *Journal of Chemical Physics*. 1999;111(19):9025-33. doi: 10.1063/1.480245. PubMed PMID: WOS:000083437400032.

23. Anandarajah, A. "Influence of particle orientation on one-dimensional compression of montmorillonite." *Journal of Colloid and Interface Scien*ce. 1997;194(1):44-52. doi: 10.1006/jcis.1997.5068. PubMed PMID: WOS:A1997YG92600006.

24. Boek, ES, Coveney, PV, and Skipper, NT. "Monte Carlo molecular modeling studies of hydrated Li-, Na-, and K-smectites: Understanding the role of potassium as a clay swelling inhibitor." *Journal of the American Chemical Society.* 1995;117(50):12608-17. doi: 10.1021/ja00155a025. PubMed PMID: WOS:A1995TL73300025.

25. Karaborni, S, Smit, B, Heidug, W, Urai, J, and Van Oort, E. "The Swelling of Clays: Molecular Simulations of the Hydration of Montmorillonite." *Science*. 1996;271(5252):1102-4.

26. Katti, D, Ghosh, P, Schmidt, S, and Katti, K. "Mechanical properties of the sodium montmorillonite interlayer intercalated with amino acids." *Biomacromolecules*. 2005;6(6):3276-82. doi: 10.1021/bm0503219. PubMed PMID: WOS:000233392100053.

27. Katti D, Schmidt, S, Ghosh, P, and Katti, K. "Modeling the response of pyrophyllite interlayer to applied stress using steered molecular dynamics." *Clays and Clay Minerals.* 2005;53(2):171-8. doi: 10.1346/CCMN.2005.0530207. PubMed PMID: WOS:000228649900007.

28. Schmidt, SR, Katti, DR, Ghosh, P, and Katti KS. "Evolution of mechanical response of sodium montmorillonite interlayer with increasing hydration by molecular dynamics." *Langmuir*. 2005;21(17):8069-76. doi: 10.1021/la050615f. PubMed PMID: WOS:000231389200063.

29. Katti, DR, Schmidt, SR, Ghosh, P, and Katti, KS. "Molecular modeling of the mechanical behavior and interactions in dry and slightly hydrated sodium montmorillonite interlayer."

Canadian Geotechnical Journal. 2007;44(4):425-35. doi: 10.1139/t06-127. PubMed PMID: WOS:000248085200005.

30. Katti, D, Matar, M, Katti, K, and Amarasinghe, P. "Multiscale modeling of swelling clays: A computational and experimental approach." *KSCE J Civ Eng*. 2009;13(4):243-55. doi: 10.1007/s12205-009-0243-0.

31. Pradhan, SM, Katti, KS, and Katti, DR. "Evolution of Molecular Interactions in the Interlayer of Na-Montmorillonite Swelling Clay with Increasing Hydration." *International Journal of Geomechanics*. 2015;15(5). doi: 10.1061/(asce)gm.1943-5622.0000412. PubMed PMID: WOS:000361555300011.

32. Katti, DR, Srinivasamurthy, L, and Katti, KS. "Molecular modeling of initiation of interlayer swelling in Na-montmorillonite expansive clay." *Canadian Geotechnical Journal.* 2015;52(9):1385-95. doi: 10.1139/cgj-2014-0309. PubMed PMID: WOS:000360296600014.

33. Kadoura, A, Nair, AKN, and Sun, SY. "Molecular Simulation Study of Montmorillonite in Contact with Variably Wet Supercritical Carbon Dioxide." *Journal of Physical Chemistry C.* 2017;121(11):6199-208. doi: 10.1021/acs.jpcc.7b01027. PubMed PMID: WOS:000397546300041.

34. Sun, L, Tanskanen, JT, Hirvi, JT, Kasa, S, Schatz, T, and Pakkanen, TA. "Molecular dynamics study of montmorillonite crystalline swelling: Roles of interlayer cation species and water content." *Chemical Physics*. 2015;455:23-31. doi: 10.1016/j.chemphys.2015.04.005. PubMed PMID: WOS:000355342100004.

35. Greathouse, JA, Hart, DB, Bowers, GM, Kirkpatrick, RJ, and Cygan, RT. "Molecular Simulation of Structure and Diffusion at Smectite-Water Interfaces: Using Expanded Clay Interlayers as Model Nanopores." *Journal of Physical Chemistry C*. 2015;119(30):17126-36. doi: 10.1021/acs.jpcc.5b03314. PubMed PMID: WOS:000359031900012.

36. Makaremi, M, Jordan, KD, Guthrie, GD, and Myshakin, EM. "Multiphase Monte Carlo and Molecular Dynamics Simulations of Water and CO2 Intercalation in Montmorillonite and Beidellite." *Journal of Physical Chemistry C*. 2015;119(27):15112-24. doi: 10.1021/acs.jpcc.5b01754. PubMed PMID: WOS:000357964900034.

37. Pradhan, SM, Katti, KS, Katti DR. Evolution of Molecular Interactions in the Interlayer of Na-Montmorillonite Swelling Clay with Increasing Hydration. International Journal of Geomechanics. 2015;15(5):04014073. doi: 10.1061/(asce)gm.1943-5622.0000412. PubMed PMID: WOS:000361555300011.

38. Katti DR, Patwary ZR, Katti KS. Modelling clay-fluid interactions in montmorillonite clays. Environmental Geotechnics. 2016.

39. Skipper NT, Sposito G, Chang FRC. Monte-Carlo Simulation of Interlayer Molecular-Structure In Swelling Clay-Minerals .2. Monolayer Hydrates. Clays and Clay Minerals. 1995;43(3):294-303. doi: 10.1346/ccmn.1995.0430304. PubMed PMID: WOS:A1995RV42800004.

40. van Olphen H, Fritpiat JJ. Data Handbook for Clay Materials and Other Non-Metallic Minerals. New York: Pergamon Press; 1979.

41. Katti DR, Ghosh P, Schmidt S, Katti KS. Mechanical properties of the sodium montmorillonite interlayer intercalated with amino acids. Biomacromolecules. 2005;6(6):3276-82. doi: 10.1021/bm0503219. PubMed PMID: WOS:000233392100053.

42. Humphrey W, Dalke A, Schulten K. VMD: Visual molecular dynamics. Journal of Molecular Graphics. 1996;14(1):33-&. PubMed PMID: ISI:A1996UH51500005.

43. MacKerell AD, Bashford D, Bellott M, Dunbrack RL, Evanseck JD, Field MJ, Fischer S, Gao J, Guo H, Ha S, Joseph-McCarthy D, Kuchnir L, Kuczera K, Lau FTK, Mattos C, Michnick S, Ngo T, Nguyen DT, Prodhom B, Reiher WE, Roux B, Schlenkrich M, Smith JC, Stote R, Straub J, Watanabe M, Wiorkiewicz-Kuczera J, Yin D, Karplus M. All-atom empirical potential for molecular modeling and dynamics studies of proteins. Journal of Physical Chemistry B. 1998;102(18):3586-616. PubMed PMID: WOS:000073632700037.

44. Jorgensen WL, Chandrasekhar J, Madura JD, Impey RW, Klein ML. Comparison of Simple Potential Functions for Simulating Liquid Water. Journal of Chemical Physics. 1983;79(2):926-35. doi: 10.1063/1.445869. PubMed PMID: WOS:A1983QZ31500046.

45. Katti DR, Katti KS, Amarasinghe P, Pradhan S. "Interlayer Fluid Flow and the Role of Clay-Fluid Molecular Interactions on the Swelling Behavior of Montmorillonite Clays." *Poro-Mechanics Iv*. 2009:836-41. PubMed PMID: WOS:000270143600126.

46. Katti, DR, Patwary, ZR, and Katti, KS. "Modelling clay-fluid interactions in montmorillonite clays." *Environmental Geotechnics.* 2016;0(0):17. doi: doi:10.1680/jenge.14.00027.

47. Phillips, JC, Braun, R, Wang, W, Gumbart, J, Tajkhorshid, E, Villa, E, Chipot, C, Skeel, RD, Kale, L, and Schulten, K. "Scalable molecular dynamics with NAMD." *Journal of Computational Chemistry*. 2005;26(16):1781-802. doi: 10.1002/jcc.20289. PubMed PMID: ISI:000233021400007.

48. Brooks, BR, Bruccoleri, RE, Olafson, BD, States, DJ, Swaminathan, S, and Karplus, M. "CHARMM - A Program for Macromolecular Energy, Minimization, and Dynamics Calculations." *Journal of Computational Chemistry*. 1983;4(2):187-217. doi: 10.1002/jcc.540040211. PubMed PMID: WOS:A1983QP42300010.

49. Feller, SE, Zhang, YH, Pastor, RW, and Brooks, BR. "Constant-Pressure Molecular-Dynamics Simulation - The Langevin Piston Method." *Journal of Chemical Physics.* 1995;103(11):4613-21. doi: 10.1063/1.470648. PubMed PMID: WOS:A1995RU11000023.

50. Amarasinghe, PM, Katti, KS, and Katti, DR. "Molecular Hydraulic Properties of Montmorillonite: A Polarized Fourier Transform Infrared Spectroscopic Study." *Applied Spectroscopy*. 2008;62(12):1303-13. PubMed PMID: WOS:000261594500004.

51. Katti, KS, Sikdar, D, Katti, DR, Ghosh, P, and Verma, D. "Molecular interactions in intercalated organically modified clay and clay-polycaprolactam nanocomposites: Experiments and modeling. Polymer. 2006;47(1):403-14. doi: 10.1016/j.polymer.2005.11.055. PubMed PMID: WOS:000234617600051.

52. Katti, DR, Upadhyay, HB, and Katti, KS. "Molecular interactions of kerogen moieties with Na-montmorillonite: An experimental and modeling study." *Fuel.* 2014;130:34-45. doi: 10.1016/j.fuel.2014.04.009. PubMed PMID: WOS:000336035600005.

53. Ambre, A, Katti, KS, and Katti, DR. "In situ mineralized hydroxyapatite on amino acid modified nanoclays as novel bone biomaterials." *Materials Science & Engineering C-Materials for Biological Applications*. 2011;31(5):1017-29. doi: 10.1016/j.msec.2011.03.001. PubMed PMID: WOS:000291778800030.

54. Ambre, A, Katti, KS, and Katti, DR. "In situ mineralized hydroxyapatite on amino acid modified nanoclays as novel bone biomaterials." *Materials Science & Engineering C-Materials for Biological Applications*. 2011;31(5):1017-29. doi: 10.1016/j.msec.2011.03.001. PubMed PMID: WOS:000291778800030.

55. Sikdar, D, Katti, KS, and Katti, DR. "Molecular interactions alter clay and polymer structure in polymer clay nanocomposites." *Journal of Nanoscience and Nanotechnology*. 2008;8(4):1638-57. doi: 10.1166/jnn.2008.032. PubMed PMID: WOS:000255790400006.

56. Fu, MH, Zhang, ZZ, and Low, PF. "Changes in the Properties of a Montmorillonite-Water System During the Adsorption and Desorption of Water - Hysteresis." *Clays and Clay Minerals*. 1990;38(5):485-92. doi: 10.1346/ccmn.1990.0380504. PubMed PMID: WOS:A1990ED26200004.

57. Cases, JM, Berend, I, Besson, G, Francois, M, Uriot, JP, Thomas, F, and Poirier, JE. "Mechanism of Adsorption and Desorption of Water-Vapor by Homoionic Montmorillonite .1. The Sodium-Exchanged Form." *Langmuir*. 1992;8(11):2730-9. doi: 10.1021/la00047a025. PubMed PMID: WOS:A1992JZ53400025.

58. Berend, I, Cases, JM, Francois, M, Uriot, JP, Michot, L, Masion, A, and Thomas, F. "Mechanism of Adsorption and Desorption of Water-Vapor by Homoionic Montmorillonites .2. The LI+, NA+, K+, RB+ and Cs+-Exchanged Forms." *Clays and Clay Minerals.* 1995;43(3):324-36. doi: 10.1346/ccmn.1995.0430307. PubMed PMID: WOS:A1995RV42800007.

59. Chapuis, RP. "Sand-Bentonite Liners - Predicting Permeability From Laboratory Tests." *Canadian Geotechnical Journal*. 1990;27(1):47-57. doi: 10.1139/t90-005. PubMed PMID: WOS:A1990CW62700005.

60. Tang, AM, Cui, YJ, and Barnel, N. "Thermo-mechanical behaviour of a compacted swelling clay." *Geotechnique*. 2008;58(1):45-54. doi: 10.1680/geot.2008.58.1.45. PubMed PMID: WOS:000253013100005.

61. Choy, JH, Choi, SJ, Oh, JM, and Park, T. "Clay minerals and layered double hydroxides for novel biological applications." *Applied Clay Science*. 2007;36(1-3):122-32. doi: 10.1016/j.clay.2006.07.007. PubMed PMID: WOS:000245765100011.

62. Yu, JY, Feng, PC, Zhang, HL, and Wu, SP. "Effect of organo-montmorillonite on aging properties of asphalt." *Construction and Building Materials.* 2009;23(7):2636-40. doi: 10.1016/j.conbuildmat.2009.01.007. PubMed PMID: WOS:000266524800022.

63. Sebastian, E, Cultrone, G, Benavente, D, Fernandez, LL, Elert, K, and Rodriguez-Navarro, C. "Swelling damage in clay-rich sandstones used in the church of San Mateo in Tarifa (Spain)." *Journal of Cultural Heritage*. 2008;9(1):66-76. doi: 10.1016/j.culher.2007.09.002. PubMed PMID: WOS:000254660700008.

64. Grim, RE. *Clay mineralogy*. Mcgraw-Hill Book Company, Inc; New York; Toronto; London; 1953.

65. Wyckoff, RWG. *Crystal structures*; Krieger; 1964.

66. Van Olphen, H. *An introduction to clay colloid chemistry : for clay technologists, geologists, and soil scientists*. 2d ed.. ed. New York: New York : Wiley; 1977.

67. Grahame DC. "Diffuse Double Layer Theory for Electrolytes of Unsymmetrical Valence Types." *Journal of Chemical Physics*. 1953;21(6):1054-60. doi: 10.1063/1.1699109. PubMed PMID: WOS:A1953UC11200015.

68. Verwey, EJW. "Theory of the Stability of Lyophobic Colloids." J*ournal of Physical and Colloid Chemistry*. 1947;51(3):631-6. doi: 10.1021/j150453a001. PubMed PMID: WOS:A1947YD72900001.

69. Katti, DR, Matar, MI, Katti, KS, and Amarasinghe, PM. "Multiscale modeling of swelling clays: A computational and experimental approach." *Ksce Journal of Civil Engineering*. 2009;13(4):243-55. doi: 10.1007/s12205-009-0243-0. PubMed PMID: WOS:000267600900004.

70. Cygan, RT, Liang, JJ, and Kalinichev, AG. "Molecular models of hydroxide, oxyhydroxide, and clay phases and the development of a general force field." J*ournal of Physical Chemistry B*. 2004;108(4):1255-66. doi: 10.1021/jp0363287. PubMed PMID: WOS:000188535700014.

71. Smith, DE. "Molecular computer simulations of the swelling properties and interlayer structure of cesium montmorillonite." *Langmuir*. 1998;14(20):5959-67. doi: 10.1021/la980015z. PubMed PMID: WOS:000076221800045.

72. Mignon, P, Ugliengo, P, Sodupe, M, and Hernandez, ER. "Ab initio molecular dynamics study of the hydration of Li+, Na+ and K+ in a montmorillonite model. Influence of isomorphic substitution." *Physical Chemistry Chemical Physics*. 2010;12(3):688-97. doi: 10.1039/b915689e. PubMed PMID: WOS:000273037900016.

73. Segad, M, Jonsson, B, Akesson, T, and Cabane, B. "Ca/Na Montmorillonite: Structure, Forces and Swelling Properties." *Langmuir*. 2010;26(8):5782-90. doi: 10.1021/la9036293. PubMed PMID: WOS:000276562300064.

74. Tambach, TJ, Hensen, EJM, and Smit B. Molecular simulations of swelling clay minerals. Journal of Physical Chemistry B. 2004;108(23):7586-96. doi: 10.1021/jp049799h. PubMed PMID: WOS:000221833400010.

75. Marry V, Rotenberg B, Turq P. Structure and dynamics of water at a clay surface from molecular dynamics simulation. Physical Chemistry Chemical Physics. 2008;10(32):4802-13. doi: 10.1039/b807288d. PubMed PMID: WOS:000258271800016.

76. Hensen EJM, Smit B. Why clays swell. Journal of Physical Chemistry B. 2002;106(49):12664-7. doi: 10.1021/jp0264883. PubMed PMID: WOS:000179732100003.

77. Katti DR, Thapa KB, Katti KS. Modeling molecular interactions of sodium montmorillonite clay with 3D kerogen models. Fuel. 2017;199:641-52.

78. Carrier B, Vandamme M, Pellenq RJM, Van Damme H. Elastic Properties of Swelling Clay Particles at Finite Temperature upon Hydration. Journal of Physical Chemistry C. 2014;118(17):8933-43. doi: 10.1021/jp412160e. PubMed PMID: WOS:000335433100025.

79. Zartman GD, Liu H, Akdim B, Pachter R, Heinz H. Nanoscale Tensile, Shear, and Failure Properties of Layered Silicates as a Function of Cation Density and Stress. Journal of Physical Chemistry C. 2010;114(4):1763-72. doi: 10.1021/jp907012w. PubMed PMID: WOS:000273947600004.

80. Ebrahimi D, Pellenq RJM, Whittle AJ. Nanoscale Elastic Properties of Montmorillonite upon Water Adsorption. Langmuir. 2012;28(49):16855-63. doi: 10.1021/la302997g. PubMed PMID: WOS:000312122300018.

81. Qomi MJA, Ebrahimi D, Bauchy M, Pellenq R, Ulm FJ. Methodology for Estimation of Nanoscale Hardness via Atomistic Simulations. Journal of Nanomechanics and Micromechanics. 2017;7(4). doi: 10.1061/(asce)nm.2153-5477.0000127. PubMed PMID: WOS:000424163400001.

82. Cornelis K, Dutrow B. Manual of mineral science. John Wiley & Sons, Inc; 2007.

83. Katti DR, Thapa KB, Katti KS. The role of fluid polarity in the swelling of sodium-montmorillonite clay: A molecular dynamics and Fourier transform infrared spectroscopy study. Journal of Rock Mechanics and Geotechnical Engineering. 2018.

84. Fripiat JJ, Van Olphen H, Clay Minerals S, Organisation for Economic Co-operation and D. Data handbook for clay materials and other non-metallic minerals : providing those involved in clay research and industrial application with sets of authoriative data describing the physical and

chemical properties and mineralogical composition of the available reference materials. Oxford ; New York: Oxford ; New York : Pergamon Press; 1979.

85. Sikdar D, Katti DR, Katti KS. A molecular model for epsilon-caprolactam-based intercalated polymer clay nanocomposite: Integrating modeling and experiments. Langmuir. 2006;22(18):7738-47. doi: 10.1021/la060243q. PubMed PMID: WOS:000239921800041.

86. Kale L, Skeel R, Bhandarkar M, Brunner R, Gursoy A, Krawetz N, Phillips J, Shinozaki A, Varadarajan K, Schulten K. NAMD2: Greater scalability for parallel molecular dynamics. Journal of Computational Physics. 1999;151(1):283-312. doi: 10.1006/jcph.1999.6201. PubMed PMID: WOS:000080181500013.

87. Martyna GJ, Tobias DJ, Klein ML. Constant-Pressure Molecular-Dynamics Algorithms. Journal of Chemical Physics. 1994;101(5):4177-89. doi: 10.1063/1.467468. PubMed PMID: WOS:A1994PE11000084.

88. Katti DR, Sharma A, Ambre AH, Katti KS. Molecular interactions in biomineralized hydroxyapatite amino acid modified nanoclay: In silico design of bone biomaterials. Materials Science & Engineering C-Materials for Biological Applications. 2015;46:207-17. doi: 10.1016/j.msec.2014.07.057. PubMed PMID: WOS:000347757100027.

89. Grim RE. Clay Mineralogy McGraw-Hill. New York. 1968:206.

90. Buzzi O, Fityus S, Sloan SW. Use of expanding polyurethane resin to remediate expansive soil foundations. Canadian Geotechnical Journal. 2010;47(6):623-34. doi: 10.1139/t09-132. PubMed PMID: WOS:000279224600003.

91. Guggenheim S, Martin RT. Reply to the comment by DM Moore on “Definition of clay and clay mineral: Joint report of the AIPEA nomenclature and CMS nomenclature committees”. Clays and Clay Minerals. 1996;44(5):713-5.

92. Grim RE. Modern concepts of clay materials. Journal of Geology. 1942;50(3):225-75. PubMed PMID: WOS:000188564600001.

93. Hendricks SB, Jefferson ME. Structures of kaolin and talc-pyrophyllite hydrates and their bearing on water sorption of the clays. American Mineralogist. 1938;23(12):863-75. PubMed PMID: WOS:000187829100002.

94. Massat L, Cuisinier O, Bihannic I, Claret F, Pelletier M, Masrouri F, Gaboreau S. Swelling pressure development and inter-aggregate porosity evolution upon hydration of a compacted swelling clay. Applied Clay Science. 2016;124:197-210. doi: 10.1016/j.clay.2016.01.002. PubMed PMID: WOS:000375162300023.

95. Bihannic I, Tchoubar D, Lyonnard S, Besson G, Thomas F. X-ray scattering investigation of swelling clay fabric 1. The dry state. Journal of Colloid and Interface Science. 2001;240(1):211-8. doi: 10.1006/jcis.2001.7690. PubMed PMID: WOS:000170111900024.

96. Keller LM, Schuetz P, Erni R, Rossell MD, Lucas F, Gasser P, Holzer L. Characterization of multi-scale microstructural features in Opalinus Clay. Microporous and Mesoporous Materials. 2013;170:83-94. doi: 10.1016/j.micromeso.2012.11.029. PubMed PMID: WOS:000315614700011.

97. Likos WJ, Wayllace A. Porosity Evolution of Free and Confined Bentonites During Interlayer Hydration. Clays and Clay Minerals. 2010;58(3):399-414. doi: 10.1346/ccmn.2010.0580310. PubMed PMID: WOS:000289446300011.

98. Jullien M, Raynal J, Kohler E, Bildstein O. Physicochemical reactivity in clay-rich materials: Tools for safety assessment. Oil & Gas Science and Technology-Revue D Ifp Energies Nouvelles. 2005;60(1):107-20. doi: 10.2516/ogst:2005007. PubMed PMID: WOS:000229877900008.

99. Norrish K. The swelling of montmorillonite. Discussions of the Faraday society. 1954;18:120-34.

100. Sposito G, Prost R. Structure of Water Adsorbed On Smectites. Chemical Reviews. 1982;82(6):553-73. doi: 10.1021/cr00052a001. PubMed PMID: WOS:A1982PY80900001.

101. Yong RN. Soil suction and soil-water potentials in swelling clays in engineered clay barriers. Engineering Geology. 1999;54(1-2):3-13. doi: 10.1016/s0013-7952(99)00056-3. PubMed PMID: WOS:000082578000002.

102. Pusch R, Yong R. Water saturation and retention of hydrophilic clay buffer - microstructural aspects. Applied Clay Science. 2003;23(1-4):61-8. doi: 10.1016/s0169-1317(03)00087-5. PubMed PMID: WOS:000186093500008.

103. Perdrial JN, Warr LN. Hydration Behavior of Mx80 Bentonite In A Confined-Volume System: Implications For Backfill Design. Clays and Clay Minerals. 2011;59(6):640-53. doi: 10.1346/ccmn.2011.0590609. PubMed PMID: WOS:000300339900009.

104. Salles F, Beurroies I, Bildstein O, Jullien M, Raynal J, Denoyel R, Van Damme H. A calorimetric study of mesoscopic swelling and hydration sequence in solid Na-montmorillonite. Applied Clay Science. 2008;39(3-4):186-201. doi: 10.1016/j.clay.2007.06.001. PubMed PMID: WOS:000256276900010.

105. Salles F, Douillard J-M, Denoyel R, Bildstein O, Jullien M, Beurroies I, Van Damme H. Hydration sequence of swelling clays: Evolutions of specific surface area and hydration energy. Journal of Colloid and Interface Science. 2009;333(2):510-22. doi: 10.1016/j.jcis.2009.02.018. PubMed PMID: WOS:000265121500012.

106. Jonas EC, Oliver RM. Size and shape of montmorillonite crystallites. Clays Clay Miner. 1967;15:27-33.

107. Karaborni S, Smit B, Heidug W, Urai J, vanOort E. The swelling of clays: Molecular simulations of the hydration of montmorillonite. Science. 1996;271(5252):1102-4. doi: 10.1126/science.271.5252.1102. PubMed PMID: WOS:A1996TW70100033.

108. Smith DE, Wang Y, Whitley HD. Molecular simulations of hydration and swelling in clay minerals. Fluid Phase Equilibria. 2004;222:189-94. doi: 10.1016/j.fluids.2004.06.023. PubMed PMID: WOS:000223777100022.

109. Katti DR, Schmidt SR, Ghosh P, Katti KS. Modeling the response of pyrophyllite interlayer to applied stress using steered molecular dynamics. Clays and Clay Minerals. 2005;53(2):171-8. doi: 10.1346/ccmn.2005.0530207. PubMed PMID: WOS:000228649900007.

110. Katti DR, Patwary ZR, Katti KS. Modelling clay-fluid interactions in montmorillonite clays. Environmental Geotechnics. 2017;4(5):322-38. doi: 10.1680/jenge.14.00027. PubMed PMID: WOS:000417320900002.

111. Van Olphen H, Fripiat J-J. Data handbook for clay materials and other non-metal lic minerals: providing those involved in clay research and indus trial application with sets of authoritative data describing the physical and chemical properties and mineralogical composition of the available reference materials1979.

112. Skipper NT, Chang FRC, Sposito G. Monte-Carlo Simulation of Interlayer Molecular-Structure in Swelling Clay-Minerals .1. Methodology." *Clays and Clay Minerals*. 1995;43(3):285-93. doi: 10.1346/ccmn.1995.0430303. PubMed PMID: WOS:A1995RV42800003.

113. Vanommeslaeghe, K, Hatcher, E, Acharya, C, Kundu, S, Zhong, S, Shim, J, Darian, E, Guvench, O, Lopes, P, Vorobyov, I, and MacKerell, AD. "CHARMM General Force Field: A Force Field for Drug-Like Molecules Compatible with the CHARMM All-Atom Additive Biological Force Fields." *Journal of Computational Chemistry*. 2010;31(4):671-90. doi: 10.1002/jcc.21367. PubMed PMID: WOS:000274922000002.

114. Payne, MC, Teter, MP, Allan, DC, Arias, TA, and Joannopoulos, JD. "Iterative Minimization Techniques for Abinitio Total-Energy Calculations - Molecular-Dynamics and Conjugate Gradients." *Reviews of Modern Physics*. 1992;64(4):1045-97. doi: 10.1103/RevModPhys.64.1045. PubMed PMID: WOS:A1992JV36300004.

115. Young, D. *Computational chemistry: a practical guide for applying techniques to real world problems*: John Wiley & Sons; 2004.

116. Michot, LJ, Bihannic, I, Porsch, K, Maddi, S, Baravian, C, Mougel, J, and Levitz, P. "Phase diagrams of Wyoming Na-montmorillonite clay. Influence of particle anisotropy." *Langmuir*. 2004;20(25):10829-37. doi: 10.1021/la0489108. PubMed PMID: WOS:000225500700008.

117. Cadene, A, Durand-Vidal, S, Turq, P, and Brendle, J. "Study of individual Na-montmorillonite particles size, morphology, and apparent charge." *Journal of Colloid and Interface Science*. 2005;285(2):719-30. doi: 10.1016/j.jcis.2004.12.016. PubMed PMID: WOS:000228732900035.

118. Segad, M, Jönsson, B, and Cabane, B. "Tactoid formation in montmorillonite." *The Journal of Physical Chemistry C*. 2012;116(48):25425-33.

119. Olive, WW, Chleborad, AF, Frahme, CW, Schlocker, J, Schneider, RR, and Schuster, RL. *Swelling clays map of the conterminous United States*. 1989.

120. Sridharan, A, Rao, SN, and Rao, GV. "Shear strength characteristics of saturated montmorillonite and kaolinite clays." *Soils and Foundations*. 1971;11(3):1-22.

121. SinhaRay, S, and Biswas, M. "Preparation and evaluation of composites from montmorillonite and some heterocyclic polymers: 3. A water dispersible nanocomposite from pyrrole-montmorillonite polymerization system." *Materials Research Bulletin*. 1999;34(8):1187-94. doi: 10.1016/s0025-5408(99)00121-x. PubMed PMID: WOS:000083047900001.

122. Alonso, EE, Vaunat, J, and Gens, A. "Modelling the mechanical behaviour of expansive clays." *Engineering Geology*. 1999;54(1-2):173-83. doi: 10.1016/s0013-7952(99)00079-4. PubMed PMID: WOS:000082578000020.

123. Alstadt, KN, Katti, KS, and Katti, DR. "Nanoscale Morphology of Kerogen and In Situ Nanomechanical Properties of Green River Oil Shale." *Journal of Nanomechanics and Micromechanics*. 2015:04015003.

124. Wang, ZJ. "Fundamentals of seismic rock physics." *Geophysics*. 2001;66(2):398-412. doi: 10.1190/1.1444931. PubMed PMID: WOS:000168101200004.

125. Das, BM, and Sobhan, K. *Principles of geotechnical engineering: Cengage Learning*; 2013.

126. Zhang, GP, Wei, ZX, and Ferrell, RE. "Elastic modulus and hardness of muscovite and rectorite determined by nanoindentation." *Applied Clay Science*. 2009;43(2):271-81. doi: 10.1016/j.clay.2008.08.010. PubMed PMID: WOS:000263390200020.

127. Kadali, S, Sharma, S, and Singh, DN. "Application of nanoindentation to establish influence of heat on soils." *Engineering Geology*. 2013;162:14-21. doi: 10.1016/j.enggeo.2013.05.004. PubMed PMID: WOS:000322054500002.

128. Mallikarjunachari, G, Nallamilli, T, Ravindran, P, and Basavaraj, MG. "Nanoindentation of clay colloidosomes." *Colloids and Surfaces a-Physicochemical and Engineering Aspects*. 2018;550:167-75. doi: 10.1016/j.colsurfa.2018.04.041. PubMed PMID: WOS:000432552600020.

129. Vanorio, T, Prasad, M, and Nur, A. "Elastic properties of dry clay mineral aggregates, suspensions and sandstones." *Geophysical Journal International.* 2003;155(1):319-26. doi: 10.1046/j.1365-246X.2003.02046.x. PubMed PMID: WOS:000185348000024.

130. Oliver, WC, and Pharr, GM. "An Improved Technique for Determining Hardness and Elastic-Modulus Using Load and Displacement Sensing Indentation Experiments." *Journal of Materials Research*. 1992;7(6):1564-83. doi: 10.1557/jmr.1992.1564. PubMed PMID: WOS:A1992HY10600033.

131. Wang, ZJ, Wang, H, and Cates, ME. "Effective elastic properties of solid clays." *Geophysics.* 2001;66(2):428-40. doi: 10.1190/1.1444934. PubMed PMID: WOS:000168101200007.